NASA Contractor Report 201667

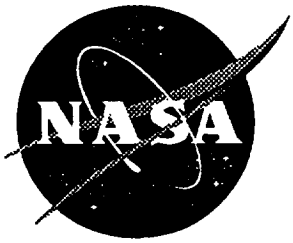

A Unique Test Facility to Measure Liner Performance With a Summary of Initial Test Results

K. K. Ahuja and R. J. Gaeta, Jr.
Georgia Institute of Technology, Atlanta, Georgia

Contract NAS1-19061

March 1997

National Aeronautics and
Space Administration
Langley Research Center
Hampton, Virginia 23681-0001

Foreword/Acknowledgments

This report was prepared by the Acoustics and Aerodynamics Branch of the Aerospace and Transportation Laboratory of Georgia Tech Research Institute (GTRI) for NASA Langley Research Center, Hampton, Virginia, under Task Assignment 14 of Contract NAS1-19061.

Mr. Tony Parrot and Ms. Sherry Tanner were the Project Managers for NASA Langley Research Center. GTRI's Project Director was Dr. Krish K. Ahuja.

The authors would like to acknowledge the assistance of Mike Dewey, Pat McPherson, and Todd Elsbrend of GTRI for their assistance in the data acquisition and hardware design.

TABLE OF CONTENTS

List of Figures

Summary

A very ambitious study was initiated to obtain detailed acoustic and flow data with and without a liner in a duct containing a mean flow so that available theoretical models of duct liners can be validated. A unique flow-duct facility equipped with a sound source, liner box, flush-walled microphones, traversable microphones and traversable pressure and temperature probes was built. A unique set of instrumentation boxes equipped with computer controlled traverses were designed and built that allowed measurements of Mach number, temperature, SPLs and phases in two planes upstream of a liner section and two planes downstream at a large number of measurement points. Each pair of planes provided acoustic pressure gradients for use in estimating the particle velocities. Specially-built microphone probes were employed to make measurements in the presence of the flow. A microphone traverse was also designed to measure the distribution of SPLs and phases from the beginning of the liner to its end along the duct axis. All measurements were made with the help of cross-correlation techniques to reject flow noise and/or other obtrusive noise, if any. The facility was designed for future use at temperatures as high as 1500° F. In order to validate 2-D models in the presence of mean flow, the flow duct was equipped with a device to modify boundary layer flow on the smaller sides of a rectangular duct to simulate 2-D flow.

A massive amount of data was acquired for use in validating duct liner models and will be provided to NASA in an electronic form.

It was found that the sound in the plane-wave regime is well behaved within the duct and the results are repeatable from one run to another. At the higher frequencies corresponding to the higher-order modes, the SPLs within a duct are not repeatable from run to run. In fact, when two or more modes have the same frequency (i.e., for the degenerate modes), the SPLs in the duct varied between 2 dB to 12 dB from run to run. This made the calibration of the microphone probes extremely difficult at the higher frequencies.

Most of the data presented in this report is for zero mean flow. Data with flow were also acquired but were not analyzed at the time of the preparation of this report. The flow data will be published separately in due course. The technique based upon cross-correlation measurements used to reject flow noise was found to work well in measurements made with flow.

1.0 INTRODUCTION

1.1 BACKGROUND

The standing-wave tube has been a standard tool for determining the acoustic properties of liner materials for a long time. A number of methods based upon two microphone measurements have recently been developed that allow faster measurements of the sound absorption properties at a range of frequencies simultaneously (Munjal, Ref. 1.1 and Chung and Blaser, Ref. 1.2). Most of the available methods still rely on data acquired for plane wave sound propagation. As such, the microphones are mounted either flush with the tube or duct wall or at the center of the duct. In addition, methods of measuring acoustic properties are well developed for zero mean-flow conditions. Few facilities have been developed to measure the acoustic properties in the presence of the flow (Dean and Vaidya, Ref. 1.3). What is lacking, however, is a facility that will allow measurements of the sound field as well as the flow field in two or more planes in the interior of a given duct with and without a liner both for unheated and heated flow conditions. Such a facility is needed to validate duct liner analytical models. For example, to predict the performance of a liner mounted on the walls of a duct with flow, a model developed by Watson (Ref. 1.4) requires sound pressure levels and phase information along with the appropriate flow data in three planes in the duct. In particular, such information is needed in two planes upstream of the liner and one plane downstream of the liner. In addition, distribution of sound pressure levels and phases in the liner section is desired. Such a unique facility was designed, built, and tested in the present program.

1.2 STUDY OBJECTIVE AND PROGRAM DESCRIPTION

Thus the objective of this study was to develop a flow-duct facility that would allow measurements of detailed acoustic and flow data with and without a liner in a duct containing cold or heated mean flow so that available theoretical models of duct liners can be validated. A capability of generating known sound upstream was implemented. A unique set of instrumentation boxes equipped with computer controlled traverses was designed and built that allowed measurements of Mach number, temperature, SPLs and phases in two planes upstream of a liner section and two planes downstream at a large number of measurement points. Each pair of planes provided acoustic pressure gradients for use in estimating the particle velocities in the measurement planes. Specially-built microphone probes were employed to make measurements in the presence of the flow. A microphone traverse was also designed to measure the distribution of SPLs and phases from the beginning of the liner to its end along the duct axis. All measurements were made with the help of cross-correlation techniques to reject flow noise or other obtrusive noise, if any.

The facility was designed for future use at temperatures as high as 1500° F. In order to validate 2-D models in the presence of mean flow, a rectangular duct was equipped with a device to modify boundary layer flow on the smaller sides of a rectangular duct to simulate 2-D flow.

A massive amount of benchmark experimental data was acquired in sufficient detail to enable validation of theoretical duct liner models. All of the data acquired will be provided to NASA Langley Research Center in electronic form. Selected results are presented here to highlight some of the features of the measured results and to direct the reader as to how best to use the massive amount of data saved in the electronic form.

Most of the data presented in this report is for zero mean flow. Data with flow were acquired but were not analyzed at the time of the preparation of this report. The flow data will be published separately in due course. The technique based upon cross-correlation measurements which was used to reject flow noise was, however, found to work well in measurements made with flow.

1.3 REPORT OUTLINE

A detailed description of the unique facility mentioned above is provided in Section 2. Development of a test methodology is presented in Section 3. This section describes the calibrations of the specially-built microphone probes and methods of rejecting flow noise using cross-correlation techniques. Typical in-duct flow and acoustic measurements are presented. Methods developed for modifying boundary layer flows are also discussed. Selected acoustic data in various planes of measurements are then provided. Section 4 includes the effect of the liner on the sound field. Selected results are presented here to highlight some of the features of the measured results. Finally, the overall conclusions are given in Section 5.

2.0 TEST FACILITY AND EXPERIMENTAL SET-UP

2.1 INTRODUCTION

Interest in the detailed measurements of the acoustic field inside a flow-duct at locations upstream and downstream of a potential duct liner was the impetus for developing the test facility described below. In general, the following design requirements were adhered to:

1. Develop a rectangular duct that is made up of modular sections which can be mixed and matched in any order.

2. Develop a probe-measurement system which can provide smooth two-axis (planar) in-duct traversing within the rectangular duct at a given axial location with and without mean flow. Furthermore, provide for a small axial offset of the measurement probe to estimate acoustic pressure gradients. Also, ensure a leak-free environment during testing with mean flow.

3. Develop a method of controlling the boundary layer of the short side of the rectangular duct by mass addition and mass removal techniques.

4. Develop a liner-housing section that can be integrated with the measurement system and provide for acoustic lining on the long sides of the rectangular duct.

5. Fabricate duct sections from steel to provide a flow-duct that can operate at elevated temperatures (up to 1500° F).

A schematic of the liner facility is shown in Figure 2.1. A photographic view is provided in Figure 2.2.

The discussion below includes a detailed description of the general test facility where the rectangular flow-duct was housed, the details of the flow-duct, and the data acquisition system used for the present experimental work. Also, a brief description of the acoustic properties for the liner tested in this facility is provided.

2.2 FLOW FACILITY

All of the work discussed in this report was performed in GTRI's Hot Jet Flow Facility. The Hot Jet Flow Facility can produce a single or coaxial flow. The primary flow enters through a 25.6-cm (10.1-inch) diameter plenum, followed by a contraction to a 10.2-cm (4.0-inch) diameter plenum exit dimension. An outer coannular plenum exists to provide a source of secondary air. For the present tests, only the primary air system was used. The plenum exit is flanged to accept nozzles or duct extensions as needed. A circular duct section equipped with the acoustic sound source was placed at the plenum exit. Four equally (circumferentially) spaced tubes in the circular duct section lead to four acoustic drivers which provide an upstream sound source. To accommodate a rectangular flow-duct apparatus required for the present study, a duct transition from a circular to a rectangular cross section was fabricated. The overall contraction ratio from the primary plenum to the rectangular duct is 8.5:1. For all of the present experiments, the downstream sound propagation set-up was used.

2.3 RECTANGULAR FLOW-DUCT

The following sections describe the modular pieces which make up the flow-duct used for the present study. Once the flow-duct converges to a rectangular cross section, it maintains a constant-area cross section until the duct-exhaust exit. All of the sections were designed to attach to each other in any order. The possibility of using heated flow was taken into account in the design of this flow-duct and is reflected in the use of stainless steel as the main fabrication material. This will allow for greater capability for the study of high temperature acoustic liners in any future validation of duct liner models.

Figure 2.3 provides the terminology and flow-duct coordinate system that will be used for the remainder of this report.

2.3.1 Round-to-Rectangular Transition

In order to provide compatibility with the existing primary plenum's exit geometry, a round-to-rectangular transition duct was fabricated which converged from a 81.7 cm^2 (12.57 in^2) circular area to a 60.5 cm^2 (9.4 in^2) rectangular area. The transition duct section was made from a 10.2-cm (4.0-inch) inner-diameter steel pipe. The flowpath of the pipe was tapered to a diameter of 11.91 cm (4.69 inches). The pipe was then cut to allow two steel

plates to be welded onto its end. This provided a rectangular duct cross section with a height of 5.08 cm (2.00 inches) and a width of 11.91 cm (4.69 inches) at the exit of the transition. Figure 2.4 shows a photograph of the transition duct. The transition duct was positioned downstream of the acoustic source section.

2.3.2 Boundary-Layer Control Section

The objective for the Boundary-Layer Control Section (BLCS) was to develop a way to approximate a two-dimensional flow field in the rectangular flow-duct. The catalyst for the quasi-2D flowfield was the existence of 2-D finite element codes at NASA Langley Research Center (LaRC) which can predict acoustic liner performance. NASA LaRC's code was developed by Dr. W. Watson (Ref. 2.1). Since the flow downstream of the round-to-rectangular transition is expected to be turbulent and nearly fully-developed, complete removal of the boundary layer would not be possible. Still it was desired to provide a capability of minimizing the boundary layer thickness on the sidewall of the duct as much as possible in order to more closely match the 2-D assumptions of the 2-D model to be validated. Additionally, it may be desirable in the future to enhance the three dimensionality of the flow in the duct in a controlled manner to represent a more realistic flow environment. The BLCS was, thus, designed with this alternate purpose in mind.

Two concepts were considered to minimize the sidewall boundary layer: 1) boundary layer suction and 2) tangential slot blowing. The former concept removes low momentum boundary layer flow via a vacuum system and the latter adds momentum to the boundary layer via a high pressure wall jet. There are advantages and disadvantages to each concept and it was decided that each concept can be employed with a common duct section module. Each concept will now be discussed in turn.

Boundary Layer Suction

Removal of low momentum fluid near the sidewall of the flow-duct is achieved by creating a low pressure cavity on either side of the duct over a small 3.8 cm (1.5 inches) segment. This segment of the sidewall was equipped with a section which was replaced with reticulated steel foam. This porous material is expected to provide smooth, even, flow removal across the side wall. Figure 2.5 shows a schematic of the BLCS with the suction system concept. The design

allows for multi-layers of reticulated foam for controlled flow resistance and hence a finer control on boundary layer suction. The plenum cavity which backs the porous foam was bolted to the side wall of the rectangular duct. Initial tests were performed with a standard 5 hp shop-vacuum. However, future tests could incorporate a "quiet" vacuum system which would muffle any noise from the pump. A smooth contracting bell mouth is used to remove the extracted flow from the attached cavities with minimal disturbances.

Tangential Blowing

An alternate method of controlling the sidewall boundary layer is that of mass addition in the form of tangential blowing. This concept relies on the addition of mass (and momentum) into the boundary layer to reduce the boundary layer thickness. A continuous slot area across each sidewall at a prescribed axial location in the duct will allow air to be forced along the wall. By controlling the mass flow and thus the momentum of the injected air, a single axial location on the sidewall can be optimized for maximum reduction of boundary layer thickness. This concept has been used in the past by many researchers. In particular, GTRI has extensive experience in this type of boundary layer control. Specifically, GTRI's low speed wind tunnel currently uses this concept to properly simulate ground effects for hydroplane race vehicles (see Englar, Ref. 2.2). However, the effectiveness of such a system will be somewhat limited by the presence of fully-developed duct flow.

Figure 2.6 shows a schematic of the tangential blowing apparatus. The side plenum cavity is common to the cavity which houses the boundary layer suction device discussed earlier. The air diffuser/muffler has two functions: 1) it evenly distributes high-pressure air in the plenum and 2) it helps attenuate any noise which may accompany the incoming jet. The air in the plenum was forced through an adjustable slot in the sidewall around a "Coanda" surface to ensure a tangential exit. The slot height can be adjusted with a single push-rod which is controlled from outside of the plenum cavity. The push-rod was connected to a micrometer head to achieve variable slot heights precisely.

Preliminary Tests of the Upstream Boundary-Layer Control Section

The Boundary-Layer Control Section was tested for its basic operation and its effectiveness in minimizing the sidewall boundary layer in the rectangular duct. The Round-to-Rectangular

transition was bolted to the plenum of the Hot Jet Flow Facility and the BLCS was attached to the exit of this section. In addition, a 17.8-cm (7-in) long rectangular nozzle was attached downstream of the BLCS. In the full set-up of the flow-duct, the exit of the BLCS will be approximately 20 cm (8 in) from the beginning of the liner material.

The tangential-blowing arrangement of the BLCS was assembled first. While blowing is designed to occur on both sidewalls of the duct, only measurements on the left side (viewing in the upstream direction) were taken. A probe traverse system was built to measure boundary layer profiles on the major-axis of the flow-duct. High pressure 550 kPa (80 psig) shop air was used to supply the blowing plenum.

The character of the flow profile in the duct was first established with the tangential slot "closed" and with no secondary air in the plenum. Typical flow-duct Mach numbers of 0.1, 0.2, and 0.3 were produced at ambient temperatures. A boundary-layer pitot probe was used to acquire flow velocities at the exit of the exhaust nozzle, which was at a distance of approximately 18 cm (7 in) downstream of the blowing slot. Velocities were computed using isentropic flow relations and assuming that ambient static pressure exists everywhere at the exit. Measurements were taken along the flow-duct's major axis (see Figure 2.3). Pressure measurements were made every 2 mm from the wall to just over half way across the duct. The flow in the duct was found to be nearly fully-developed for all Mach numbers tested. By arbitrarily defining the boundary layer height to be where the velocity is 99% of the maximum duct velocity, the boundary layer thickness in the duct is approximately 3.18 - 3.8 cm (1.25 - 1.5 in) from the duct wall. Also, the profile shape is consistent with turbulent, fully developed pipe flow profiles in the literature (Schlichting, Ref. 2.3).

Various slot areas were examined which, due to inlet-area constraints, gave a decreasing plenum pressure with increasing slot area. It was relatively easy to produce an "inverted" velocity flow profile, i.e., one which had higher velocities near the wall compared to the duct centerline. The calculation of the displacement thickness involves integration of the velocity profile (Ref. 2.3). It is then possible for the displacement thickness to have a value of zero for an inverted velocity profile. Thus, the displacement thickness is not the best measure of a 2-dimensional flow profile. Strictly speaking, boundary layer thickness is the best measure of two-dimensionality of the flow, but since our duct is nearly fully developed, it will be extremely difficult to reduce the thickness appreciably with tangential blowing. While not

optimized, it was found that a slot height of about 1.2 mm (0.05 in) provided reasonable results. Figures 2.7 - 2.9 show the non-dimensional velocity profiles for M = 0.1, 0.2, 0.3, respectively, with and without tangential blowing. It was found that the boundary layer was modified noticeably in the first 1.3 cm (0.5 in) from the wall. While the result of the tangential blowing was to make the boundary layer more "two-dimensional," it tended to produce a more "jagged" velocity profile. This was due to the fact that the tangential mass addition near the wall created a shear layer as the added velocity was much larger than the duct velocity. This shear layer needed more axial distance to fully mix so as to provide a smoother velocity profile. We, however, believe that the tangential blowing system can, with further work, be made quite effective in altering the velocity boundary layer characteristics in any future work.

Preliminary tests of the boundary layer suction technique were also performed. In this test, a 5 horsepower shop vacuum was used to remove the low momentum boundary layer flow from the left sidewall (looking upstream). A 1.3-cm (0.5-in) thick piece of reticulated nichrome foam (porosity: 60 ppi) was used, which acted as a porous wall. Figure 2.10 shows a photograph of the porous sidewall. Figures 2.11 shows the normalized velocity profiles with and without suction for a duct Mach numbers of 0.1. It can be seen that compared with the tangential blowing results, suction provides a smoother velocity profile.

The ability to control the sidewall boundary layer has thus been demonstrated with two different techniques. However, acoustic data with the flow-duct was not acquired with these sidewall flow modifications for this report.

2.3.3 Instrumentation Section

The instrumentation section of the flow duct is the modular duct segment in which both acoustic and flow measurements can be made in a plane perpendicular to the mean flow direction. The design of this section presented somewhat of a unique challenge. It required an intrusive probe to move in two dimensions inside a high-pressure duct without any flow leakage. Furthermore, the flow along the sidewall where the probe entered the duct needed to be as "clean" as possible. Figure 2.12 shows a schematic of the concept that achieves these objectives. The figure focuses on just the probe-insertion location and the probe's translational degrees of freedom. Note that the vertical travel of the probe in the duct is accomplished by a "slide rule" type traverse sled. This concept allows for vertical travel while still maintaining a

flush inner-duct flowpath. Horizontal travel is achieved by the probe translating in and out through a circular slot in a traverse sled. The horizontal and vertical motions are actuated via stepper motors for accuracy. Two such instrumentation sections were built to provide planar in-duct measurements upstream and downstream of the liner housing section.

Air is allowed to leak out of the duct through of the probe entry opening as well as around the vertical sled groove into an air-tight containment. It was felt that if this section outside the duct could be isolated inside an air-tight enclosure, the pressure inside the enclosure would equalize with that inside of the duct. Figure 2.13 shows a cross sectional view of the instrumentation section showing the outer containment box concept. It shows how the translating sensing probe is enclosed, providing an air-tight method of intrusive duct-flow and acoustic measurements. Note that the stepper motors are located outside of the outer enclosure. Placement of the motors outside of the enclosure will protect them from the potentially hot environment if heated duct flows are experienced. Data from the probes is transmitted out through the enclosure via sealed electrical interfaces and pressure connections. Figure 2.14 shows an inside view of the instrumentation box. The traverse system can accept either a 0.64-cm (0.25-in) diameter probe. All parts are fabricated from stainless steel to facilitate heated duct flows.

An additional feature of the 2-D probe traverse system is an axial offset mechanism. This was designed to provide measurements in two planes which are offset axially (in the x-direction) by 0.76 cm (0.3 in). This requirement was introduced in the design in order to provide a streamwise gradient in acoustic (complex) pressure from which the acoustic particle velocity can be computed. The 0.76-cm (0.3-in) offset was chosen from LaRC's numerical analysis experience. It was suggested that no greater than a tenth of an acoustic wavelength would be a sufficiently small spatial offset. Thus, a 0.76-cm (0.3-in) offset satisfies this condition for acoustic signals up to 4 kHz. Sensing probes enter the duct from either or both of the side walls. Flow measurements include pressure, temperature, and velocity profiles upstream of the liner section. Also, in-flow sound pressure levels and phases are obtained with a microphone probe equipped with a nosecone. With these measurements, both the mean flowfield and acoustic flowfields can be determined in a cross-plane of the rectangular duct.

A spring mechanism was designed to hold the measurement probe in its place. This mechanism also served to provide a way for the probe to "slip" the required 0.76 cm (0.3 in) in

the x-direction. Once locked in an axial plane, a clamp prevented the probe from moving in the axial direction while at the same time allowing the probe to move in the transverse directions. Figure 2.15 shows a photograph of part of this probe-holding mechanism. The axial-shift mechanism was also designed to be actuated remotely from outside the instrumentation box if necessary. This arrangement allowed measurements in two planes located upstream of the liner section and two planes located downstream.

2.3.4 Liner Section

This section of the flow-duct was designed to house an acoustic liner. Specifically, the section allowed for a liner to be placed on the top and/or bottom walls of the rectangular duct. Liner material with depths up to five inches can be placed on either side of this section of the duct. Approximately 7.6 cm (3 in) of a smooth rigid-walled duct section preceded and followed this lined section. This section, as with all others, is fabricated from steel. Once a liner is installed, the top and bottom of the liner housing can be sealed with a backing plate to prevent any flow leakage. A rigid-walled duct can be simulated by placing a steel plate in place of a liner in the housing section. In general, the liner housing section is amenable to installation of a variety of liners.

As an additional source of acoustic information, flush-mounted microphone ports are located on the top and bottom of the flow-duct in the rigid-wall region just upstream and just downstream of the liner housing section. The liner section is flanged on both ends to allow attachment to any modular section of the flow-duct.

2.3.5 Exhaust Section

A relatively short rigid-walled duct section was built to provide approximately seven inches of length to the last section of the flow-duct as it opened to the ambient room conditions. As used for testing in this report, the exhaust section formed the last 17.8 cm (7 inches) of the rectangular flow-duct.

2.3.6 Axial Centerline Acoustic Measurement Apparatus

An additional need to acquire acoustic data on the duct centerline in the lined region of the duct was met with a single axially-traversing microphone. A 0.64-cm (0.25-in) microphone

was placed inside a 1.59-cm (0.625-in) OD tube which was mounted on a cylindrical support post. Figure 2.16 shows a photograph of this apparatus. The support post was mounted on a traverse sled. In order to insure accurate centerline placement in the duct and to provide stabilization during flow testing, the tube holding the microphone was equipped with support wires placed at a distance of 20.3 cm (8.0 in) from the transducer which pushed against the corners of the flow-duct. Figure 16 also shows a photograph of these support wires. The traverse and its motor are mounted just outside the flow-duct.

2.4 INSTRUMENTATION AND DATA ACQUISITION

2.4.1 Flow Measurements

Qualitative and quantitative aspects of the mean flowfield within the flow-duct were established by traversing the duct in the z-y plane at a given axial location with a combination pitot-static and thermocouple probe. In particular, this flow probe was a United Sensor type PAC-T. The thermocouple wire type was Chromium/Aluminum allowing for measurements in flows with temperatures up to 1400° F. The pressure tube part of the probe was made from stainless steel. The stock probe was modified to fit the instrumentation box dimensions and had a 0.318-cm (0.125-in) outer diameter. Figure 2.17 shows a photograph of a typical probe used for flow measurements.

The total and static pressure sensed by the flow probe exited the instrumentation box via pressure lines that connect to sealed steel tubes. Standard Tygon pressure tubing relayed the total and static pressure to a pair of SensSym SCX series electro-pneumatic transducers. Output from these transducers lead to an Analog-to-Digital (A-to-D) board which was connected to a Macintosh Centris 650 computer. The thermocouple wires exit the instrumentation box through a pressure tube which was sealed around the wire. The wire was then fed into an Omega type DP116-TF2 transducer and the A-to-D board.

Positioning of the probe in two dimensions was accomplished by actuating two stepper motors. These motors were controlled by a controller which received commands from the Centris 650 computer.

Both the positioning and the acquisition of the pressure/temperature data were controlled with a software program called LabView located on the Centris 650 platform. A program was

written in LabView which automatically controls the stepper motors for probe positioning and saves all data input onto the computer's hard drive. The program allowed the probe to sample data 1000 times a second while the probe was held at each position for 5 seconds. Figure 2.18 shows a schematic of the data acquisition system for the mean flow measurements.

The thermocouple part of the combination probe was calibrated by adjusting the transducer's zero for 0 ^{o}C (32 ^{o}F) while the probe was placed in a bath of ice water. The span was adjusted while the probe was placed in a bath of boiling water. The pressure transducers were calibrated against a mercury manometer up to 6.88 kPa (1 psi) gauge. A similar electro-pneumatic transducer to that used for the in-flow probes was used to measure the plenum pressure.

A Note on the Variations in Total Temperature in the Flow-Duct Facility

For the no-flow acoustic tests, the change in total temperature in the flow-duct from the beginning of the test to the end, averaged 10 K for the long duration tests, which were approximately 5 hours. A 10 K increase in temperature corresponds to a 6 m/s increase in the speed of sound. It is believed that this temperature change resulted primarily through the heat transfer between the stagnant air in the duct and the walls of the duct. For the acoustic tests with flow in the duct (M = 0.30), the change in total temperature was on the order of 2 K.

2.4.2 Acoustic Measurements

Acoustic data were acquired with a total of eight microphones: two in-duct microphones for planar measurements, four flush wall-mounted microphones, one in-duct microphone for axial centerline measurements, and one microphone outside the duct for reference. The microphone signals were sent to an HP 3667A Signal Processor where real time FFT's were performed on the time signals. In addition, the microphone signals were also recorded on a 14-track TEAC analog tape machine for post processing. The HP analyzer was also fed the electronic signal used for exciting the acoustic drivers located just downstream of the plenum in the flow-duct. This provided a relative phase along with an amplitude of the acoustic pressure. It allowed for cross-correlation computations between the speaker input and the microphones measuring acoustic signals in the duct. This technique is critical to the analysis of signals which contain both hydrodynamic and acoustic pressures and will be discussed further in section 3.0. Figure 2.19 shows a schematic of the acoustic data acquisition system.

The acoustic measurements made in the duct cross-planes were accomplished by using a 0.64-cm (0.25-in) Bruel and Kjaer (B&K) type 4136 microphone which has a probe-tube attached to the diaphragm of the microphone. Figure 2.20 shows a typical in-duct, in-flow microphone probe. The probe-tube tapers from a 0.64-cm (0.25-in) outer diameter to a 0.318-cm (0.125-in) outer diameter before turning 90 degrees from the diaphragm axis. A bulleted nose cone (B&K type UA 0355) is attached to the tip of the probe end. In order to minimize flow blockage by the probe, a recently developed small diameter B&K type 2633 preamplifier was used. This preamplifer has an outer diameter of 0.64 cm (0.25 in).

Calibration of this microphone probe is discussed in section 3.0. A B&K 4136 0.64-cm (0.25-in) microphone with a bulleted nose cone (B&K type UA 0385) attachment was used to acquire acoustic data along the axial centerline of the duct. Again, the nose cone allowed for the in-flow acoustic measurements. Figure 2.16 shows a photograph of this microphone fitted with a nose cone and attached to its stabilizing boom.

Flush wall-mounted microphones were placed upstream and downstream of the liner section, in the center of the top and bottom walls. These were B&K type 4133 1.27-cm (0.50-in) microphones. A special mounting device was fabricated to allow for microphones with protection grids to be flush with the bottom and top walls of the duct and also to prevent any air leakage around the microphone. Figure 2.21 shows a photograph of a typical microphone with mounting device. The flush wall-mounted ports were designed with the flexibility for allowing for a water-cooled mounting design to be used in the future.

Finally, an additional B&K 4133 microphone was placed outside of the exhaust section of the flow-duct. This microphone can be located by the duct coordinates of z = -20.3 cm (-8 in), y = -38.1 cm (-15 in) at a distance of 30.5 cm (12 in) downstream of the exhaust duct exit.

2.5 NORMAL INCIDENT ACOUSTIC CHARACTERISTICS OF SOUND ABSORBING TEST LINER

Some of the acoustic results presented in this report have been acquired with a liner present in the flow-duct. This liner was of the locally-reacting type and was made from a ceramic material. The material, consisting of a tubular structure, was provided by NASA LaRC. This material is referred to as CT73 ceramic liner by NASA LaRC personnel and will

be referred to as CT73 liner in this report also. Its general acoustic properties were examined in a normal incident impedance tube before being tested in a flow-duct environment. Furthermore, the sample tested in the impedance tube was used to check the effectiveness of the backing used in the flow-duct testing. Thus, the frequency response of the normal incident absorption was determined for CT73 liner.

The impedance tube used for these tests was a B&K 4206 Two-Microphone Impedance Tube. This impedance tube utilizes the two-microphone method of determining material impedance (see Ref. Chung & Blaser, Ref. 2.4). The B&K 4206 impedance tube provides impedance data for a range of frequencies simultaneously through broadband sound generated by an acoustic driver located at one end of the impedance tube. This feature allows relatively quick determination of input impedance of liner materials compared to a standing wave impedance tube which acquires data at one frequency at a time. A frequency range of 50 Hz to 6400 Hz is possible by configuring the impedance tube with two measurement tube diameters.

Since the impedance tube relies on plane wave impingement of sound onto the test sample, the tube diameter is critical to the frequency range of interest. The B&K 4206 impedance tube is provided with 10.0-cm (3.94 in.) and 2.9-cm (1.14 in.) diameter tube sections. This ensures plane wave propagation from 50 Hz to 1600 Hz with the 10.0 cm diameter tube and from 500 Hz to 6400 Hz with the 2.9 cm diameter tube. More details of the B&K 4206 impedance tube are provided in volume I of this report. For the present impedance tests, a 2.9 cm-diameter test sample of CT73 was used.

It was desired that the CT73 liner have a rigid wall backing when installed in the liner housing. Since the material was made up of fine tubular cells, it was also desired that there be no "cross-talk" between individual cells. The rigid backing was achieved by using a 0.159mm (0.0625-in.) thick rubber gasket material with aluminum tape on one side and a 1.27 cm (0.5 in.) thick steel plate on the other. The metal tape side rested on the back side of the CT73 (see Figure 2.22). It was felt that this would provide a sealed, rigid-walled backing for the liner.

The effect of the rubber backing and metal tape was also examined in the aforementioned impedance tube. The impedance tube sample was approximately 8.89 cm (3.5 inches) thick, which corresponded to the tested flow-duct liner thickness. Figure 2.23 shows the absorption

coefficient spectra of CT73 and the relative effect of the type of backing. Figure 2.24 shows the normalized impedance components of the liner for the same backing conditions. It is evident that the rubber backing with the metal tape has little or no effect on the liners normal incident impedance, thus this backing can be used with confidence in the flow-duct testing.

3.0 DEVELOPMENT OF A TEST METHODOLOGY TO EVALUATE LINER PERFORMANCE

3.1 INTRODUCTION

The flow-duct described in section 2.0 has many unique features. Its main function is centered around the measurement of the acoustic field and the associated flow field in a duct with an acoustic liner present. These measurements require an experimental technique that allows for the separation of the acoustic fluctuations from the total measured fluctuations, which under some flow conditions may be buried within the hydrodynamic fluctuations associated with the flow in the duct. In some cases, if a noisy jet is present, the jet noise may propagate upstream and contaminate known acoustic signals generated by the upstream acoustic driver. In general, as the mean flow speed increases, the associated "flow noise" increases. This problem can typically be overcome by maintaining a reasonable signal-to-noise ratio which can be accomplished to a limit by increasing the amplitude of the acoustic source. In some cases, this may be impractical and may damage the drivers. There exist, however, signal processing methods that allow eduction of the low level acoustic signals buried in the flow noise. One such method relies on the cross-correlation of the microphone signals and the electronic signal that excites the acoustic drivers. This experimental method will be discussed in more detail in the following Section 3.4.3.

Measuring acoustic fluctuations in a mean flow environment led to the development of a probe microphone which could be immersed in a flow with minimal disturbance to the flow. A basic description of the probe microphone is provided in section 2.4. The concept of the probe microphone is well documented and has been used by many researchers (Neise, Ref. 3.1). In general, the probe microphone consists of a tube with an appropriate opening by which acoustic signals can be transmitted to a remote microphone diaphragm. It is necessary to calibrate probe microphones to account for the effect that the tube has on the acoustic signal before it reaches the diaphragm. This is a critical procedure if the absolute complex acoustic pressures are desired. The same probe microphone was used for cases in which no mean flow was present. The calibration procedure for the probe microphone used in the present study will be discussed in the following Section 3.4.

Section 3.3 will also discuss typical in-duct measurements that were made to quantify the mean flow as well as the acoustic field.

3.2 TEST FACILITY AND EXPERIMENTAL SET-UP

Details of the rectangular flow-duct facility developed for the present program were provided in section 2.0. In the interest of clarity, a short summary of the test setup used to develop a test methodology to evaluate liner performance appears below. These tests were mostly carried out in GTRI's Hot Jet Flow Facility. The flow-duct configuration was set-up for downstream acoustic propagation, i.e., the acoustic liner section was placed downstream of both the acoustic source and the air plenum. The leading edge of the liner section was located approximately 78.7 cm (31 inches) downstream of the acoustic drivers. An instrumentation section, which can measure flow and acoustic properties in two-dimensional duct cross-planes, was located just upstream of the liner section. Likewise, a similar instrumentation section was located just downstream of the liner section. Figure 3.1 shows a schematic of the flow-duct. The left side (looking upstream) of the instrumentation box sections were fitted with acoustic probes, while the right side of the instrumentation sections were equipped with combination pitot-static/thermocouple probes. Both of these probes are described in detail in section 2.0 along with the pertinent information regarding data acquisition and instrumentation.

3.3 TYPICAL IN-DUCT MEAN FLOW MEASUREMENTS

The mean flow parameters in the rectangular duct were measured by a combination pitot-static/thermocouple probe which traversed two planes perpendicular to the x-axis of the duct. In this way, mean pressure, velocity, and temperature data were obtained to accompany acoustic data taken in the same plane. One measurement plane was located approximately 19.05 cm (7.5 inches) upstream of the leading edge of the acoustic liner while the other plane was located approximately 11.43 cm (4.5 inches) downstream of the trailing edge of the acoustic liner. A more detailed description of the probe's data acquisition system was provided in section 2.4. Flow data can be acquired at any prescribed point in the measurement plane. Typically a grid of points was used which covered most of the duct cross sectional area. Figure 3.2 shows a typical grid of measurement locations. Data presented in this section utilizes this typical grid.

Figures 3.3 and 3.4 show typical mean flow results at a given plenum pressure. In this case, an acoustic liner was installed on the top wall of the liner housing section. A perforated metal face sheet was used to separate the liner from the grazing flow. The face sheet was provided to test other bulk liners on future dates. It also helped maintain a constant duct flow area. The Mach number profiles (Figure 3.3) show results typical of Fanno line flow, where the effect of friction increases the centerline Mach number (and velocity) as a function of duct axial position. The non-dimensional velocity profiles (Figure 3.4) suggest a turbulent, fully developed flow (i.e., the profiles fit a curve consistent with a power law distribution; see Schlicting, Ref. 3.2) for the upstream plane as well as the downstream plane. Furthermore, note that the boundary layer near the top wall, which had the liner, at the downstream location shows an increased velocity defect compared to the same upstream region. The major axis profiles do not show this feature as the liner was installed only along one of the larger sides of the duct. The region of velocity defect corresponds to an area just downstream of the lined section of the duct.

3.4 CALIBRATION OF PROBE MICROPHONES

The probe microphone used in the present study (described in section 2.4) modifies the acoustic signal which ultimately reaches the microphone diaphragm. This means that if absolute values of sound pressure level (SPL) and phase are desired, a calibration must be performed which corrects the probe microphone measurement to a "true" value. This section will describe the methodology that was used to calibrate the particular probe microphone used in this study. In addition, calibration results will be presented for cases with and without the mean flow. The calibration methods employed in this report were developed under an existing NASA Grant to GTRI (NAG1-1734) which is, in part, tasked with developing new techniques for measuring acoustic signals in mean flow environments.

3.4.1 Methodology

The objective of the probe microphone calibration is to produce a frequency response of the probe's transfer function, i.e., for a given frequency, how should the amplitude and phase of the acoustic signal be adjusted to render "true" levels. The methodology consisted of first measuring a known acoustic signal with a conventional microphone (e.g., a B&K 4136 microphone). The probe microphone was then placed in the same physical location as the

conventional microphone to measure the same acoustic signal. Finally, by computing the difference in these two responses, the "correction" or transfer function which relates the response of the probe microphone to the "true" response was obtained. The phase corrections were also obtained using this procedure. If a broadband acoustic signal is used, the probe corrections can be made as a function of frequency. Thus, the calibration procedure produces a curve in the frequency domain from which a SPL or phase value can be added to or subtracted from a measurement. A reference microphone at a fixed location is used to account for any variations in the acoustic signal from day to day. Calibrations were performed with and without a mean flow present. These results are discussed below.

3.4.2 Results With No Mean Flow

Initial calibrations of the probe microphones took place in one of GTRI's anechoic chambers. A portable stereo system was placed in the anechoic chamber approximately 1 m (3.28 ft) from the microphone positions. A white-noise electronic signal was fed to acoustic drivers to provide a broad range of frequencies. The reference microphone was a B&K 4136 microphone. The "true" microphone was another B&K 4136 microphone. The effect of the probe microphone was determined by replacing the standard grid on the microphone diaphragm with the probe tube to be calibrated. Two probe microphones were tested in this way: probes P1 and P2 which corresponded to the probe microphones that were used in the flow-duct facility at the upstream and downstream locations, respectively.

In addition, a calibration was made in the flow-duct facility itself. This was done by placing the axial centerline microphone (a B&K 4136 equipped with a nose cone) in the center of the duct at a given location. The upstream drivers were fed a broadband signal and the sound pressure level was recorded. This was considered to be the "true" microphone measurement. (Note: microphones used in this project were brand new and were used for the first time in this study.) Then the probe microphone, installed in the instrumentation box, was moved to the same centerline position to measure the same acoustic signal. A flush wall-mounted microphone was used in each measurement as the reference microphone.

Figure 3.5 shows a comparison of the standard microphone response with the response of a probe microphone. Note that the probe increases the acoustic signal significantly below 500 Hz and above 5 kHz. Figure 3.6 shows the resulting transfer function of the anechoic chamber

calibration and compares it with the calibration performed in the flow duct. The two calibrations are in good agreement until approximately 2 kHz. Although there is not as good an agreement above 2.2 kHz, the general shape and character of the curves are similar.

Experiments to determine the performance of a liner material were conducted using acoustic tones of selected frequencies. Specifically, a Sinc waveform was generated from a Hewlett-Packard 3311A function generator. The signal was set to produce a series of tones at multiples of 500 Hz. Figure 3.7 shows the typical Fourier transform of the Sinc wavefunction from the function generator. Calibration of a probe microphone using this signal was performed. Figure 3.8 shows a comparison with the in-duct white noise calibration results. In general, below 3 kHz there is very good agreement between the white noise calibration and the Sinc wave calibration. Generally, good agreement was obtained above 3 kHz also, except for a significant discrepancy at 4.5 kHz.

There appears to be good agreement at low frequencies between the anechoic chamber and the flow-duct facility probe microphone calibrations. Furthermore, calibration with a Sinc wavefunction input agrees well with a white noise input at the lower frequencies and reasonably well at the higher frequencies. It is believed that the discrepancies above 3 kHz are due to higher order modes being present in the flow-duct. The inability of positioning the probe microphone and the reference microphone exactly at the same location in the duct could be responsible for this discrepancy.

The phase calibration of the probe microphone is accomplished by taking the difference between the phase of the probe microphone and the phase of a conventional microphone. (The phase was obtained by measuring the cross spectrum between the electronic input signal to the acoustic drivers and the microphone signals.) The phase in this case is, thus, relative to the input electronic signal. Figure 3.9 shows a typical phase calibration curve for both a white-noise input and a Sinc wave function input in the flow-duct facility. Phase measurements made in the flow-duct facility and those made in the anechoic chamber showed discrepancies at the same frequencies for which the sound pressure levels displayed discrepancies.

3.4.3 Results With Mean Flow

Before discussing the calibration of the probe microphone in the presence of a mean flow, it will be instructive to describe the method that was used to educe the acoustic signals (generated from the drivers) from the total signal reaching the microphone diaphragm. Figure 3.10 shows the overall spectrum from a standard microphone with a nose cone placed in the flow along with the educed spectrum. Here, a Sinc wave is fed into the acoustic drivers upstream of the microphone while a mean flow of $M_d = 0.3$ is present. The methodology used to reject the flow noise is described below.

Methodology for Rejecting Flow Noise from In-flow Acoustic Measurements

In general, the flow over a microphone equipped with a nose cone produces the so-called self-induced noise. Furthermore, any noise in the duct that is produced aerodynamically will be picked up by the probe microphone. One way to measure the acoustic signal that is contaminated with the self-induced and other obtrusive noise is to cross-correlate the input electronic signal fed to the acoustic drivers with the signal from a microphone, either in the flow or flush mounted on the duct wall. In this way, the cross-power spectrum can be obtained which should contain only the information that is *coherent* between the driver signal and the microphone. Figure 3.11 shows schematically how the signal path is interpreted along with a nomenclature of relevant terms.

Let x(t) be the electronic signal fed to the acoustic driver, and u(t) be the true acoustic signal that is contaminated with flow noise n(t). Let y(t) be the total signal measured by the microphone. The autospectra corresponding to signals u(t), x(t), y(t), and n(t) are denoted by $G_{uu}(f)$, $G_{xx}(f)$, $G_{yy}(f)$ and $G_{nn}(f)$, respectively. Likewise, the cross-spectra between x(t) and y(t), x(t) and u(t), y(t) and n(t), are defined as $G_{yx}(f)$, $G_{ux}(f)$, and $G_{nx}(f)$, respectively. For the sake of clarity the frequency term will not be used in the following text. Thus $G_{yx}(f)$ will be denoted by G_{yx}, etc. An overbar denotes a time average.

The objective is to determine G_{uu}, which is the autospectrum associated with the signal reaching the microphone. As shown below, G_{uu} can be *educed* by obtaining G_{yx} if G_{xx} is known.

$$G_{yx} = (S_u + S_n)S_x^* = G_{ux} + G_{nx} \quad (1)$$

$$\overline{G}_{yx} = \overline{G}_{ux} + \overline{G}_{nx} = \overline{G}_{ux} \quad (2)$$

Since x(t) and n(t) are unrelated, after many averages, $\overline{G_{nx}} = 0$

now $$H(f) = \frac{S_u(f)}{S_x(f)} = \frac{S_u S_x^*}{S_x S_x^*} = \frac{G_{ux}}{G_{xx}} \quad (3)$$

Also $$H(f) = \frac{S_u(f)}{S_x(f)} = \frac{S_u S_u^*}{S_x S_u^*} = \frac{G_{uu}}{G_{xu}} \quad (4)$$

From (3) and (4):

$$\frac{\overline{G}_{ux}}{\overline{G}_{xx}} = \frac{\overline{G}_{uu}}{\overline{G}_{xu}} \quad (5)$$

From (2) and (5):

$$\therefore \overline{G}_{yx}^2 = \overline{G}_{xx}\,\overline{G}_{uu} \quad (6)$$

From (2) and (6):

$$\overline{G}_{xy}^2 = \overline{G}_{xx}\,\overline{G}_{uu} \quad (7)$$

$$\overline{G_{xy}} = \left(\overline{G}_{xx}\,\overline{G}_{uu}\right)^{1/2} \quad (8)$$

$$\therefore 10\log\left[\overline{G}_{xy}\right] = \frac{1}{2}\left(10\log\overline{G}_{xx} + 10\log\overline{G}_{uu}\right) \quad (9)$$

$$\therefore \mathrm{SPL}_{uu} = 10\log\overline{G}_{uu} = 20\log\left[\overline{G}_{xy}\right] - 10\log\overline{G}_{xx} \quad (10)$$

Thus the sound pressure levels associated with the electronic signal, i.e., SPL_{uu}, can be separated from the contaminated signal, i.e., $10\log G_{yy}$, by using equation 10.

An example of the power of this eduction technique is seen in Figure 3.12 which shows how even if the acoustic signal (G_{uu}) is buried under the overall signal ($G_{uu} + G_{nn}$), one can obtain the input signal to the microphone. For example, tones at 4.5, 5, and 5.5 kHz were completely buried in the flow noise and have been educed. It should be noted that the input acoustic signal is a Sinc wave with a 500 Hz fundamental tone plus a series of tones every 500 Hz . The data in between these frequencies are unimportant in this case.

Mean Flow Microphone Calibration Results

The method of calibration for a probe microphone in the flow-duct with a mean flow present is the same as when no mean flow is present except that the cross-spectral technique discussed above was employed for determining the amplitudes. Typical output power spectra ($G_{uu} + G_{nn}$) as measured by in-flow microphones in the flow-duct are shown in Figure 3.13. The mean flow was approximately 300 ft/s ($M_d = 0.3$) and a 500 Hz Sinc wave was fed into the acoustic driver which was identical to that of the no flow case (see Figure 3.7). Typical cross power spectra are shown in Figure 3.14. Note that the correlated spectrum is very similar to the input power spectrum. Using the method outlined above, an educed autopower spectrum for a probe microphone is computed and compared with the output power in Figure 3.15. Using the educed power spectra, a probe microphone calibration spectrum is computed. Figure 3.16 shows the calibration transfer function. The no flow case is also shown for comparison. Below 3 kHz, there appears to be good agreement with the no flow calibration of the probe microphone. Above 3 kHz there are some differences and may be related to the change in the higher-order mode cut on frequencies due to flow. The repeatability of these differences could not be confirmed in the present program and is a topic of on-going investigation under NASA Grant NAG1-1734.

Concluding Remarks

In summary, a method for calibrating a probe microphone has been established. It appears that the calibration method can be applied to a probe microphone in a flow-duct up to certain frequencies with confidence. This upper limit on the frequency response is believed to be the result of higher order duct modes propagating in the duct. This situation is further complicated by the presence of degenerate modes at the higher frequencies as discussed below and in

Appendix A. For the flow-duct geometry presented here, higher order modes seem to be generated above 3 kHz. This will be discussed further in the next section.

3.5 TYPICAL IN-DUCT ACOUSTIC MEASUREMENTS

Based upon the calibration of microphones performed in the duct as described above and the in-duct data obtained in various planes to be described in this section, it appears that the sound in the plane-wave regime is well behaved within the GTRI flow duct and the results are repeatable from one run to another. At the higher frequencies corresponding to the higher-order modes, the SPLs within a duct are not repeatable from run to run. Much of this discrepancy may be related to the existence of degenerate modes (i.e., when two or more modes have the same frequency) in the rectangular duct. A detailed explanation of how degenerate modes can be formed and produce different nodal lines within a duct is provided in Appendix A.

Typical results of measurements taken in the flow-duct facility will now be discussed for the case with no mean flow present. It will be instructive to compute the various cut-on frequencies associated with the duct resonant modes to help interpret the results from the in-duct measurements. Furthermore, it can be assumed that the flow-duct with the acoustic drivers located upstream of the rectangular duct section will act like an open-open duct. The duct eigenfrequencies associated with the transverse modes (those in the y-z plane) for the present flow-duct dimensions were computed for two nominal temperatures, 10 °C (50 °F) and 21.4 °C (70 °F). In addition, the longitudinal eigenfrequencies were computed. Figure 3.17 shows graphically these eigenfrequencies as a function of mode orders. The frequencies as a function of mode are shown in Table 3.1.

What is important to note, however, is that near frequencies of 2.85, 3.6, 4.3, and 5.3 kHz, a number of modes have the same frequencies. This is where the modes become "degenerate" and it is near these frequencies that the calibrations were different from day to day. (See Appendix A for further description of degenerate modes.) Depending upon the ambient temperature at the time of testing, the sound amplitudes may not be repeatable at the same location since the frequencies are a function of the ambient speed of sound (and hence temperature). The frequencies may thus be the same for one day and not the other. This is

likely to change the noise amplitude at frequencies near the degenerate mode frequencies. The same situation will arrive on superimposing flow to the acoustic field. At present this appears to be the only explanation for differences in calibrations at higher frequencies.

Duct Resonant Frequencies

Open-Open Duct Conditions

T = 283 K (50 ^{o}F)

Dimensions:
L= 109.2 cm (43.0 in.)
W = 11.9 cm (4.69 in.)
H = 5.08 cm (2.0 in.)

Modal Order	(l	w	h)	Freq (Hz)
1	(1	0	0)	154
2	(2	0	0)	309
3	(3	0	0)	463
4	(4	0	0)	618
5	(5	0	0)	772
6	(6	0	0)	926
7	(7	0	0)	1081
8	(8	0	0)	1235
9	(9	0	0)	1390
10	(0	0	1)	1416
11	(10	0	0)	1544
12	(11	0	0)	1698
13	(12	0	0)	1853
14	(13	0	0)	2007
15	(14	0	0)	2162
16	(16	0	0)	2470
17	(17	0	0)	2625
18	(18	0	0)	2779
19	(0	0	2)	2831
20	(1	0	2)	2835
21	(2	0	2)	2848
22	(3	0	2)	2869
23	(19	0	0)	2934
24	(20	0	0)	3088
25	(21	0	0)	3242
26	(0	1	0)	3320

Table 3.1 Resonant frequencies for rectangular duct used in the present study.

Modal Order	(l	w	h)	Freq (Hz)
27	(22	0	0)	3397
28	(23	0	0)	3551
29	(1	1	1)	3612
30	(2	1	1)	3622
31	(24	0	0)	3706
32	(25	0	0)	3860
33	(26	0	0)	4014
34	(27	0	0)	4169
35	(0	0	3)	4247
36	(1	0	3)	4250
37	(2	0	3)	4258
38	(28	0	0)	4323
39	(1	1	2)	4366
40	(2	1	2)	4374
41	(29	0	0)	4478
42	(30	0	0)	4632
43	(31	0	0)	4786
44	(32	0	0)	4941
45	(33	0	0)	5095
46	(34	0	0)	5250
47	(1	1	3)	5393
48	(2	1	3)	5399
49	(35	0	0)	5404
50	(0	0	4)	5662
51	(37	0	0)	5713
52	(38	0	0)	5867
53	(39	0	0)	6022

Table 3.1 (Cont.) Resonant frequencies for rectangular duct used in the present study.

3.5.1 Flush-Mounted Wall Measurements

As noted in section 2.0, microphones were mounted flush on the top and bottom walls, midway of the long side of the flow-duct just upstream and downstream of the leading edge of the liner region. These opposing microphones can provide additional acoustic information inside of the duct without having to examine a large number of measurement points. For instance, one way to identify the presence of higher order modes propagating in the duct is to compare the sound pressure levels and phase between two opposing pairs of wall mounted microphones. If the opposing microphones do not provide the same sound pressure levels then, at least in one dimension (the z direction), a higher order mode is likely to be present. Figure 3.18 shows the differences in SPL of the opposing microphones for the rigid wall duct case with no mean flow and the acoustic drivers generating a Sinc waveform. Note that starting at 3 kHz, the levels of the two microphones start to diverge, indicating the presence of higher order modes. Figure 3.19 shows the same results for the lined duct case. The downstream microphone pair seem to be altered significantly due to the presence of the liner as compared to the same pair shown in Figure 3.18.

3.5.2 Axial Centerline Measurements

Axial centerline acoustic data were measured with a quarter-inch microphone fitted with a nose cone. Data were taken every 0.51 cm (0.2 inches) from the leading edge of the liner region to the trailing edge. Typical sound pressure levels as a function of axial distance are shown in Figure 3.20 for 1 kHz with and without a liner present. Note that the rigid wall case contains data some distance past the trailing edge of the liner region. Figure 3.21 shows similar data for 3 kHz. Figure 3.22 shows a typical phase comparison between the rigid-wall case and the lined-wall case at a frequency of 3.5 kHz.

3.5.3 Planar Measurements

Data were acquired with probe microphones at axial planes which are located upstream and downstream of the liner leading edge and trailing edge respectively. The extent of the measurement probe's travel relative to the duct walls is shown in Figure 3.23 along with a grid of measurement locations used. The typical time taken to acquire 64 averages of the acoustic signals of eight microphones at a given measurement point was approximately 30 seconds.

Including time to record the signals on the tape and move the probe into the next position, the data acquisition time at each location in a given plane was approximately 80 seconds. This translates into over 4.5 hours of continuous data acquisition for each plane. Time to complete the planar measurements was cut in half by measuring both the upstream and downstream planes simultaneously with different probe microphones. Still, the data acquisition process was very labor intensive.

The plenum pressure was continuously monitored during the testing and was maintained within ±0.02 psig of the target plenum pressure. For the target duct Mach number of 0.3, this maintained a Mach number of 0.300± 0.005.

Figures 3.24 through 3.27 show selected uncorrected data from the planar measurements made with and without a liner in place. The sound pressure levels at 500 Hz (Figures 3.24 and 3.26) appear to be constant across the plane. This is consistent with plane wave propagation which should exist exclusively at this frequency for this duct geometry. Also note that the 3 kHz rigid wall data (Figure 3.25) indicate a pattern of nodes and anti-nodes across the long dimension of the duct. This seems to be consistent with the (0,2,0) mode. The presence of the liner appears to "smooth" out the reflection patterns downstream of the liner at 3 kHz (Figure 3.27).

4.0 LINED VERSUS UNLINED RECTANGULAR DUCT WITH NO MEAN FLOW

4.1 INTRODUCTION

The main objective of the present effort was to acquire benchmark experimental data in sufficient detail to enable validation of theoretical duct liner models. All of the data acquired will be provided to NASA Langley Research Center in electronic form. Selected results are presented here to highlight some of the features of the measured results and to direct the reader as to how best to use the massive amount of data saved in the electronic form.

This section presents the measured acoustic data for both the lined and the unlined duct for no-mean flow only. Similar data acquired with mean flow will be analyzed under an ongoing effort under NASA Grant NAS1-1734. The following set of acoustic data are presented in this section:

1. Calibration of various microphone probes used in this study.
2. Comparison of the noise distribution at selected frequencies along the duct axis spanning the duct liner length with and without the liner.
3. Distribution of the sound pressure levels in two planes upstream of the liner section and two planes downstream of the liner section **with** the liner both for the major axis and the minor axis.
4. Distribution of the sound pressure levels in two upstream planes and the two downstream planes **without** the liner both for the major axis and the minor axis.

Note that as in the rest of the report, the liner used here was the Ceramic Honeycomb liner CT73 provided by NASA Langley Research Center.

The following 12 frequencies were selected for presentation of the data here:

500, 1000, 1500, 2000, 2500, 3000, 3500, 4000, 4500, 5000, 5500, and 6000 Hz.

It is worthy of note that the first higher-order mode for the smaller dimension of the rectangular duct is cut on at a frequency of 3321 Hz at 50°F. The corresponding frequency for

the larger dimension is: 1416 Hz at 283K (50 F). These 12 frequencies will be referred to as the "display frequencies" in the text below.

4.2 SELECTED CENTERLINE RESULTS

Figure 4.1 compares the centerline distribution of the measured sound pressure levels with and without the liner at the 12 selected frequencies. Note that the SPLs presented in this figure was measured at different times with and without the liner. All attempts were made to maintain the same levels at the leading edge of the liner for two set of measurements; but minor variations are natural. For the rigid wall case (the open symbols in the figures), the results are very similar to what one would expect in a standing wave tube. Thus, peaks and valleys are obtained as a function of distance, with the number of peaks and valleys increasing with frequency. The data with the liner (the solid symbols in the figure) show that with increasing distance from the leading edge of the liner, the liner indeed absorbs sound. It is particularly noticeable near the troughs of the standing wave pattern measured in the rigid-walled duct. The liner also appears to smooth out the "peak and valley" effect that is so obvious in the rigid-walled duct data. The liner does not seem to be very effective at frequencies of 5000 Hz and higher .

4.3 A NOTE ON THE MICROPHONE PROBE NOTATION

Three separate probe microphones, designated as P3, P2M, and P4 were used in this program as follows:

Probe P3: This probe microphone was used in the upstream planes, X1 and X2, for both the lined and the unlined cases.

Probe P4: This probe microphone was used in the downstream planes, X3 and X4, only for the lined cases. This probe broke before it could be used for the unlined duct.

Probe P2M: This probe microphone was used in the downstream planes, X3 and X4, only for the unlined cases.

4.4 A NOTE ON THE MICROPHONE PROBE CALIBRATIONS

All attempts were made to make all probe microphones identical, but minor machining differences required each probe to be calibrated separately using the procedures outlined in Section 3. Unfortunately their calibrations were found to be different on different days at the frequencies corresponding to the higher order modes in the duct. Typical results of calibration of probes P3 and P4 for two different days, as performed in the lined duct, are shown in Figure 4.2. It is seen that in the plane wave region up to a frequency of about 2500 Hz, the calibrations for each probe remain within 3dB from one day to another. But at the higher frequencies, there is a significant discrepancy. Similar results are seen to hold for the calibrations performed with the unlined duct as shown in Figure 4.3 for Probes P3 and P2M. (Note that the reference microphone referred to as U_{ft} in Figures 4.2 and 4.3 was the upstream flush mounted microphone on the top side of the duct.)

In the presentation of the SPLs measured at various points in the four planes, applying appropriate corrections in the plane wave region should be reasonable but how best to apply the corrections at the higher frequency has not been resolved at the time of preparing this report. Of course, one recourse will be to draw a mean curve through the calibration curves presented in Figures 4.2 and 4.3. We felt it best not to apply any corrections to the data at this stage, since further studies are being conducted at present by the authors to determine the best way of calibrating probe microphones. Since the majority of the data acquired in this study is to be archived electronically, the uncorrected data will be provided along with the four calibrations shown above and the mean calibrations. Which calibration should be used will be left up to the discretion of the user.

As a matter of record it should be mentioned that the data for the unlined duct were acquired on different days for the X1 and the X3 planes. The data for planes X2 and X4 were acquired on yet another day but both planes were measured on the same day. Likewise, for the lined duct, the data in the planes X1 and X3 were acquired on the same day whereas the data for the X2 and X4 planes were acquired on two different days. Because of the labor-intensive nature of these experiments, there was no other choice but to obtain these data on different days.

4.5 SELECTED MODE SHAPES UPSTREAM AND DOWNSTREAM OF THE LINER SECTION

Figures 4.4 - 4.15 show the distribution of the sound pressure levels in two planes upstream of the liner section and two planes downstream of the liner section for both the major and the minor axis. The upper portion of each figure shows the SPL profile along the major axis whereas the lower portion shows the corresponding profiles along the minor axis. The open symbols represent the data for the upstream planes, marked X1 and X2 in the figures. Likewise, the solid symbols represent the data for the downstream planes, marked X3 and X4. In each figure, the x-axis shows the SPLs. It is important to point out that the data presented here are not corrected for the response of the probe microphone. However, since each data point on a given SPL profile was acquired with the same microphone probe these figures provide an accurate measure of the mode shapes. The SPL amplitudes up to a frequency of 2500 Hz, which is the plane wave region, was found to repeatable from day to day. The SPL amplitudes at the higher frequencies corresponding to the higher order modes were not so repeatable. Sometimes the values varied up to 5 dB from one day to another. This discrepancy appears to be related to the existence of degenerate modes at many of the higher frequency discrete tones for which data were acquired in this investigation. As explained earlier in Section 3, and described in Appendix A, degeneracy occurs when two or more wave patterns or modes with the same characteristic frequency exist. If present, these degenerate modes can occur simultaneously with arbitrary amplitude and phase. This leads to a variety of nodal lines which depend very strongly on the relative amplitudes of each degenerate mode.

Keeping the above remarks in mind, it is found that almost flat SPL profiles are seen up to a frequency of 2500 Hz at each of the measurement planes. This is the region of plane waves. At the higher frequencies, some very unusual profiles are obtained in the lined duct.

Similar results were obtained for the unlined duct and are included here for the sake of completeness in Figures 4.16 - 4.27.

4.6 SELECTED PHASE RESULTS

For each SPL profile or axial distribution measured within the duct, there exists a phase profile or distribution. These phase data will be documented electronically. Typical phase

results for the major and minor axis are presented in Figures 4.28 - 4.30 for the two upstream planes in the lined duct configuration at frequencies of 500 Hz, 1000 Hz, and 1500 Hz respectively. The constancy of phases along the major and the minor axis along with constant SPLs seen above indicate that the sound waves within the duct at these frequencies were indeed plane waves.

4.7 CONCLUDING REMARKS

The main goal of the present study was to acquire detailed acoustic and flow data with and without a liner in a duct so that available theoretical models of duct liners can be validated. We believe this is the first time ever that an extensive data base has been acquired for this purpose. The data consisting of the flow velocity, SPL and phase will be made available to NASA in an electronic form. Appropriate calibrations will also be provided.

5.0 OVERALL CONCLUSIONS

A very ambitious study was initiated to obtain detailed acoustic and flow data with and without a liner in a duct containing a mean flow so that available theoretical models of duct liners can be validated. A unique flow-duct facility equipped with a sound source, liner box, flush-walled microphones, traversable microphones and traversable pressure and temperature probes was built. A unique set of instrumentation boxes equipped with computer controlled traverses were designed and built that allowed measurements of Mach number, temperature, SPLs and phases in two planes upstream of a liner section and two planes downstream at a large number of measurement points. Each pair of planes provided acoustic pressure gradients for use in estimating the particle velocities. Specially-built microphone probes were employed to make measurements in the presence of the flow. A microphone traverse was also designed to measure the distribution of SPLs and phases from the beginning of the liner to its end along the duct axis. All measurements were made with the help of cross-correlation techniques to reject flow noise and/or other obtrusive noise, if any. The facility was designed for future use at temperatures as high as 1500° F. In order to validate 2-D models in the presence of mean flow, the flow duct was equipped with a device to modify boundary layer flow on the smaller sides of a rectangular duct to simulate 2-D flow.

A massive amount of data was acquired for use in validating duct liner models and will be provided to NASA in an electronic form.

It was found that the sound in the plane-wave regime is well behaved within the duct and the results are repeatable from one run to another. At the higher frequencies corresponding to the higher-order modes, the SPLs within a duct are not repeatable from run to run. In fact, when two or more modes have the same frequency (i.e., for the degenerate modes), the SPLs in the duct varied between 2 dB to 12 dB from run to run. This made the calibration of the microphone probes extremely difficult at the higher frequencies.

Most of the data presented in this report is for zero mean flow. Data with flow were also acquired but were not analyzed at the time of the preparation of this report. The flow data will be published separately in due course. The technique based upon cross-correlation measurements used to reject flow noise was found to work well in measurements made with flow.

6.0 REFERENCES

1.1. Munjal, M. L., "Acoustics of Ducts and Mufflers," John Wiley and Sons, 1987.

1.2. Chung, J. Y. and Blaser, D. A., " Transfer Function Method of Measuring In-duct Acoustic Properties. I. Theory; II. Experiments," J. Acous. Soc. Am. 68 (3), Sept. 1980.

1.3. Vaidya, P. G., and Dean, P. D., "State of the Art of Duct Acoustics," AIAA Paper 77-1279, 1977.

1.4. Watson, Willie, R., "A Mathematical Model for Simulating Noise Suppression of Lined Ejectors," NASA Technical Paper 3425, April 1994.

2.1. Watson, Willie, R., "A Mathematical Model for Simulating Noise Suppression of Lined Ejectors," NASA Technical Paper 3425, April 1994.

2.2. Englar, R. J., Schuster, David, and Ford, Douglas, "Experimental Evaluations of Unlimited Racing Hydroplanes Operating In and Out of Ground Effects," SAE Technical Paper 901869, Presented at the Aerospace Technology Conference and Exposition, Long Beach, California, Oct. 1 - 4 , 1990.

2.3. Schlichting, H., "Boundary Layer Theory," Second Edition, McGraw-Hill, New York, 1960

2.4. Chung, J. Y. and Blaser, D. A., "Transfer Function Method of Measuring In-duct Acoustic Properties. I. Theory; II. Experiments," J. Acous. Soc. Am. 68 (3), Sept. 1980.

3.1. Neise, W., "Theoretical and Experimental Investigation of Microphone Probes for In-duct Fan Sound Power Measurements," Journal of Sound and Vibration, 111(1), pp 153-165, 1986.

3.2. Schlichting, H., "Boundary Layer Theory," Second Edition, McGraw-Hill, New York, 1960

APPENDIX A

ON DEGENERACY OF MODES

The equation for the normal mode frequencies in an open-open rectangular duct are given by

$$f_{lwh} = \frac{a_0}{2}\sqrt{\left(\frac{l}{L}\right)^2 + \left(\frac{w}{W}\right)^2 + \left(\frac{h}{H}\right)^2}$$

l, w, h = 0, 1, 2, ...

where l, w, h are the mode numbers and a_0 is the speed of sound inside the duct. L, W, and H are the dimensions of the duct.

If l2, w2, and h2 are incommensurable (meaning that l2,/w2, etc., cannot be expressed as the ratios of two integers), the frequencies are all distinct. Otherwise there can exist two or more identical frequencies for different pairs of mode numbers, l, w, h. In such a case, the normal modes are said to be degenerate. If there exist no degeneracy, the mode shapes are well defined with predictable nodes in the duct. On the other hand, if there exists degeneracy, the nodal patterns in the duct are strongly dependent on the relative amplitudes and phases of each individual degenerate mode each of the same frequency.

A good example is to consider a square duct and consider only the modes in the transverse directions with dimensions W and H, with W = H. Here l =0, w = 2 and h = 1 give the same frequency as l = 0, h =1 and w = 2. Thus the (0, 2, 1) mode and the (0, 1, 2) modes are degenerate modes. In fact, any value of l will give a degenerate mode for a duct of a square cross-section.

The two degenerate modes shown in Figure A.1a and A.1b with equal amplitudes and phases indicated by the shading combine to form a pattern with a diagonal nodal line shown in

Figure A.1c. The two modes can, however, occur with arbitrary amplitudes and phase. Thus if the amplitudes are unequal, patterns like Figure A.1d can be produced.

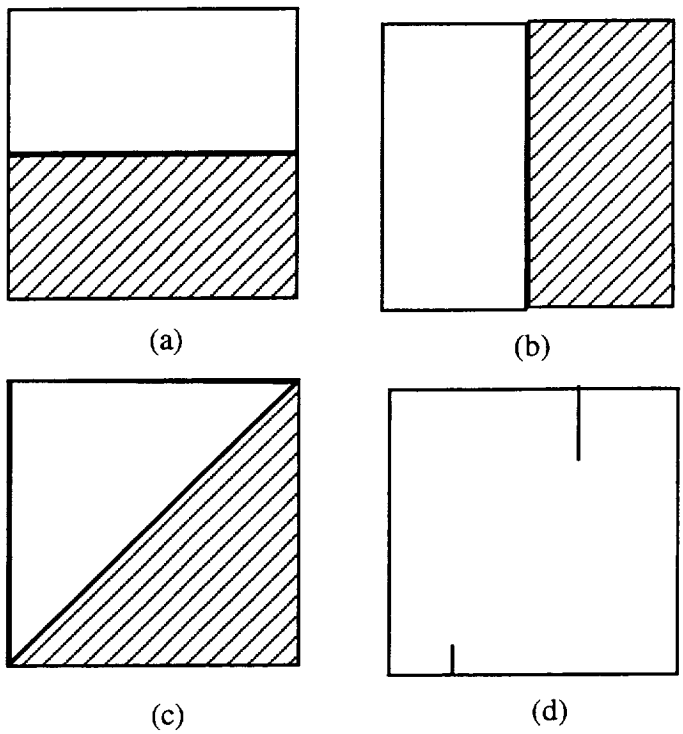

Figure A.1. Degenerate modes in a square duct.

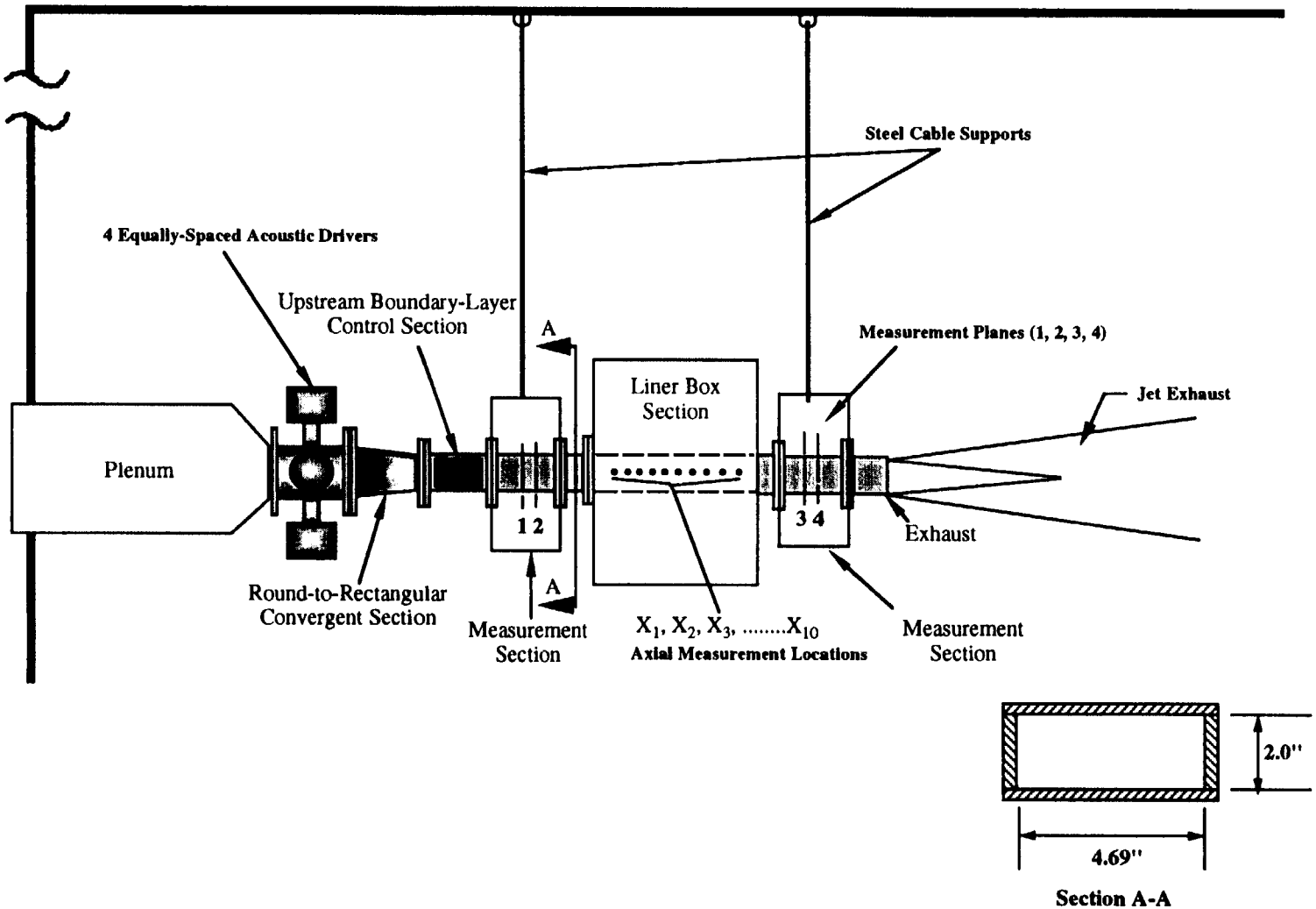

Figure 2.1 Schematic of liner performance facility.

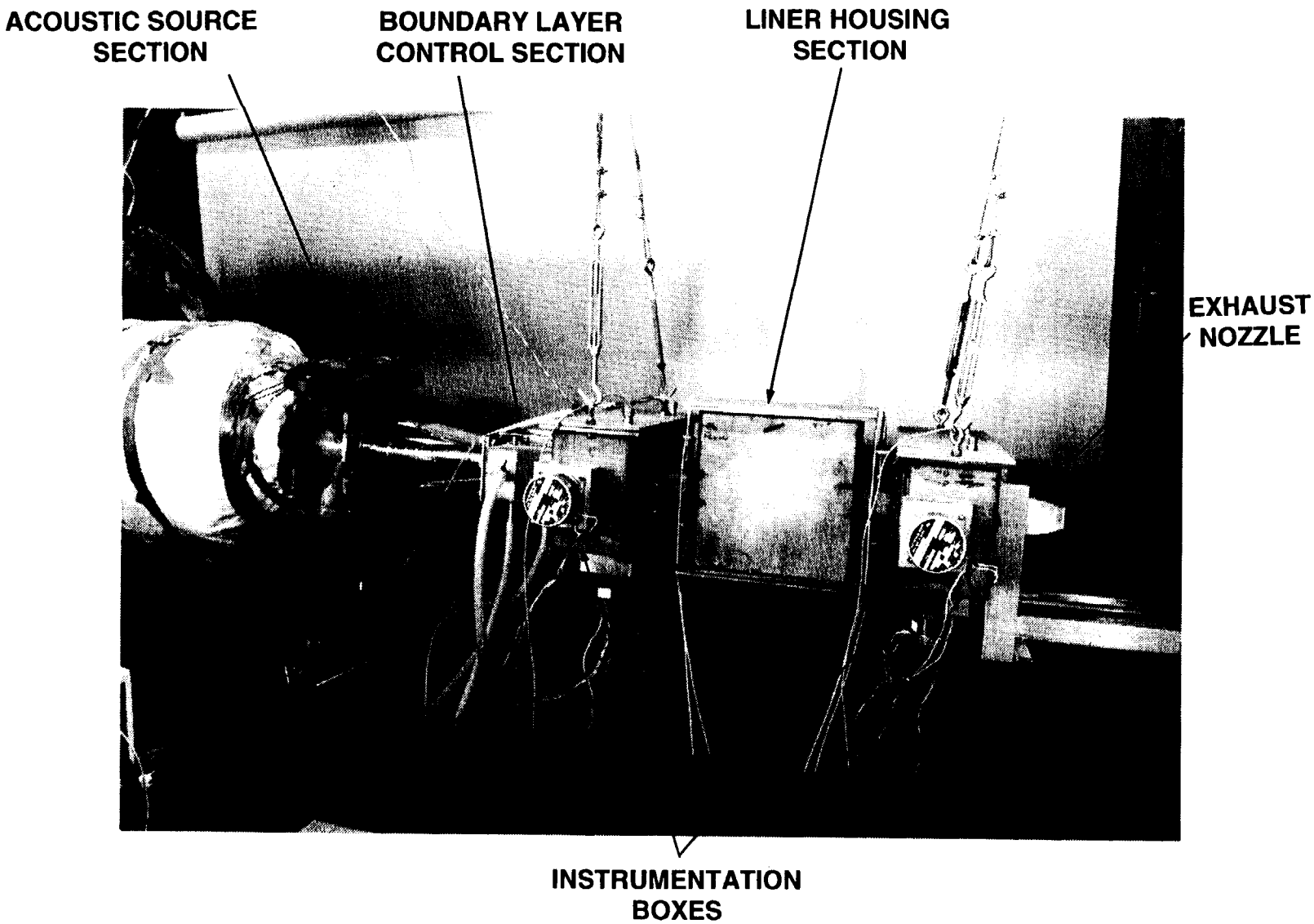

Figure 2.2 Actual liner performance facility.

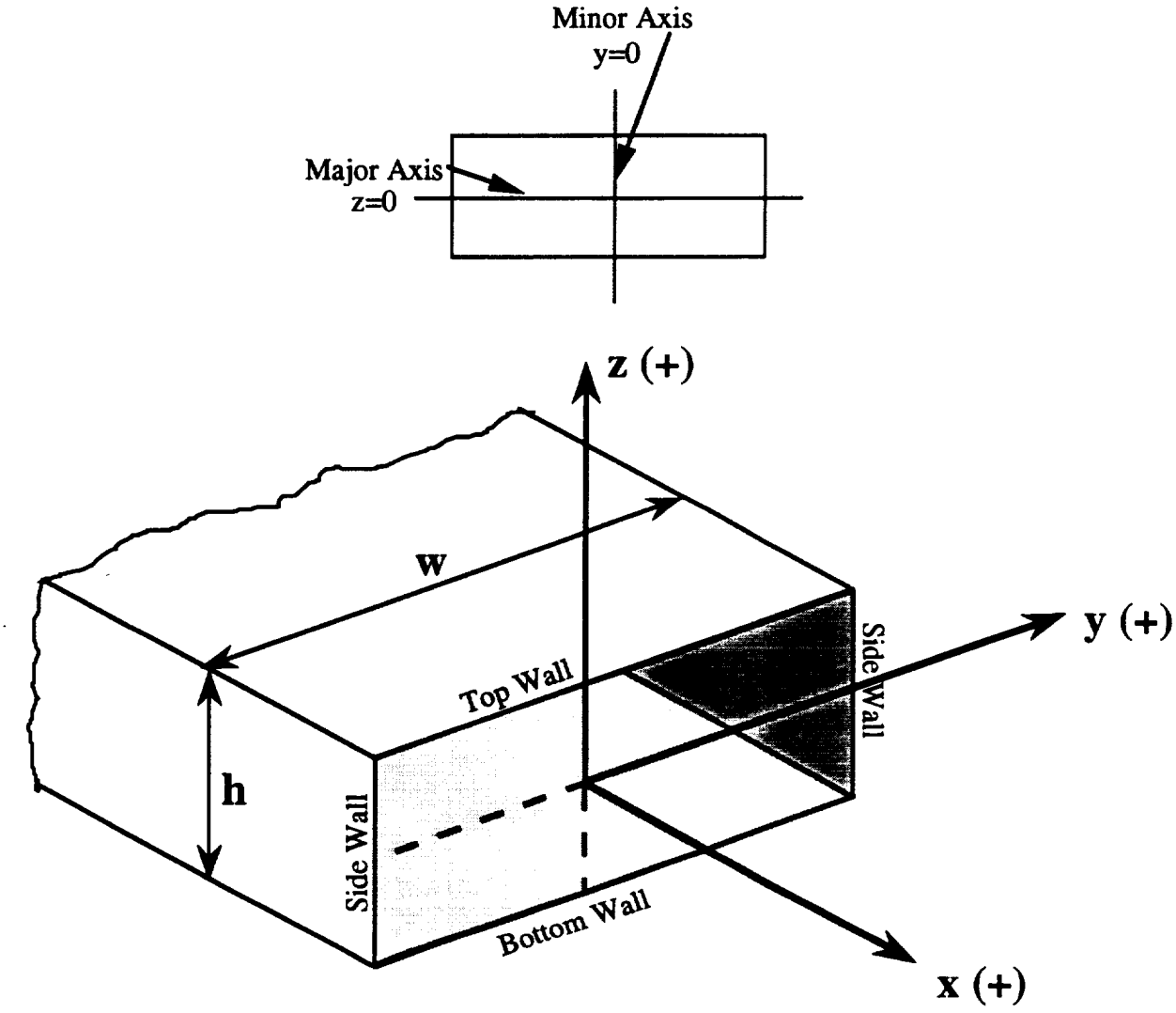

w = 11.9 cm (4.69 inches)

h = 5.08 cm (2.00 inches)

Figure 2.3 Flow-duct coordinate system and terminology.

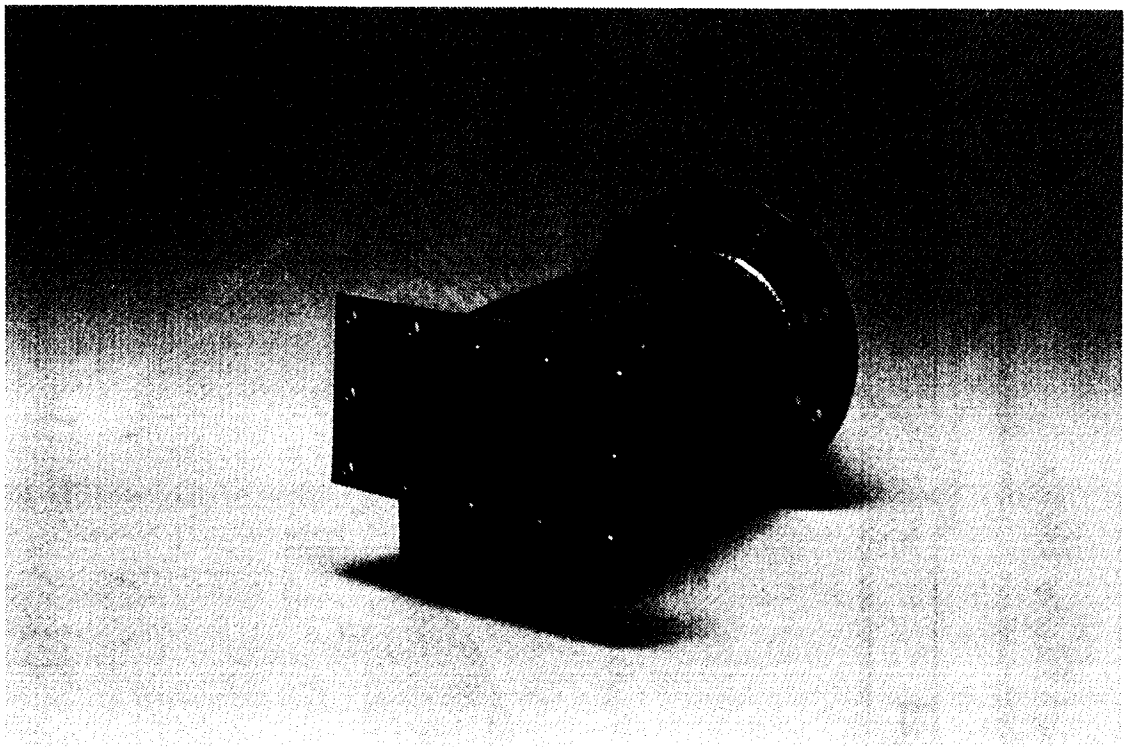

Figure 2.4 Round-to-rectangular transition duct.

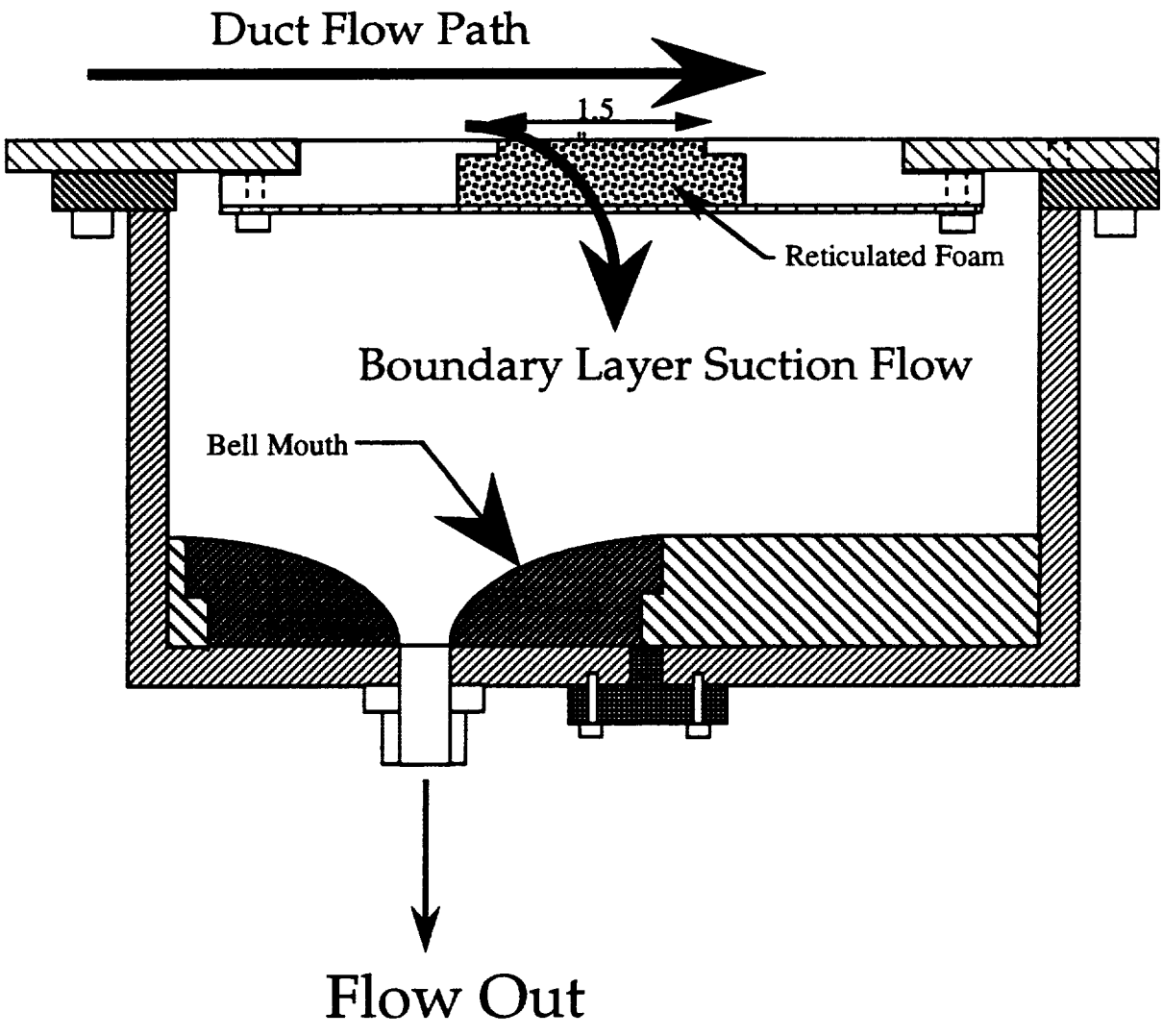

Figure 2.5 Schematic of boundary layer suction system.

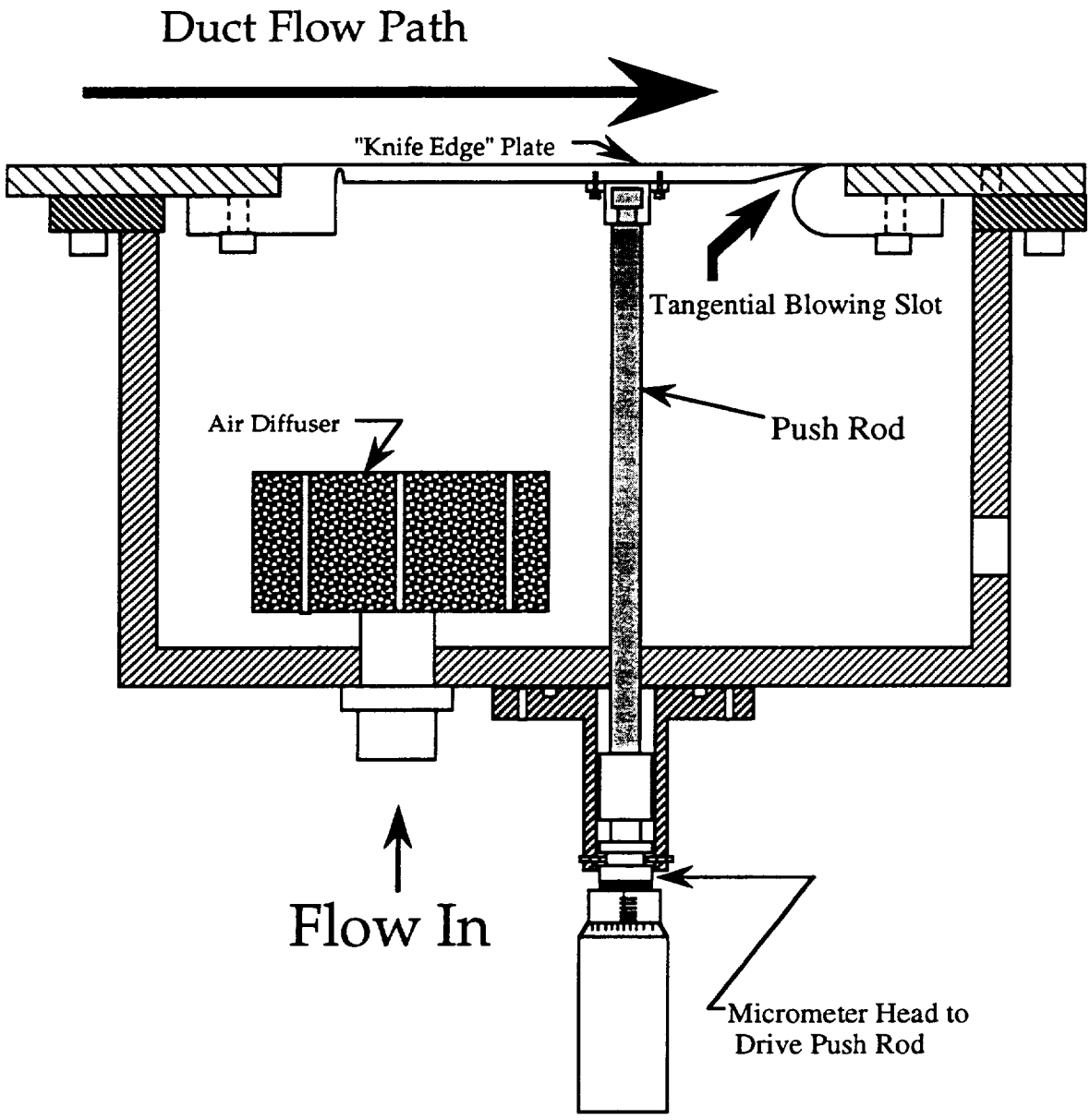

Figure 2.6 Schematic of tangential blowing system.

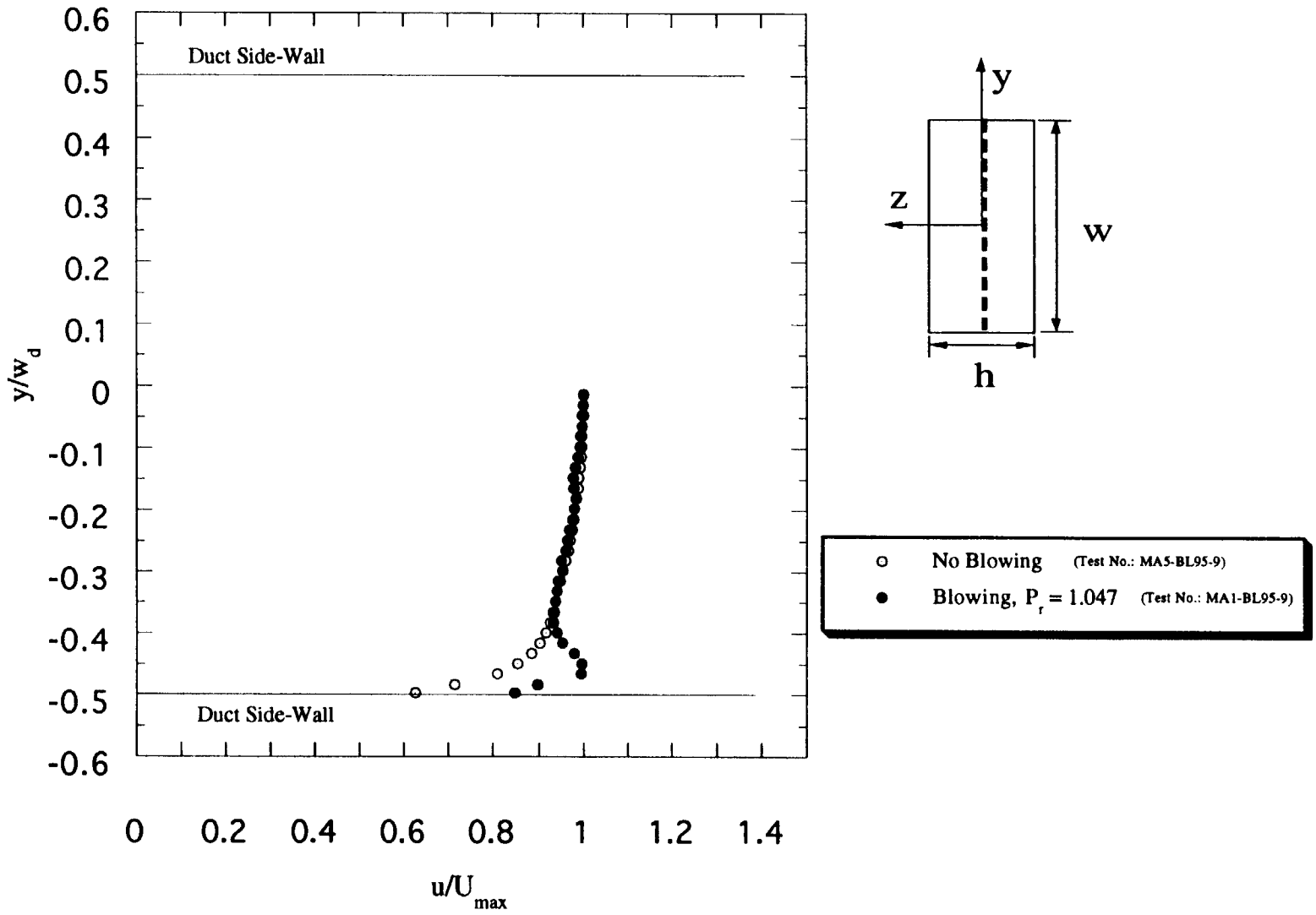

Figure 2.7 Effect of tangential blowing on side-wall boundary layer at M = 0.1.

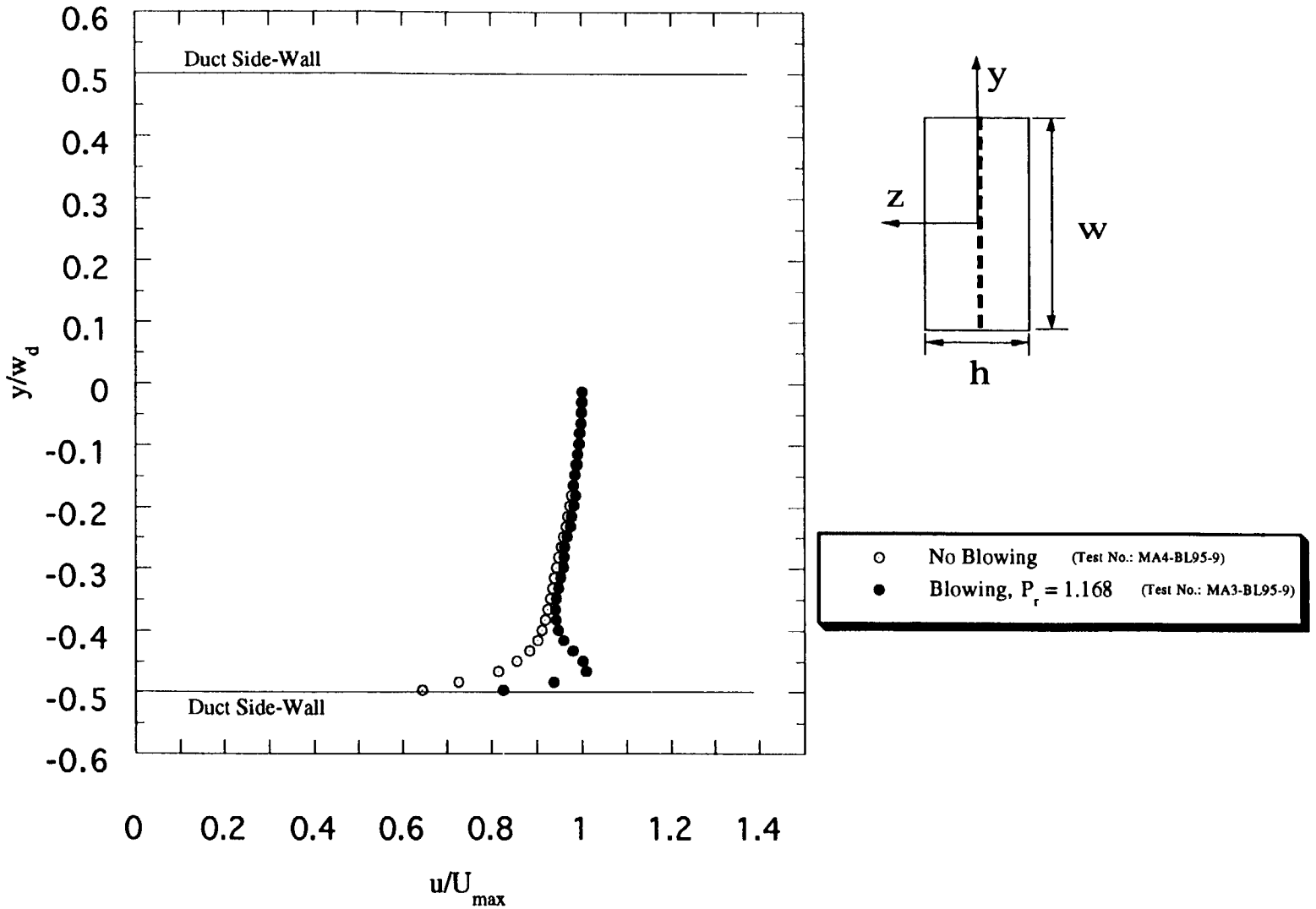

Figure 2.8 Effect of tangential blowing on side-wall boundary layer at M = 0.2.

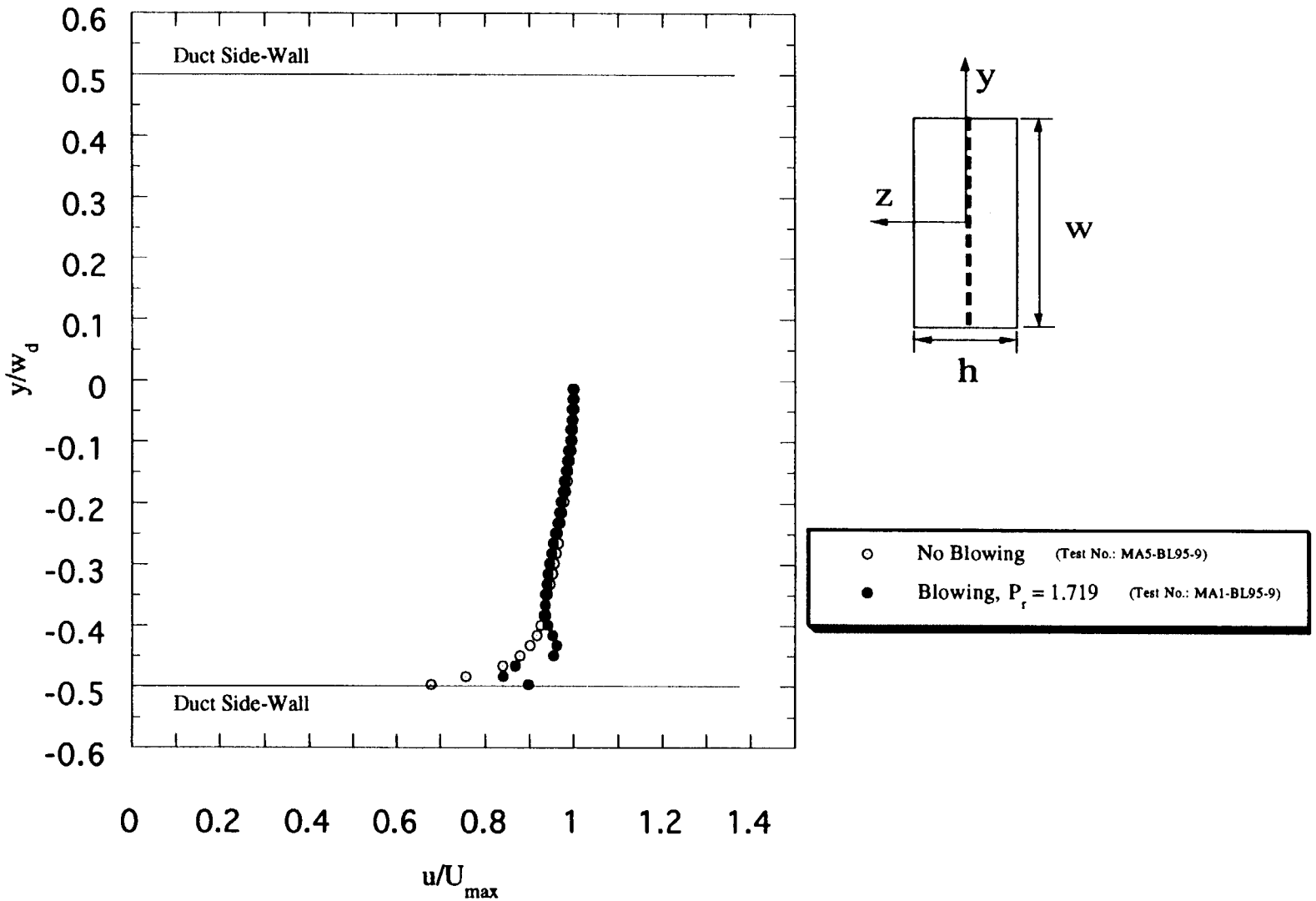

Figure 2.9 Effect of tangential blowing on side-wall boundary layer at M = 0.3.

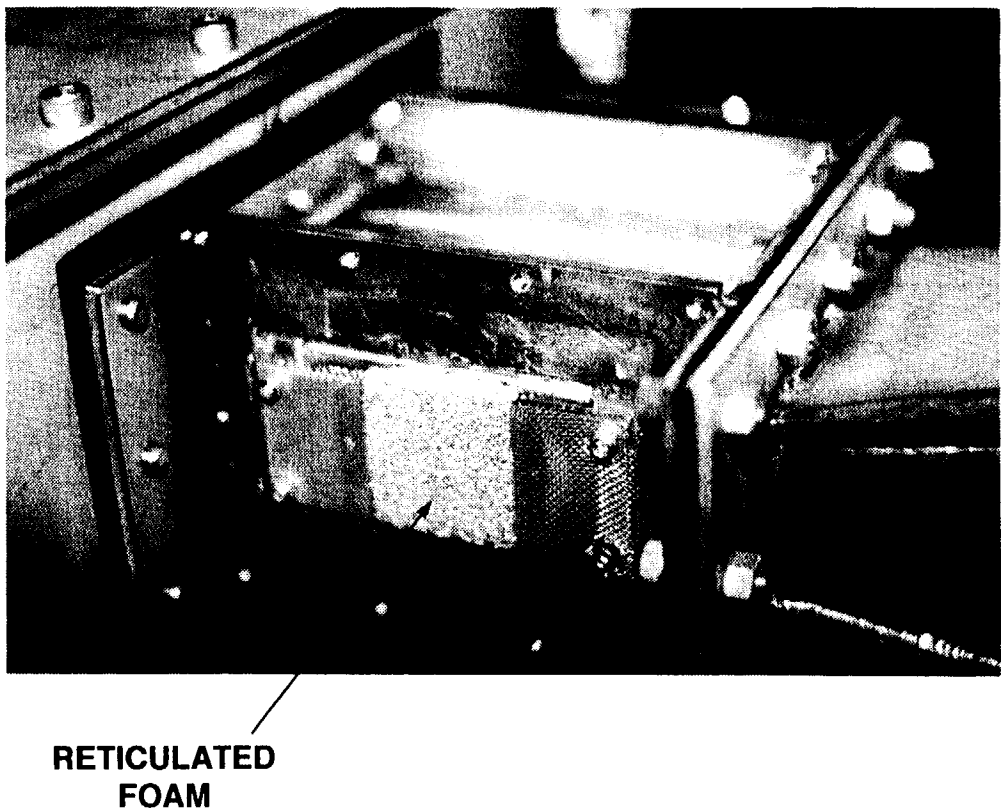

Figure 2.10 Porous side wall used in boundary layer suction apparatus.

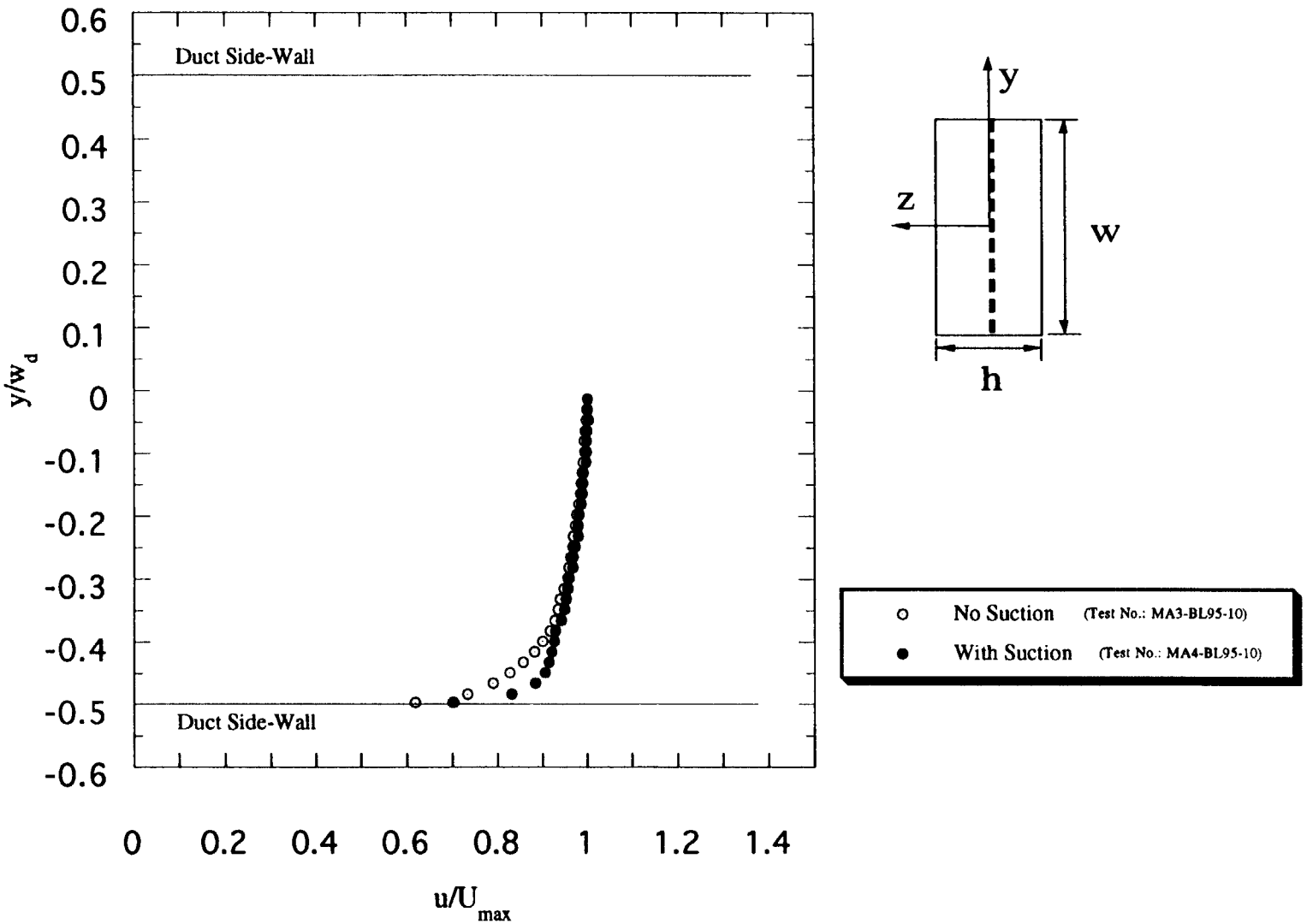

Figure 2.11 Effect of suction on side-wall boundary layer at M = 0.1.

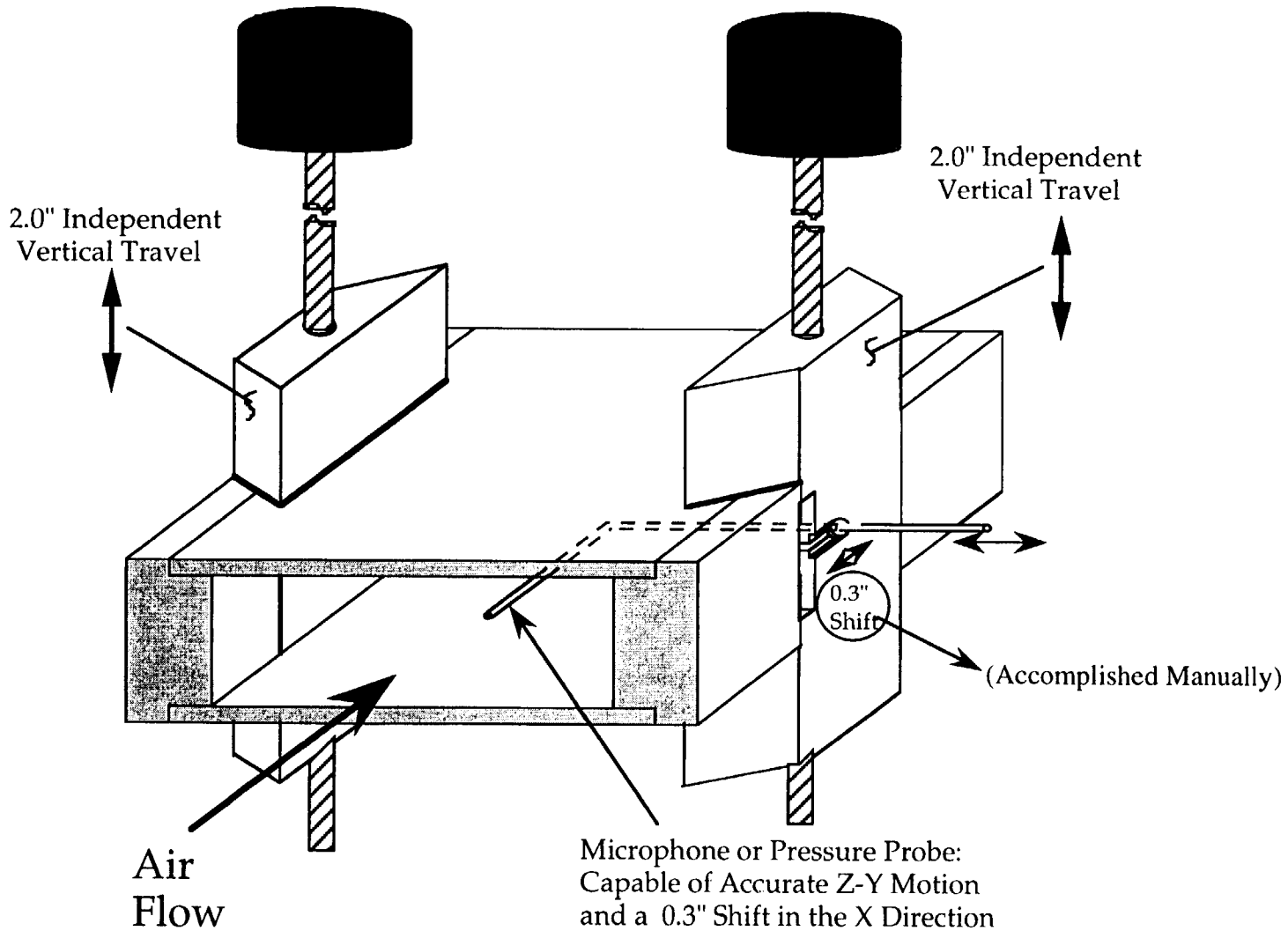

Figure 2.12 In-duct measurement probe translational degrees of freedom

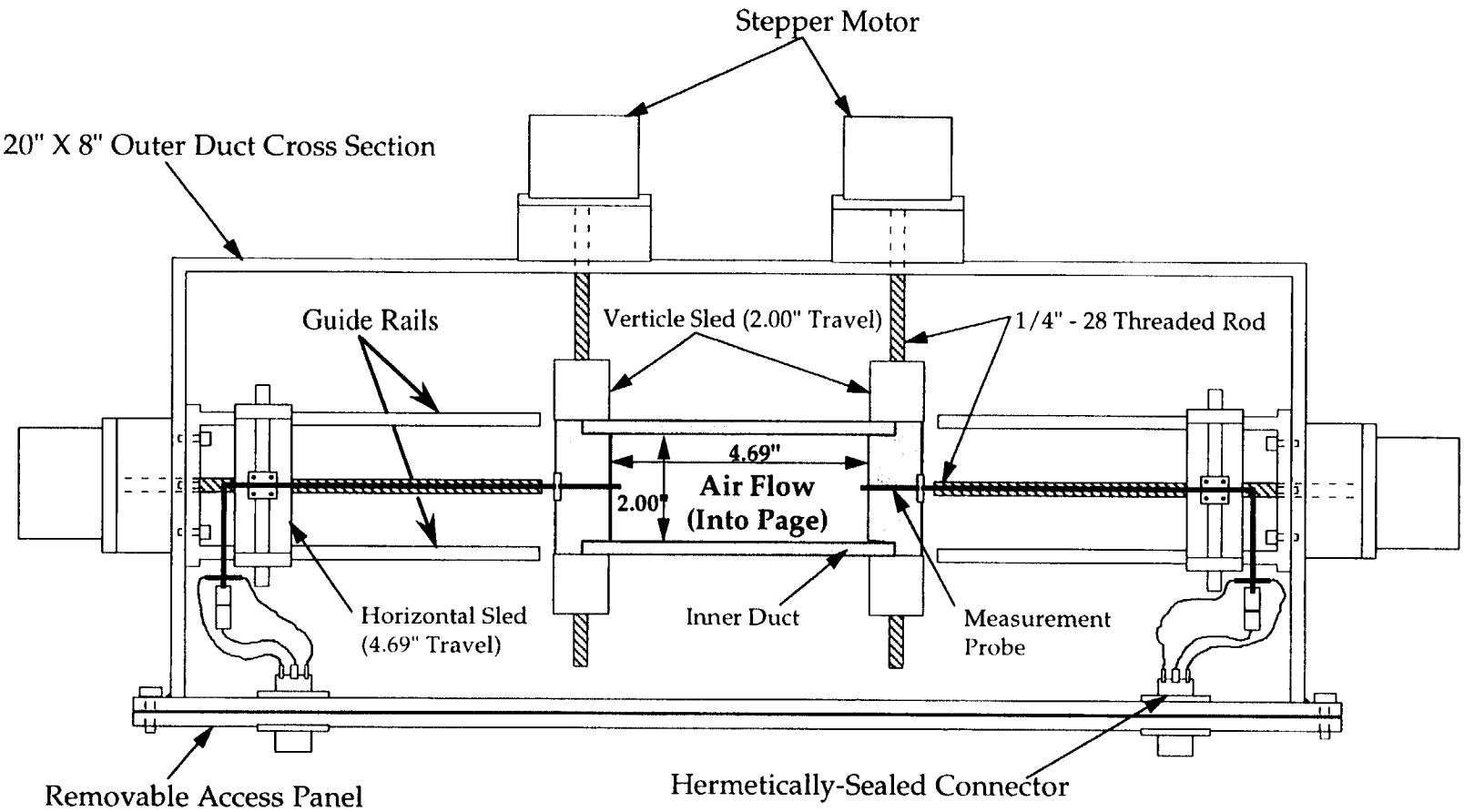

Figure 2.13 Cross sectional view of instrumentation box.

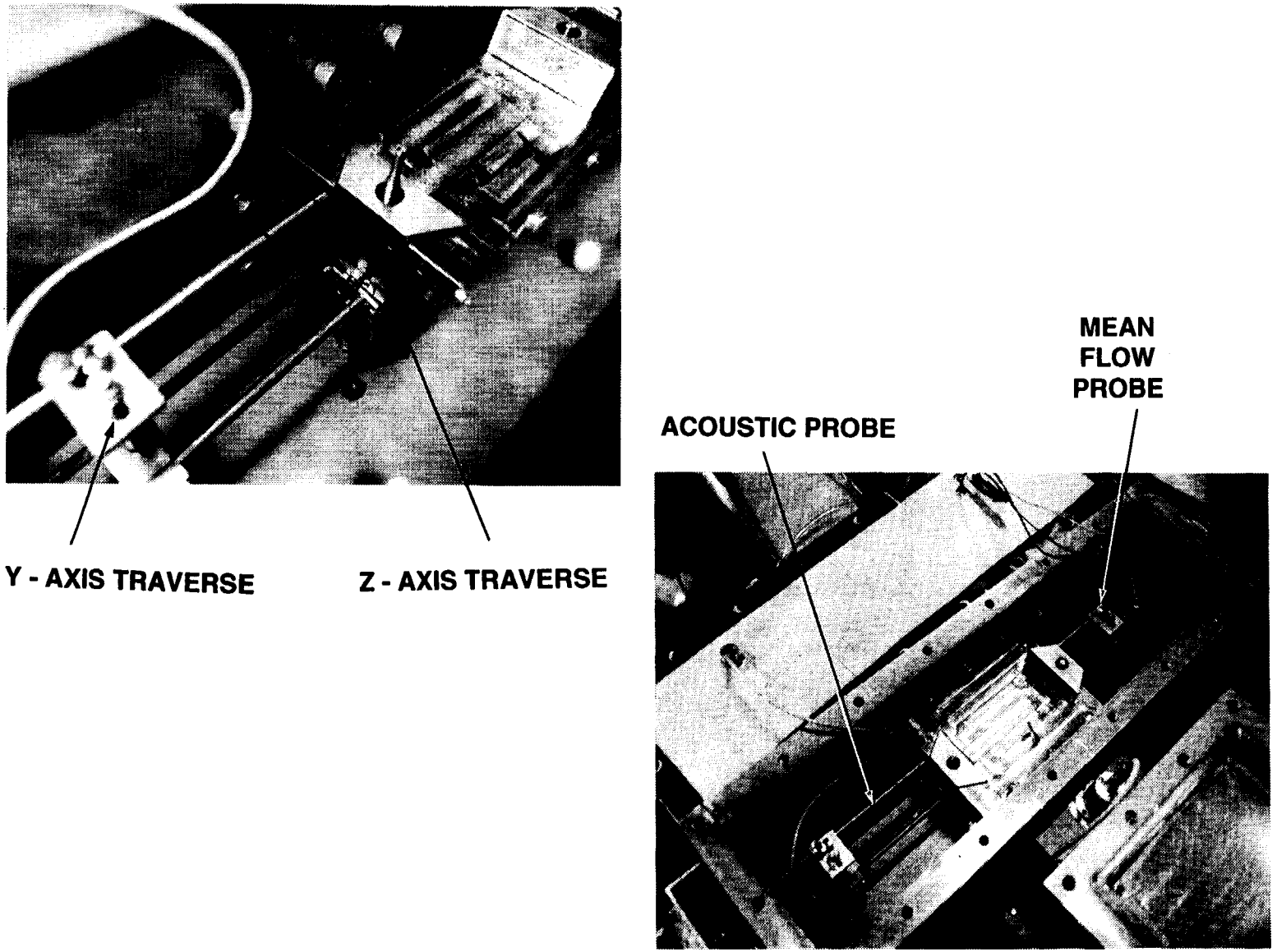

Figure 2.14 Inside views of instrumentation box.

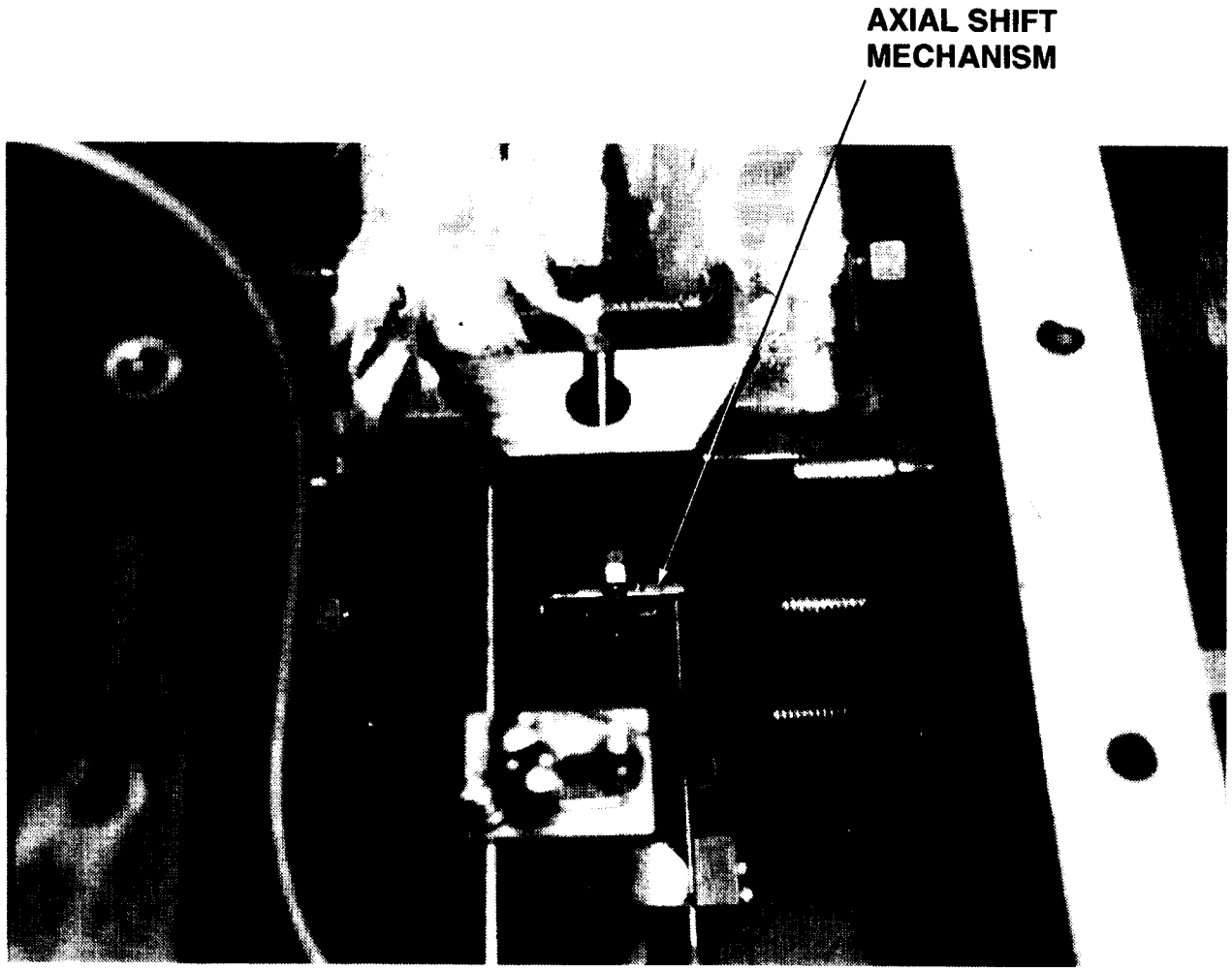

Figure 2.15 View of probe axial shift mechanism inside of instrumentation box.

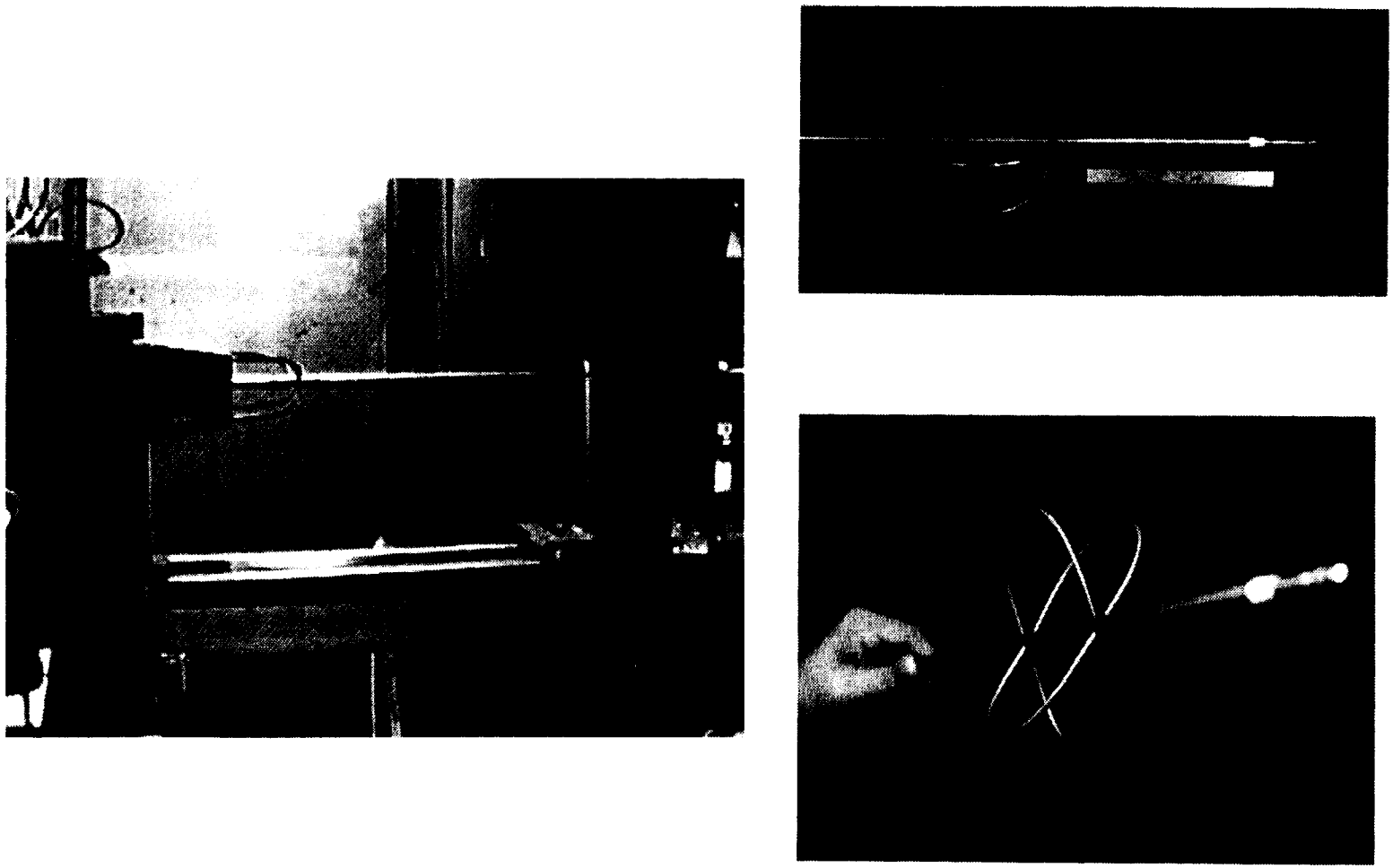

Figure 2.16 Axial centerline microphone support apparatus.

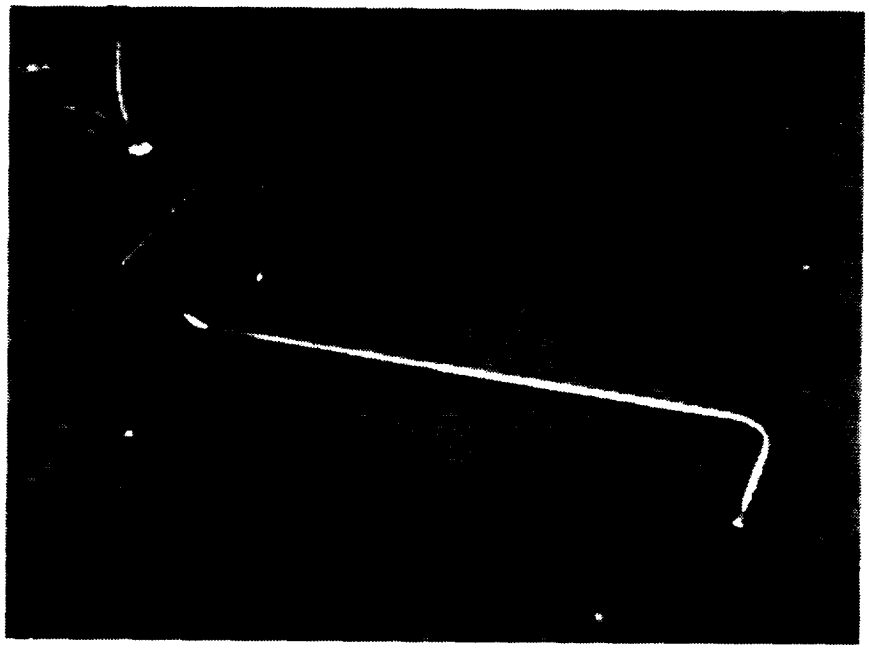

Figure 2.17 Typical mean flow probe used to measure pressure and temperature.

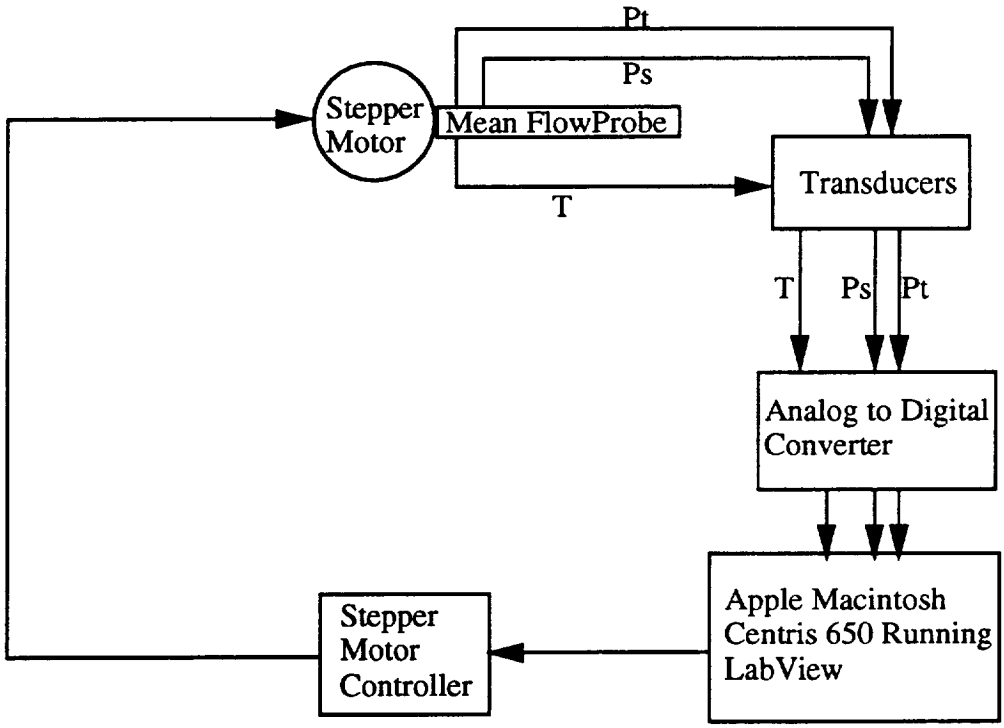

Figure 2.18 Schematic of mean flow data acquisition system.

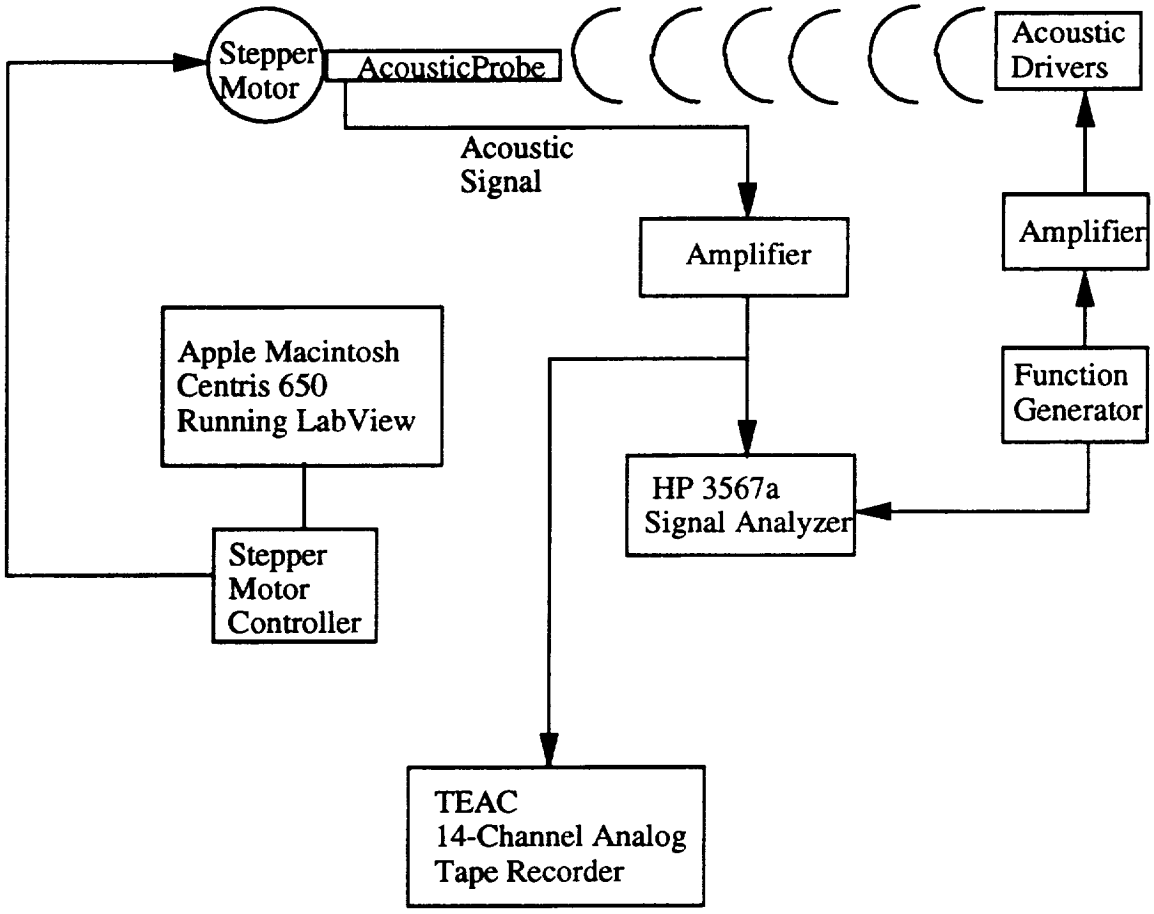

Figure 2.19 Schematic of acoustic probe microphone data acquisition system.

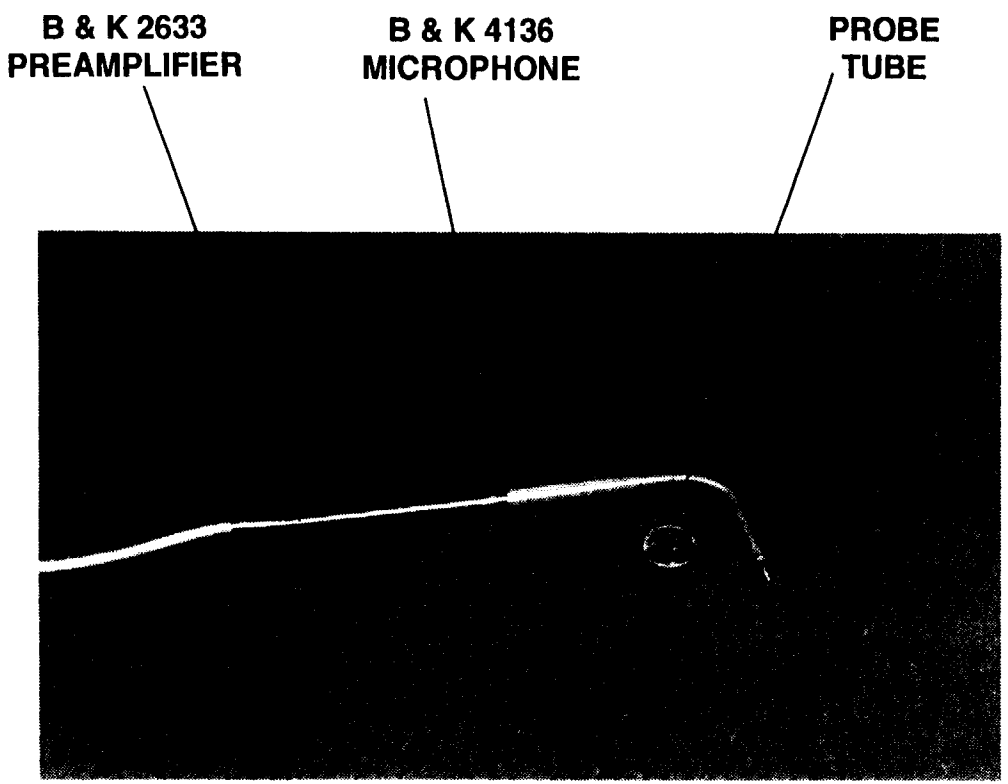

Figure 2.20 Typical probe microphone used for in-duct planar acoustic measurements.

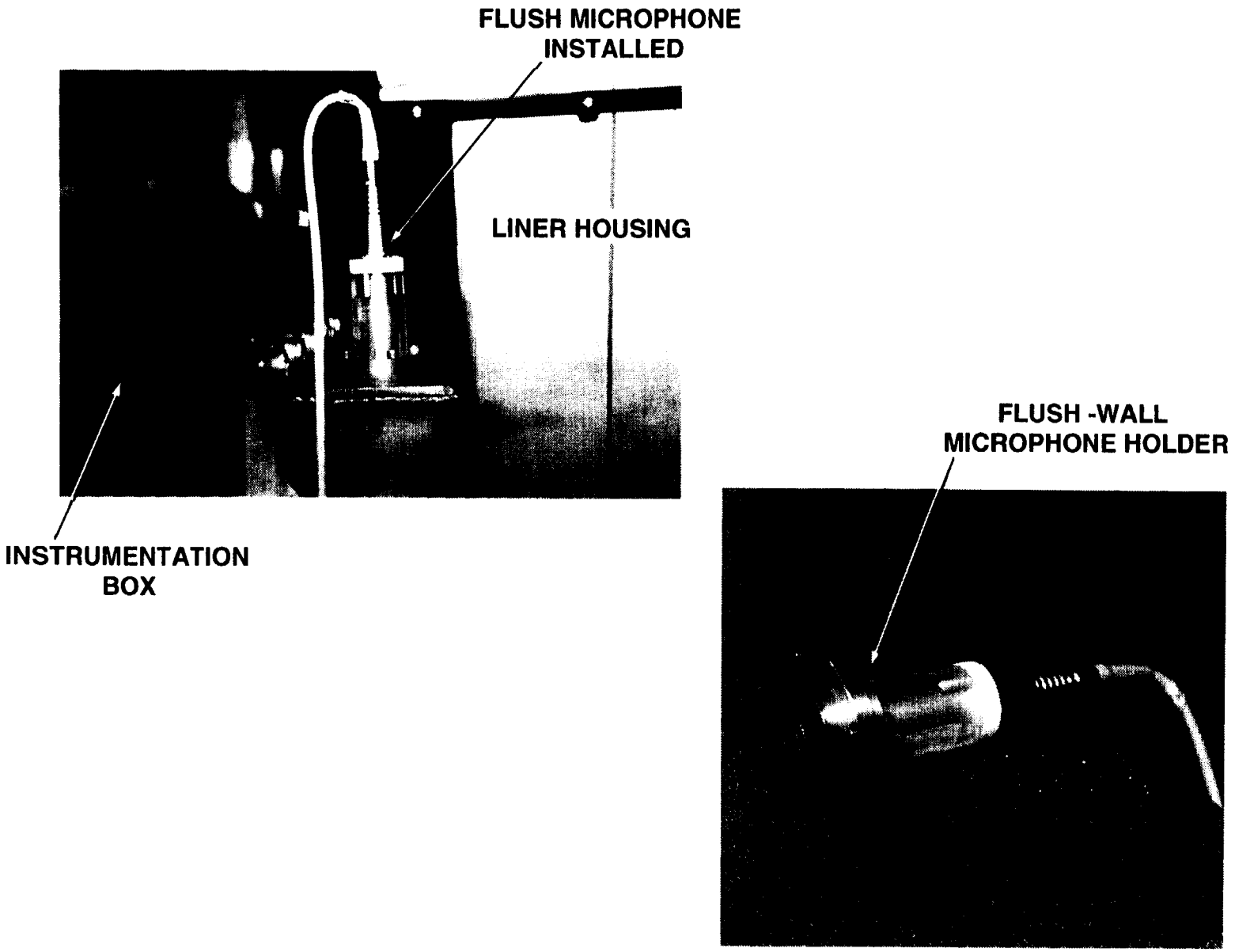

Figure 2.21 Flush wall-mounted microphones used upstream and downstream of liner section.

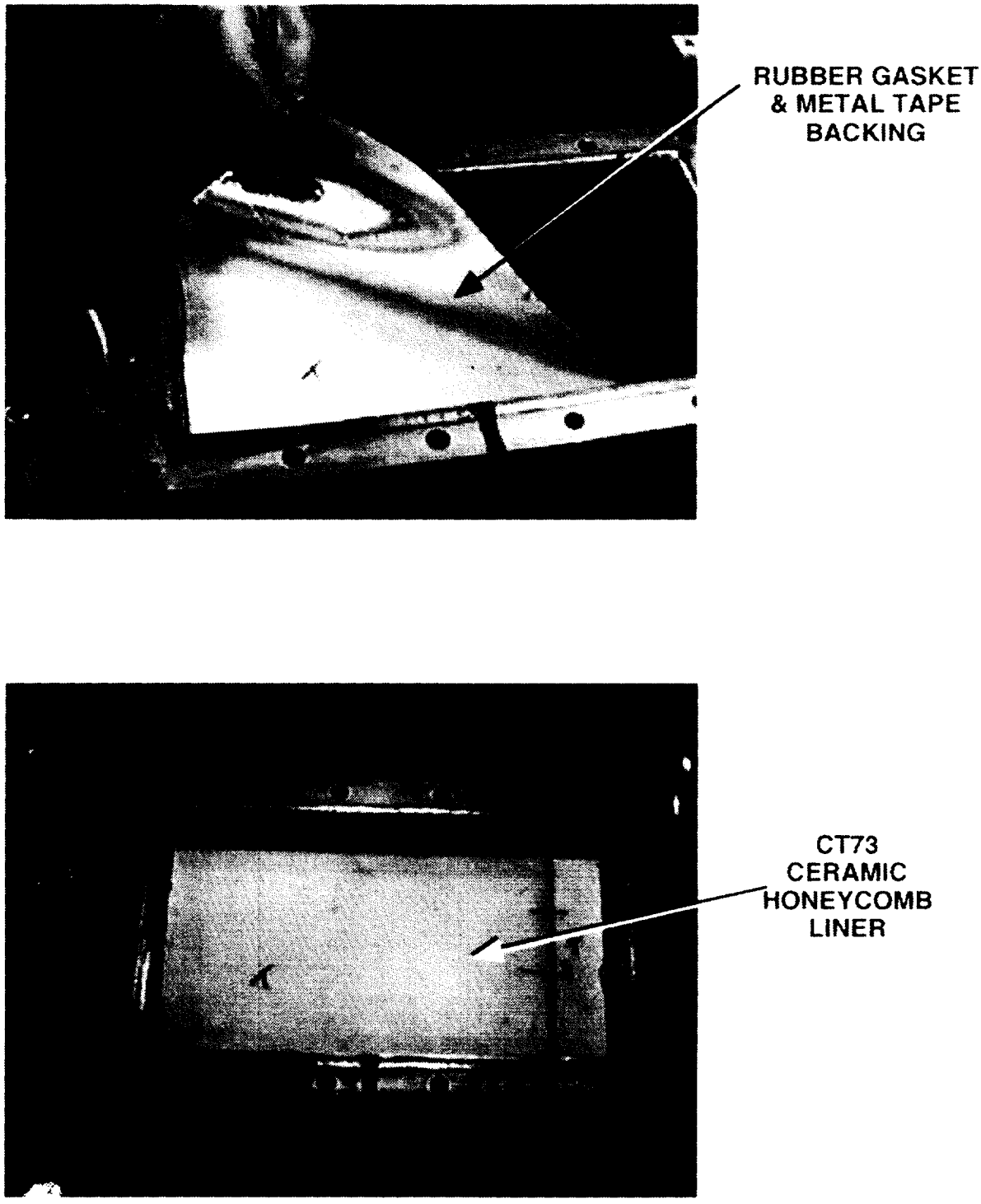

Figure 2.22 Installation of CT73 liner into liner housing section of flow-duct facility.

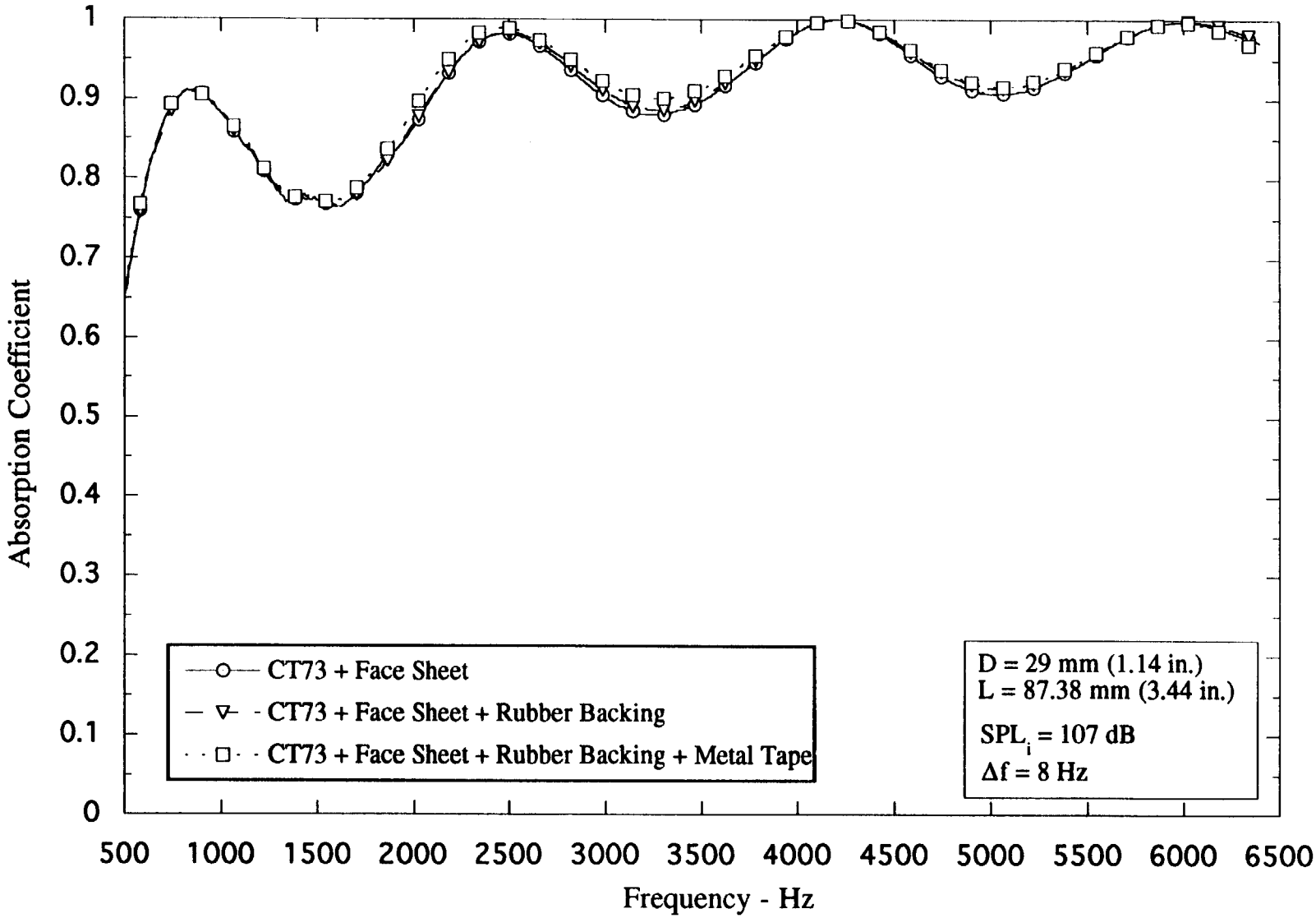

Figure 2.23 Effect of rubber backing and metal tape on the absorption of CT73 ceramic honeycomb liner.

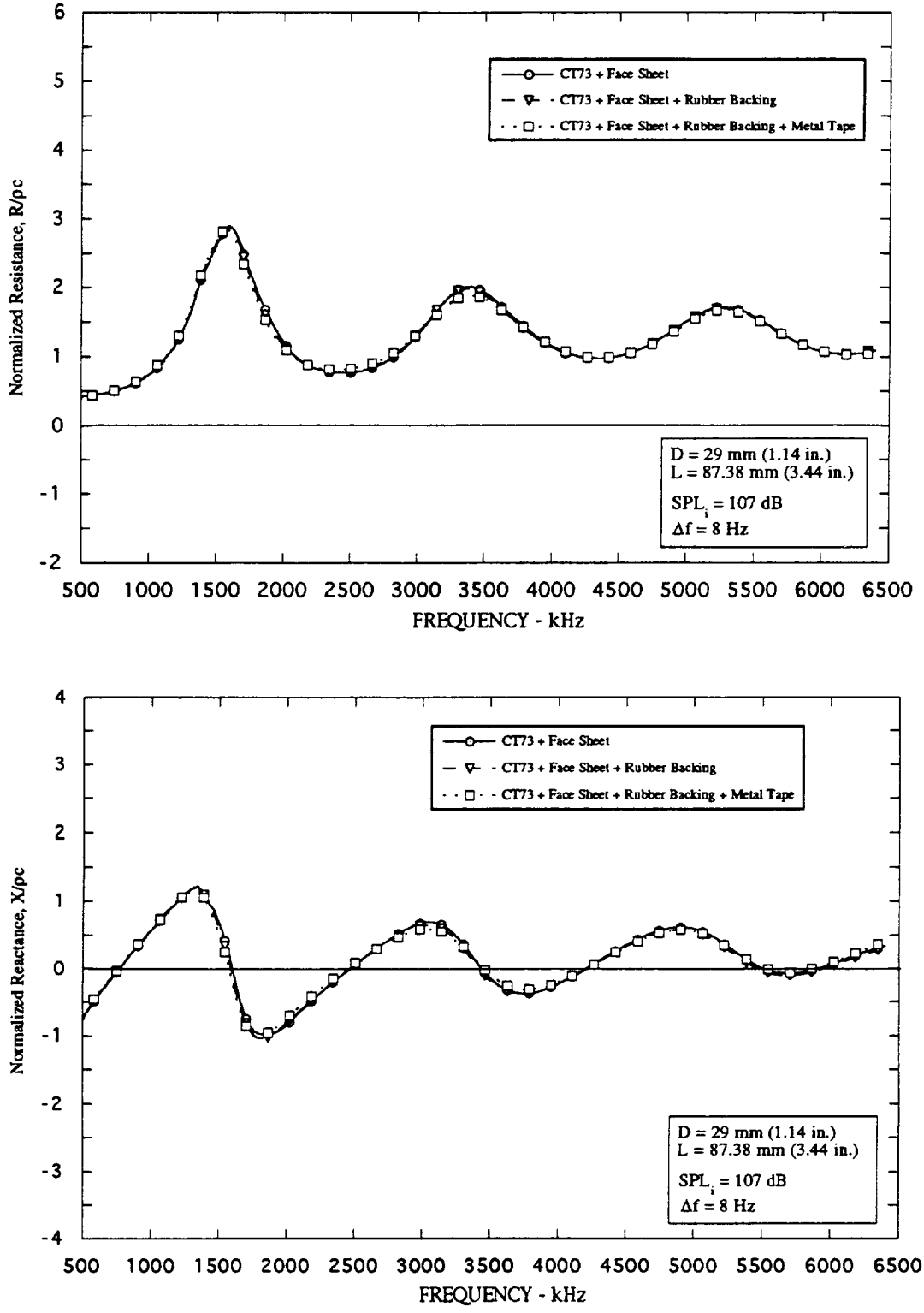

Figure 2.24 Effect of rubber backing and metal tape on the impedance of CT73 ceramic honeycomb liner.

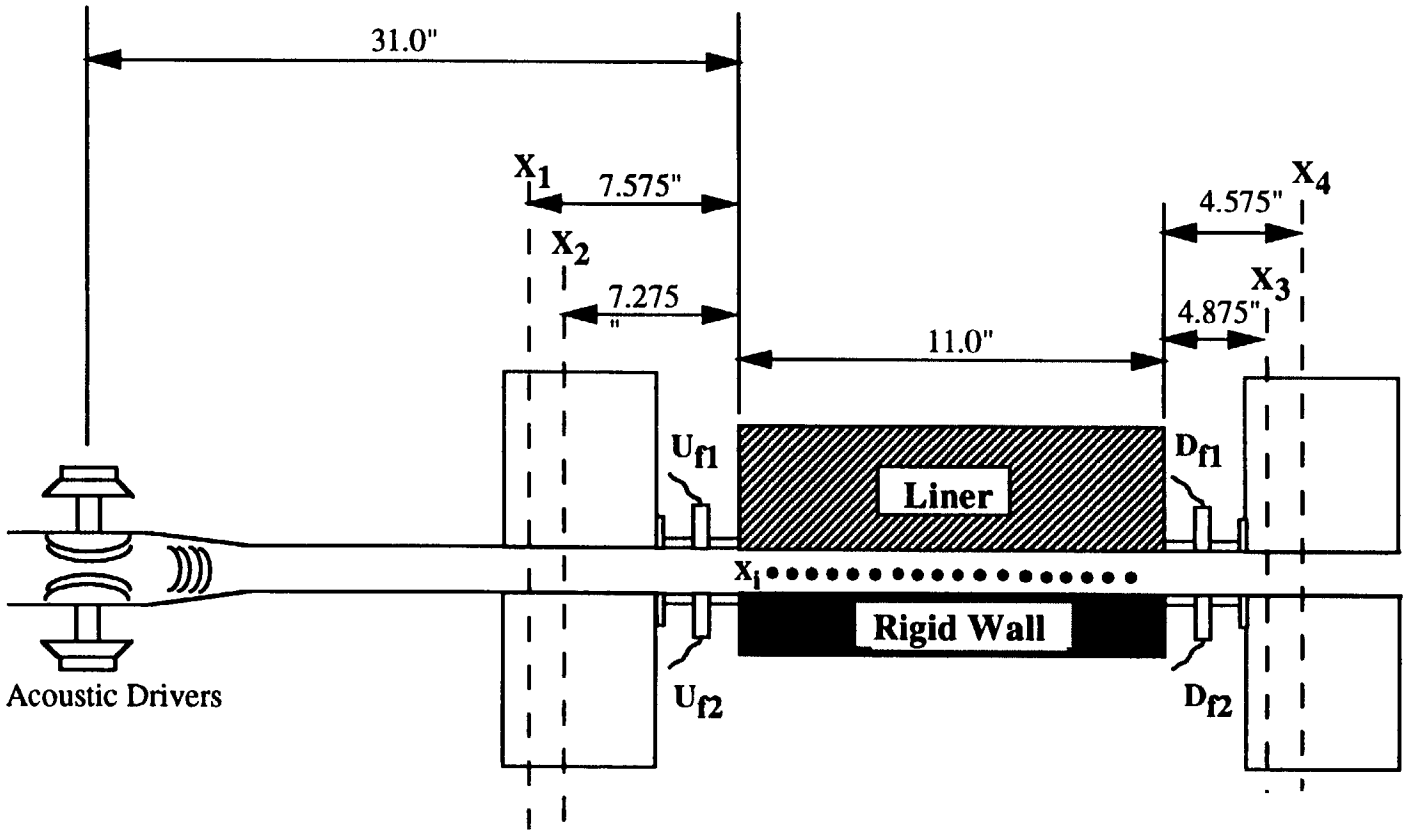

Notes:

1. U_{f1}, U_{f2}, D_{f1}, D_{f2} are flush mounted 1/2" microphones whose centers are 1.5" from liner.
2. X_1, X_2 and X_3, X_4 are upstream and downstream planes respectively.
3. X_i are axial points on the duct centerline and are 0.2 inches apart.

Figure 3.1 Locations of acoustic measurement positions relative to the leading edge and trailing edge of the liner housing section.

Flow Data Measurement Locations in Lined Duct

Aft Looking Forward

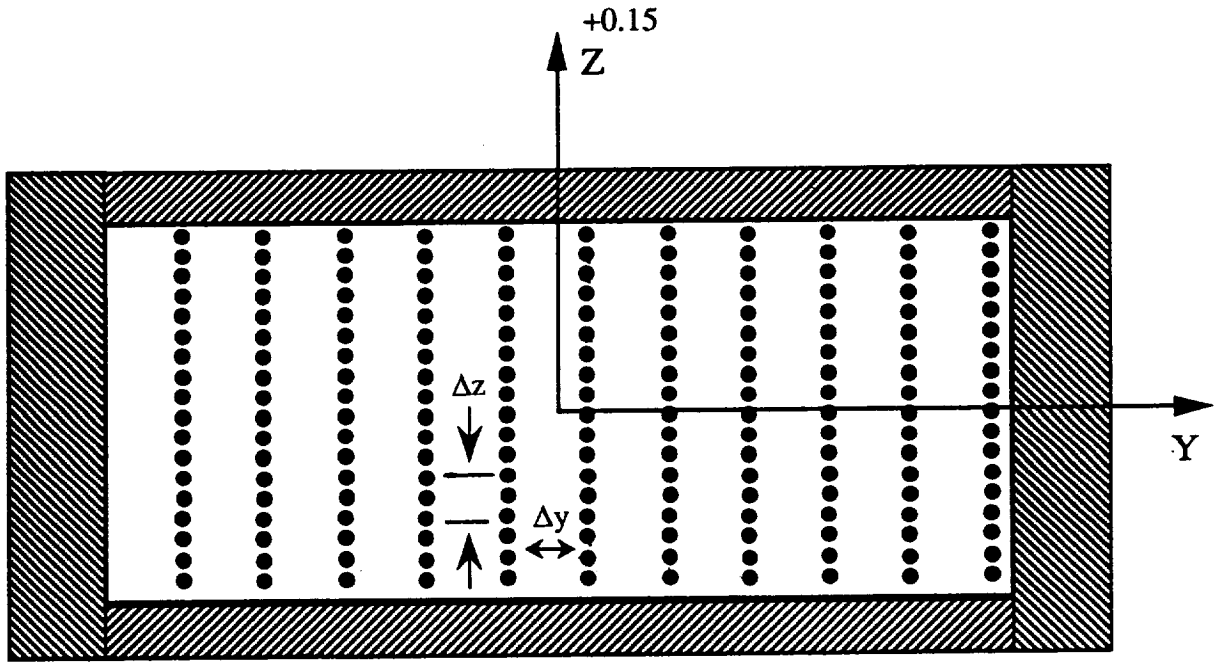

$\Delta z = 0.10$ in.
$\Delta y = 0.42$ in.

Figure 3.2 Typical grid of mean flow measurement locations in flow-duct.

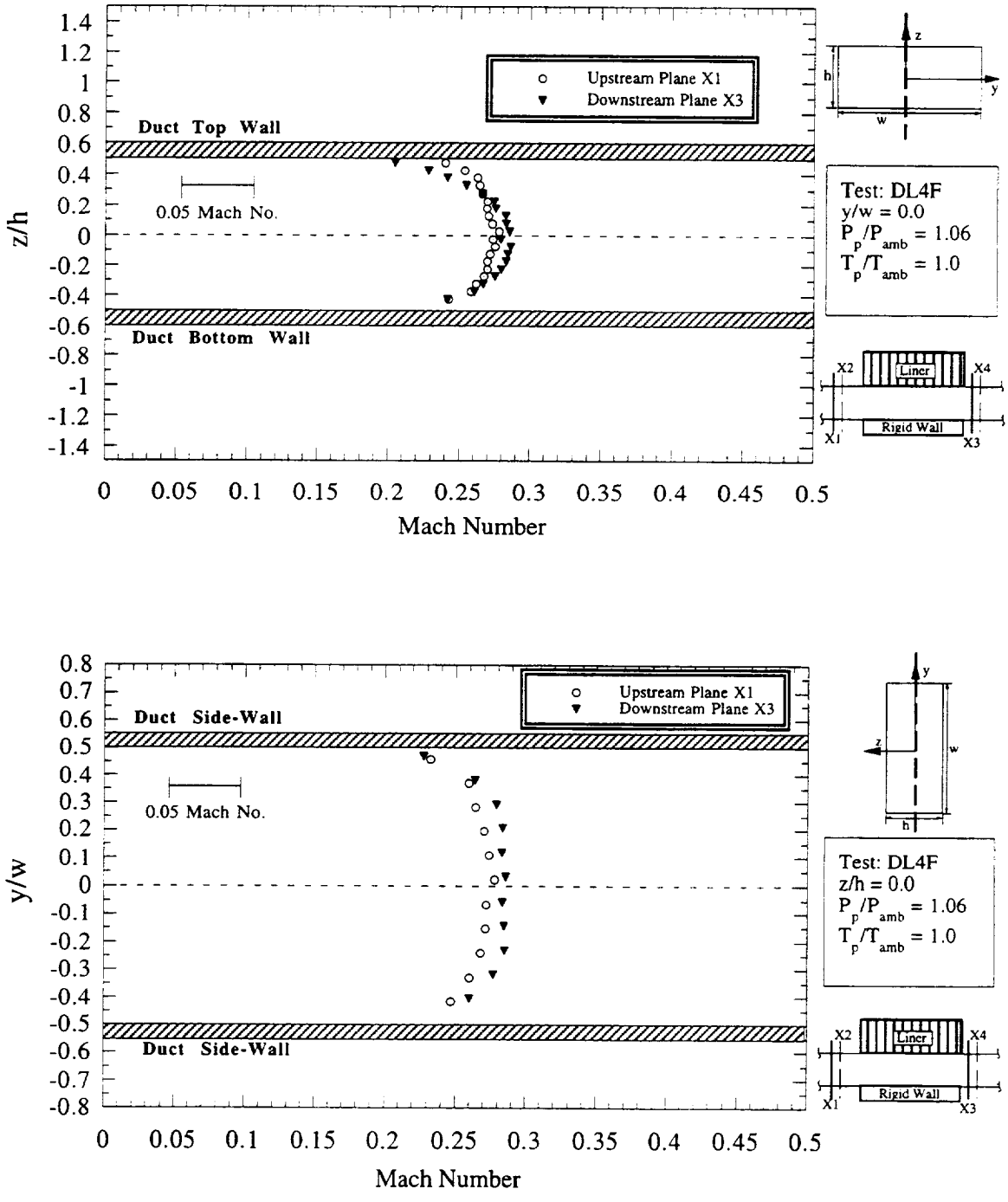

Figure 3.3 Typical mean flow Mach number profiles for $M_d = 0.3$; (a) Minor axis; (b) Major axis.

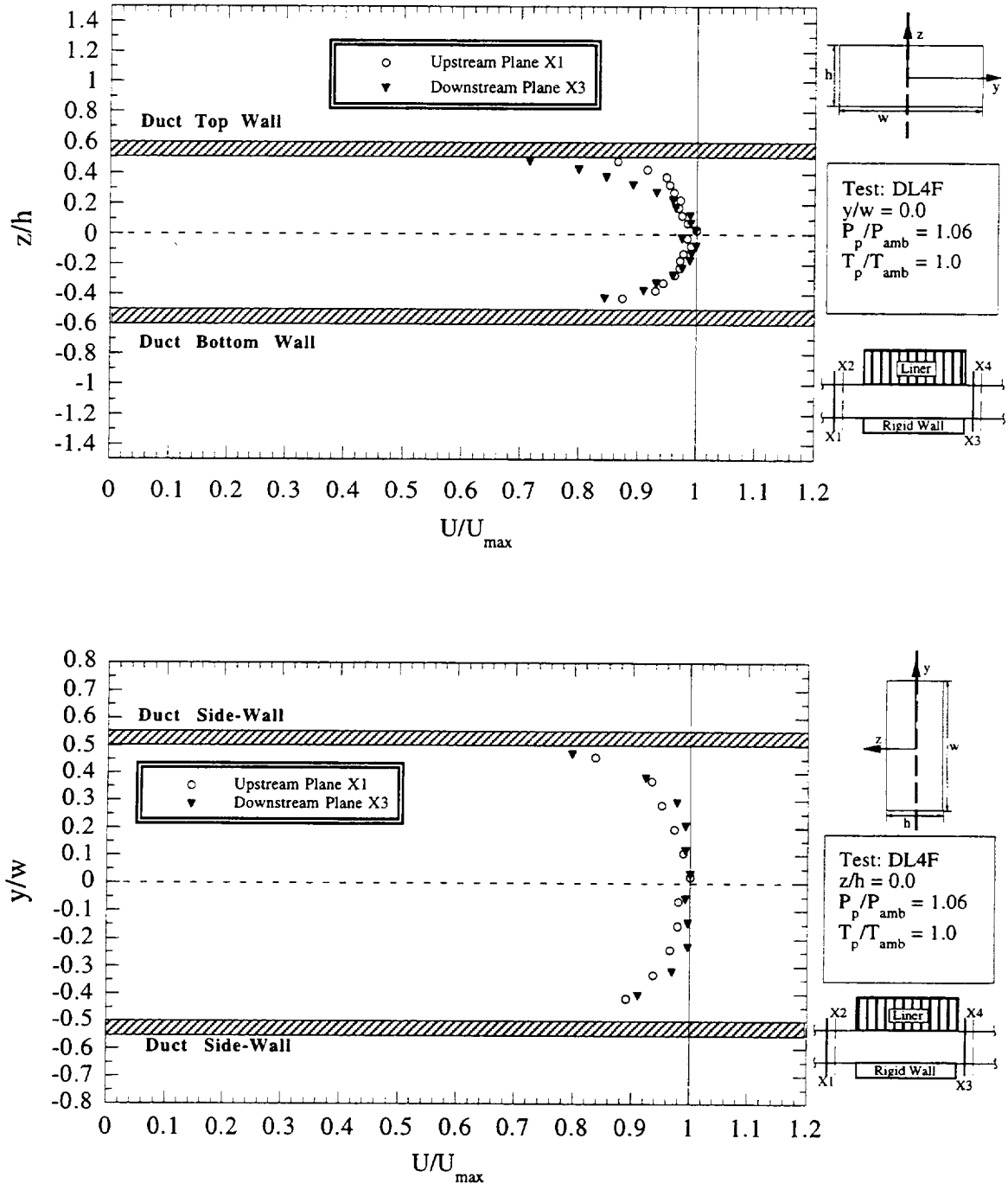

Figure 3.4 Typical mean flow velocity profiles for $M_d = 0.3$; (a) Minor axis; (b) Major axis.

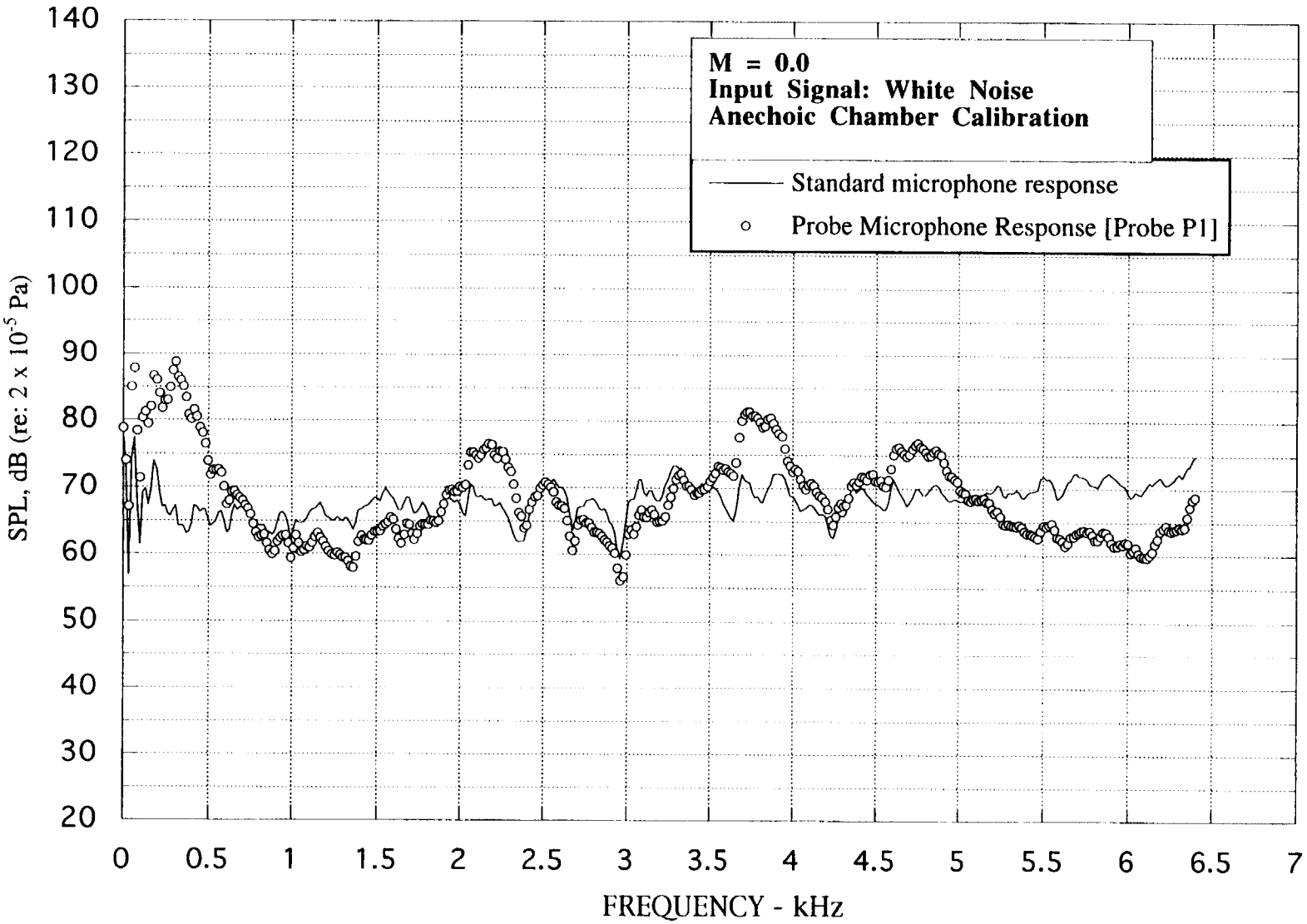

Figure 3.5 Standard microphone response compared to probe microphone in anechoic chamber (Δf = 16 Hz; 64 avgs.; Probe P1).

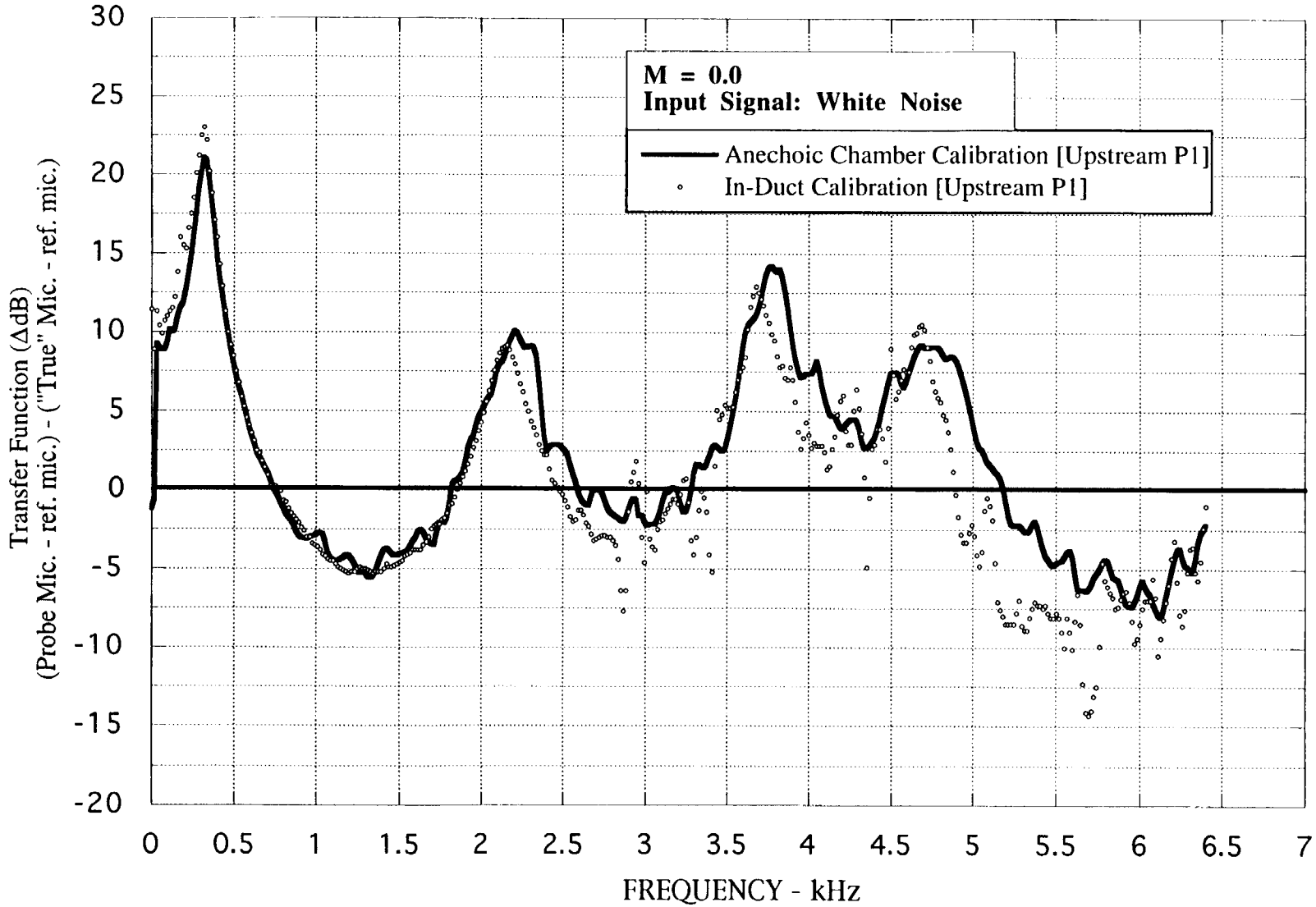

Figure 3.6 Comparison of in-duct and anechoic chamber calibrations of upstream P1 probe microphone ($M_d = 0.0$; $\Delta f = 16$ Hz; 64 avgs.).

0.0.

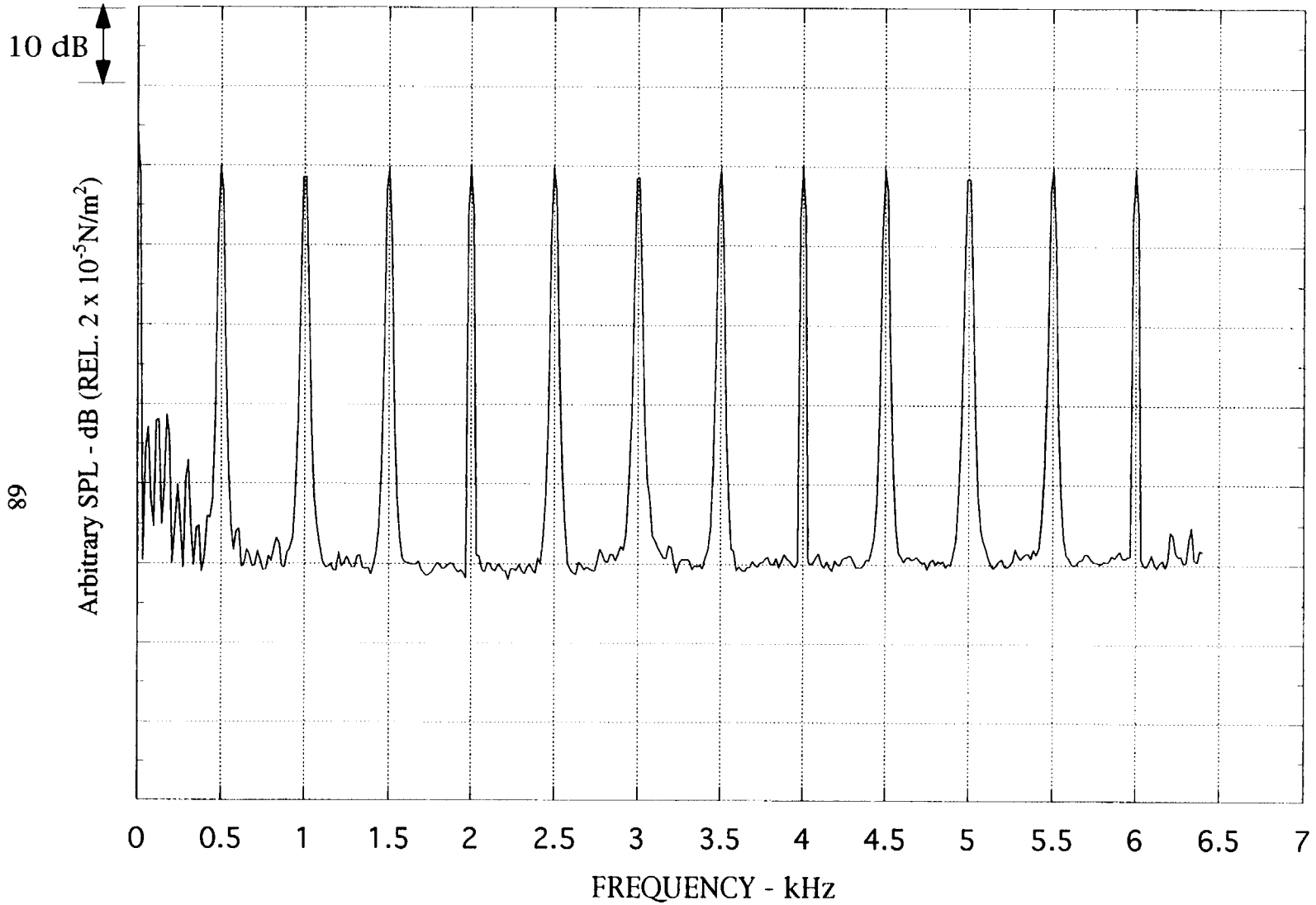

Figure 3.7 Fourier transform of Sinc wave function used as input for acoustic drivers in flow-duct facility.

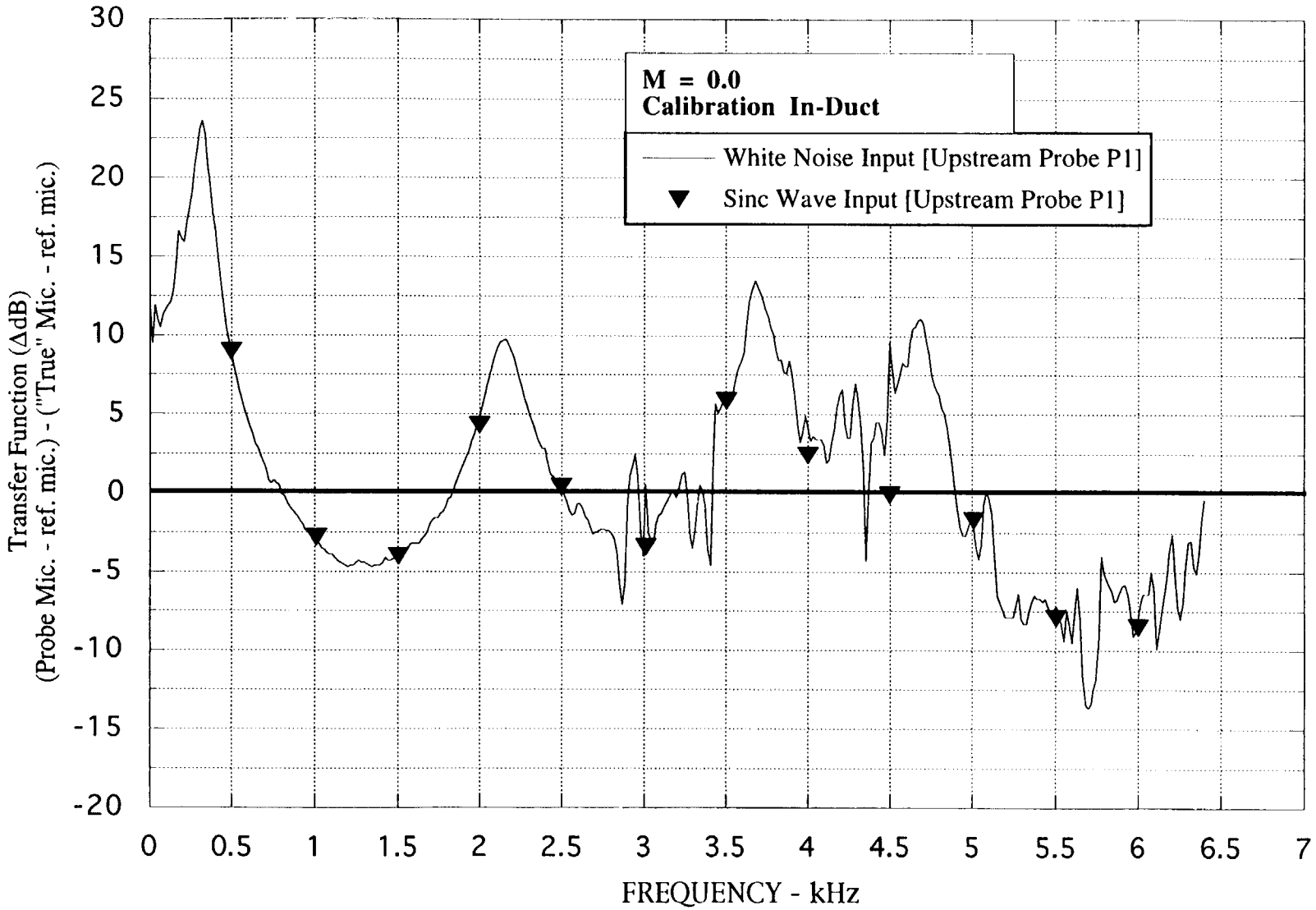

Figure 3.8 Comparison of broadband input to multi-tone input for in-duct probe microphone calibrations ($M_d = 0.0$; $\Delta f = 16$ Hz; 64 avgs.).

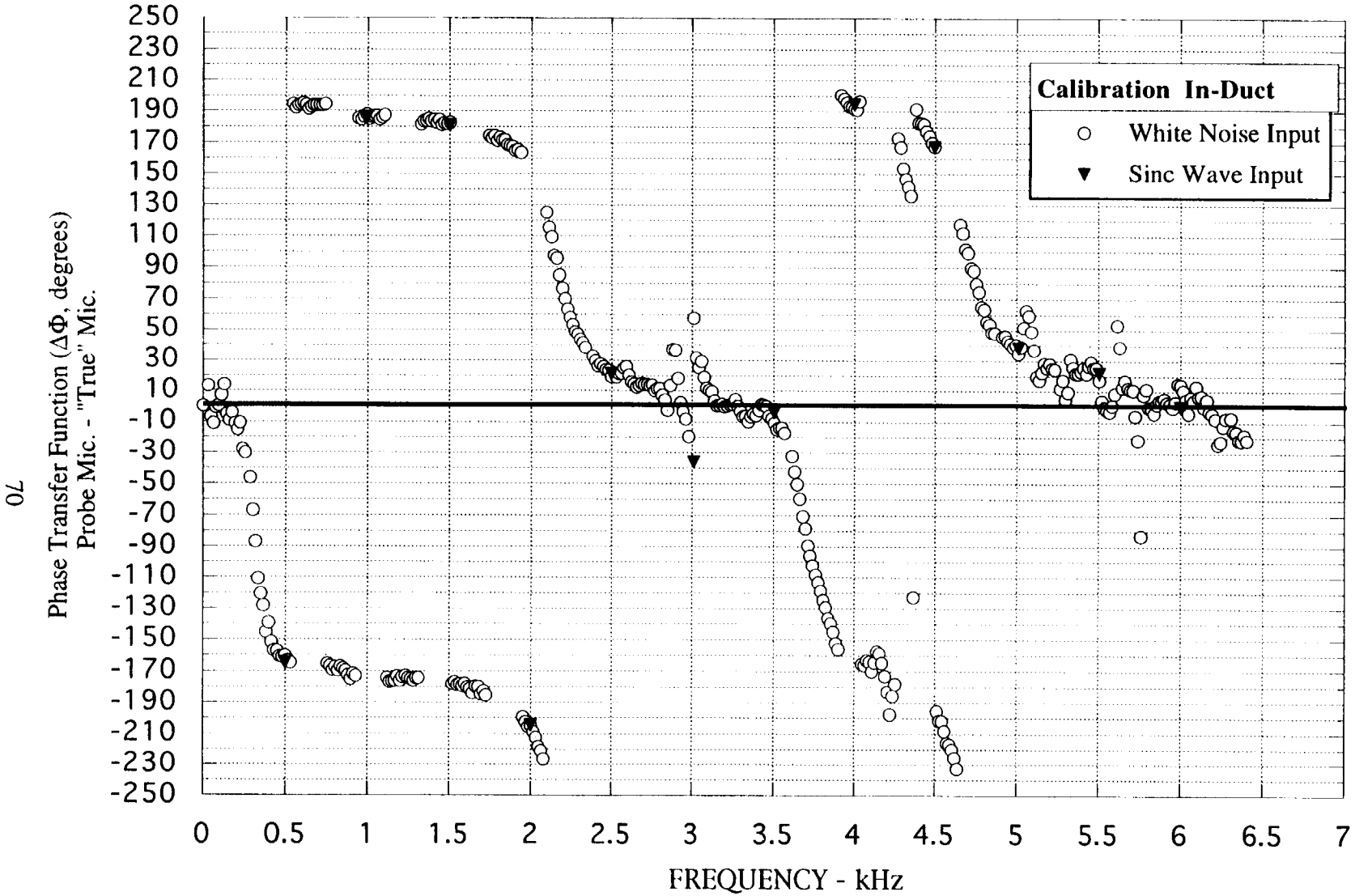

Figure 3.9 Comparison of broadband input to multi-tone input for in-duct probe microphone calibrations for phase (M_d = 0.0; Δf = 16 Hz; 64 avgs.).

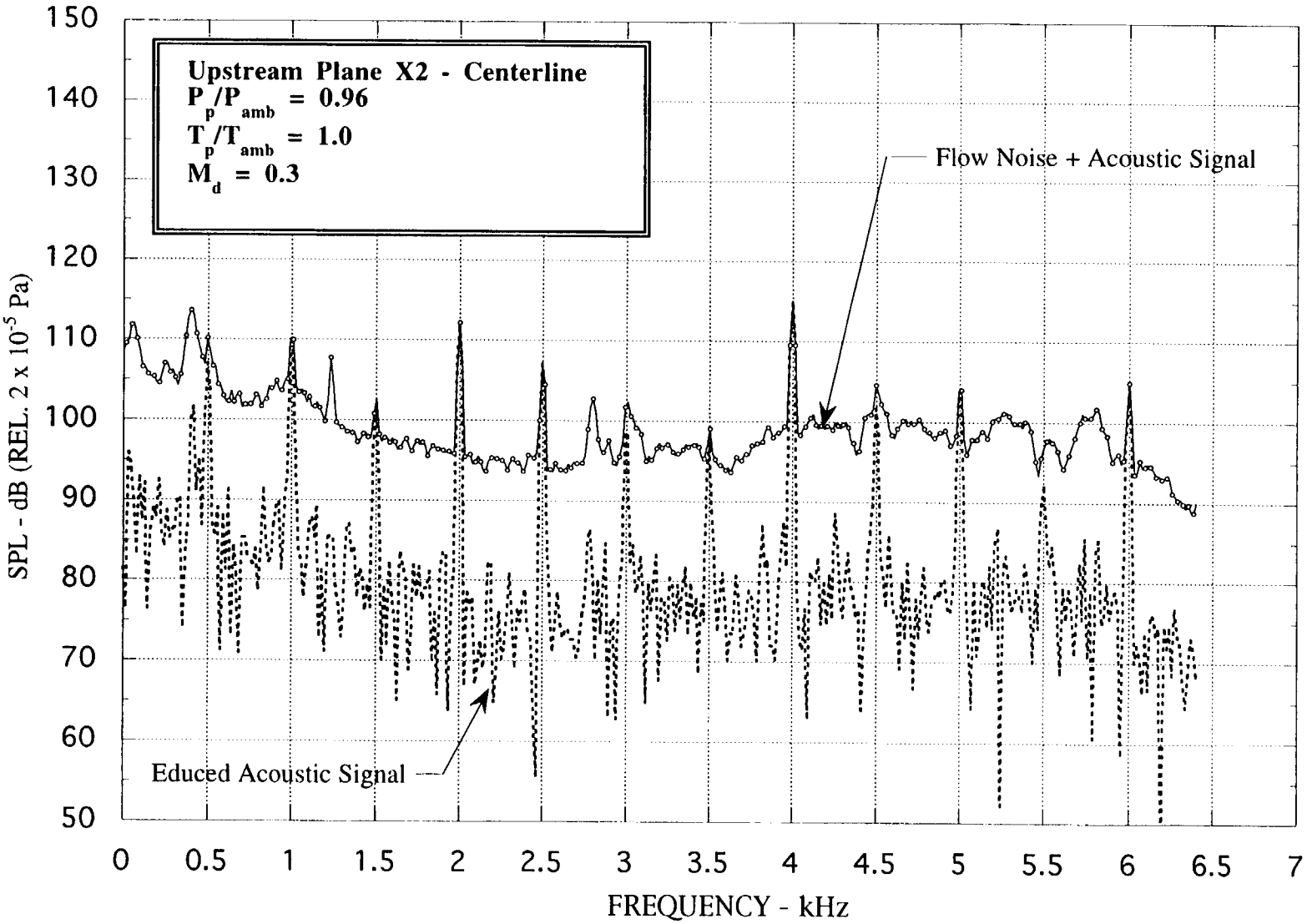

Figure 3.10 Example of educed acoustic spectra obtained from the total microphone output power (M_d = 0.3; Δf = 16 Hz; 64 avgs.).

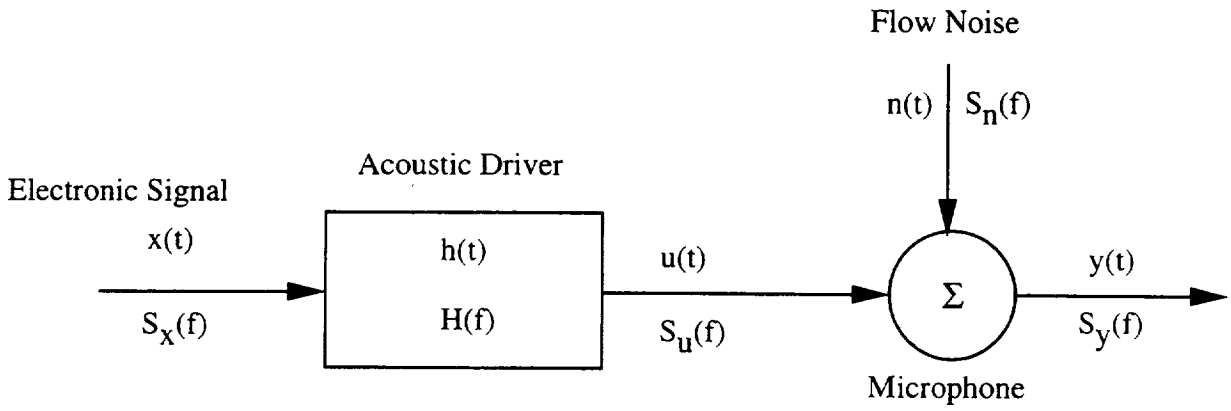

Signal Processing Path

Nomenclature:

x(t) is the electronic signal fed to the acoustic driver via an amplifier

h(t) is the transfer function of the acoustic driver

n(t) is the flow noise measured by the microphone

y(t) is the output of the microphone which includes u(t) and n(t), i.e., y(t)=u(t) + n(t)

Sx(f), H(f), Su(f), Sn(f), and Sy(f) are the corresponding frequency domain quantities

Gyx is the cross spectrum between y and x

Gxx, Gyy, Guu, and Gnn are the autospectra corresponding to x(t), y(t), u(t), and n(t) respectively

Figure 3.11 Schematic of signal processing path for a microphone placed in a mean flow along with standard terminology.

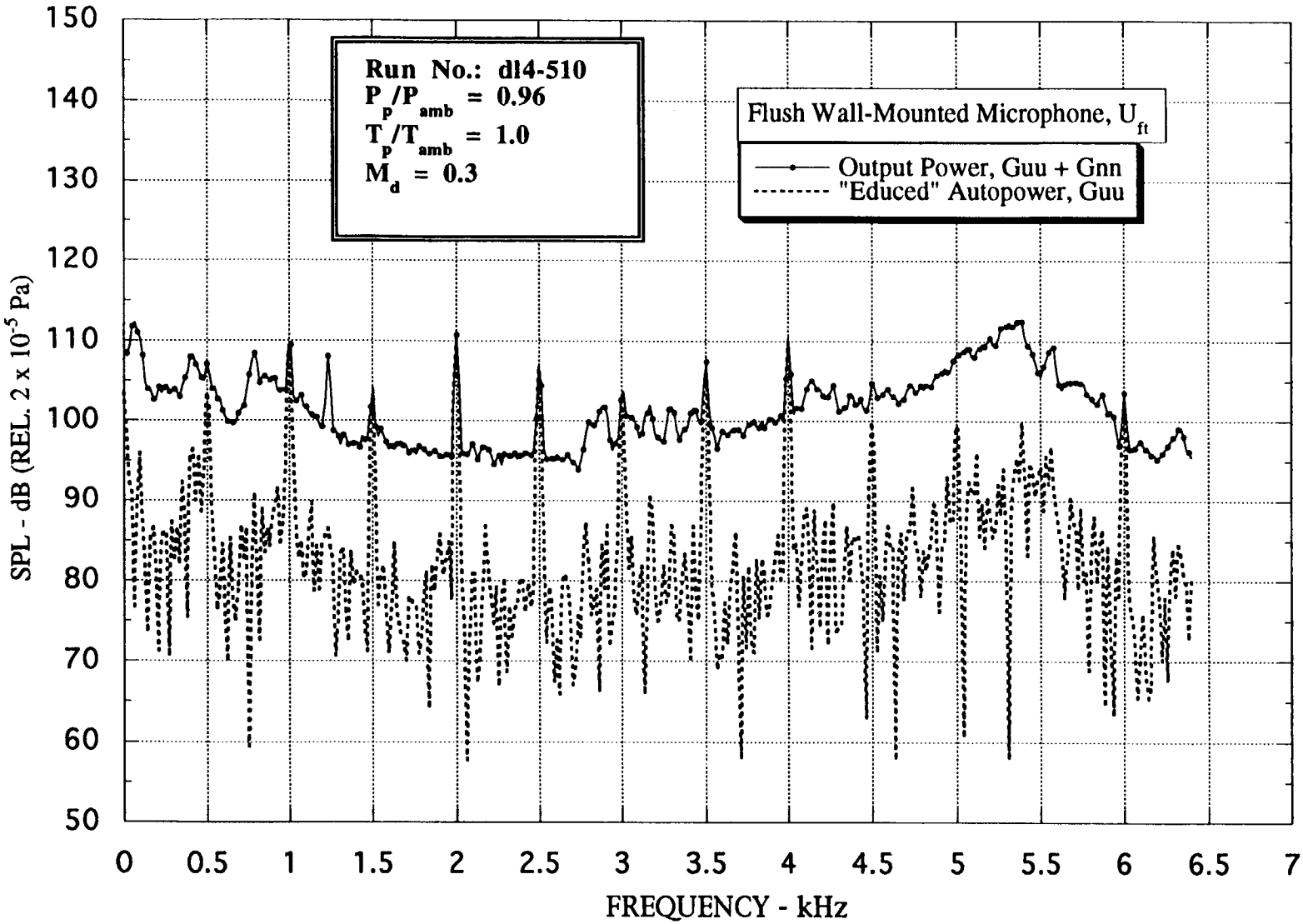

Figure 3.12 Example of educed spectra which contains tones that are completely buried under the flow noise (M_d = 0.3; Δf = 16 Hz; 64 avgs.).

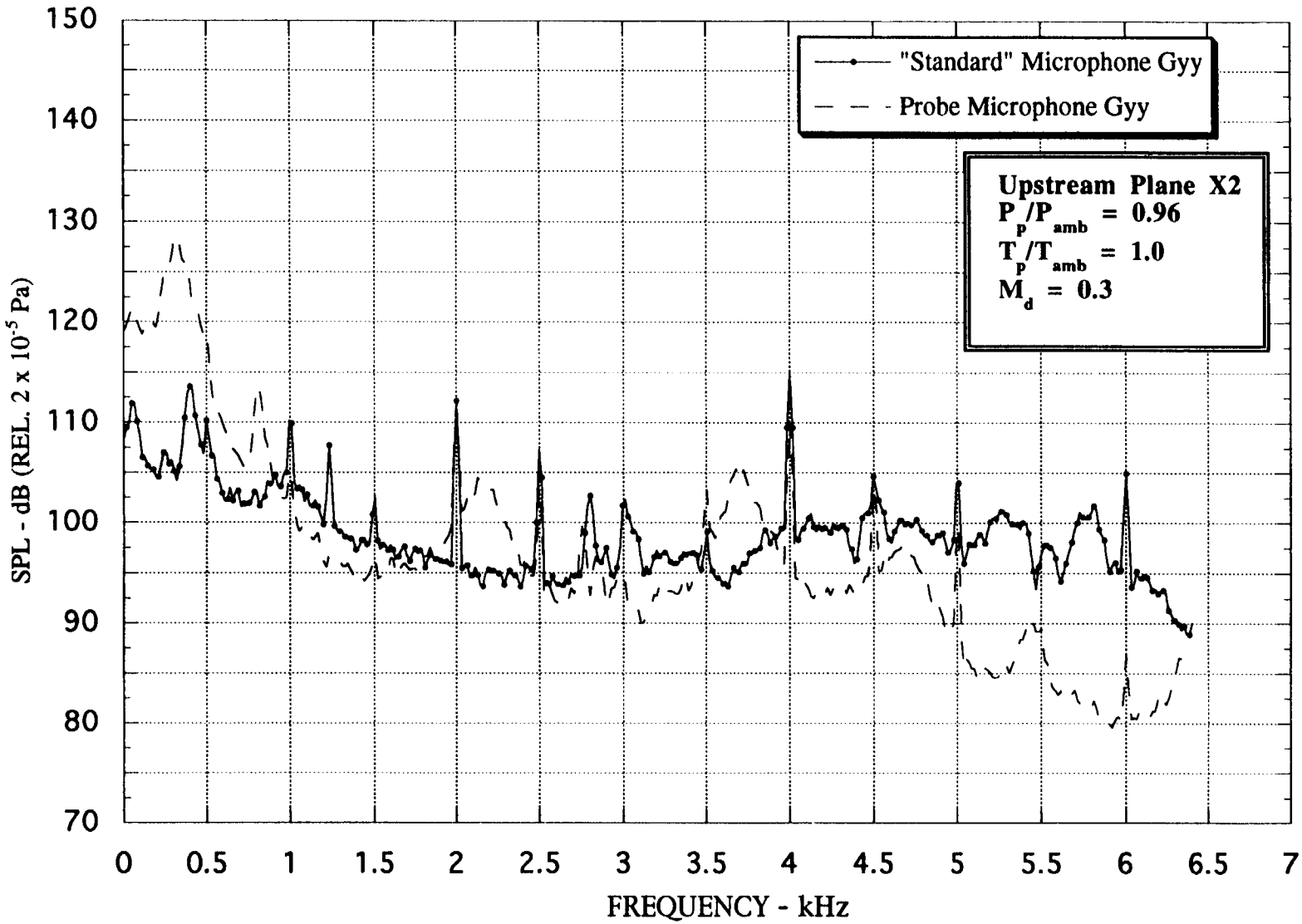

Figure 3.13 Output power spectra for a probe microphone and a "standard" microphone placed in a mean flow ($M_d = 0.3$; $\Delta f = 16$ Hz; 64 avgs.).

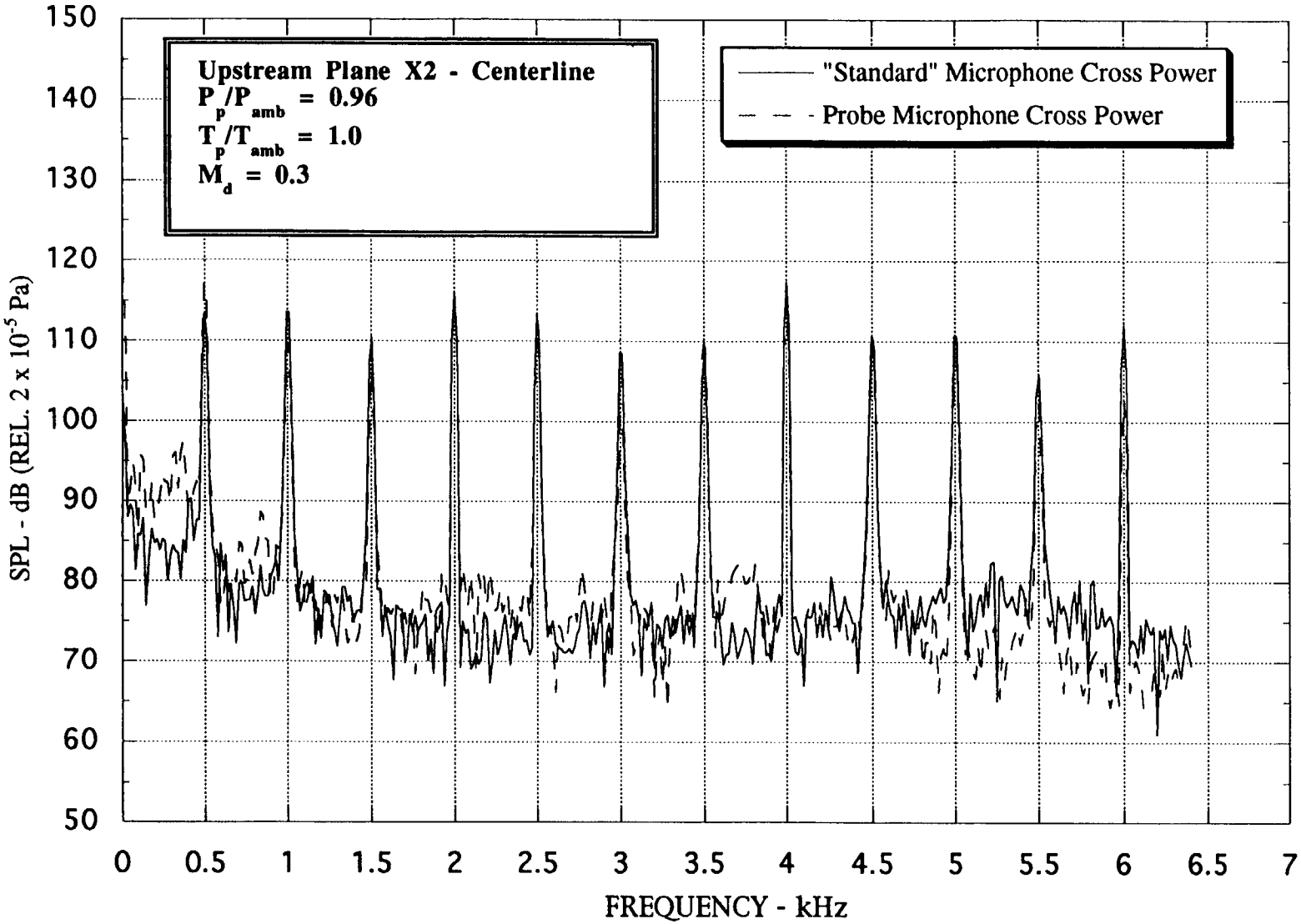

Figure 3.14 Cross power spectra for a probe microphone and a "standard" microphone placed in a mean flow ($M_d = 0.3$; $\Delta f = 16$ Hz; 64 avgs.).

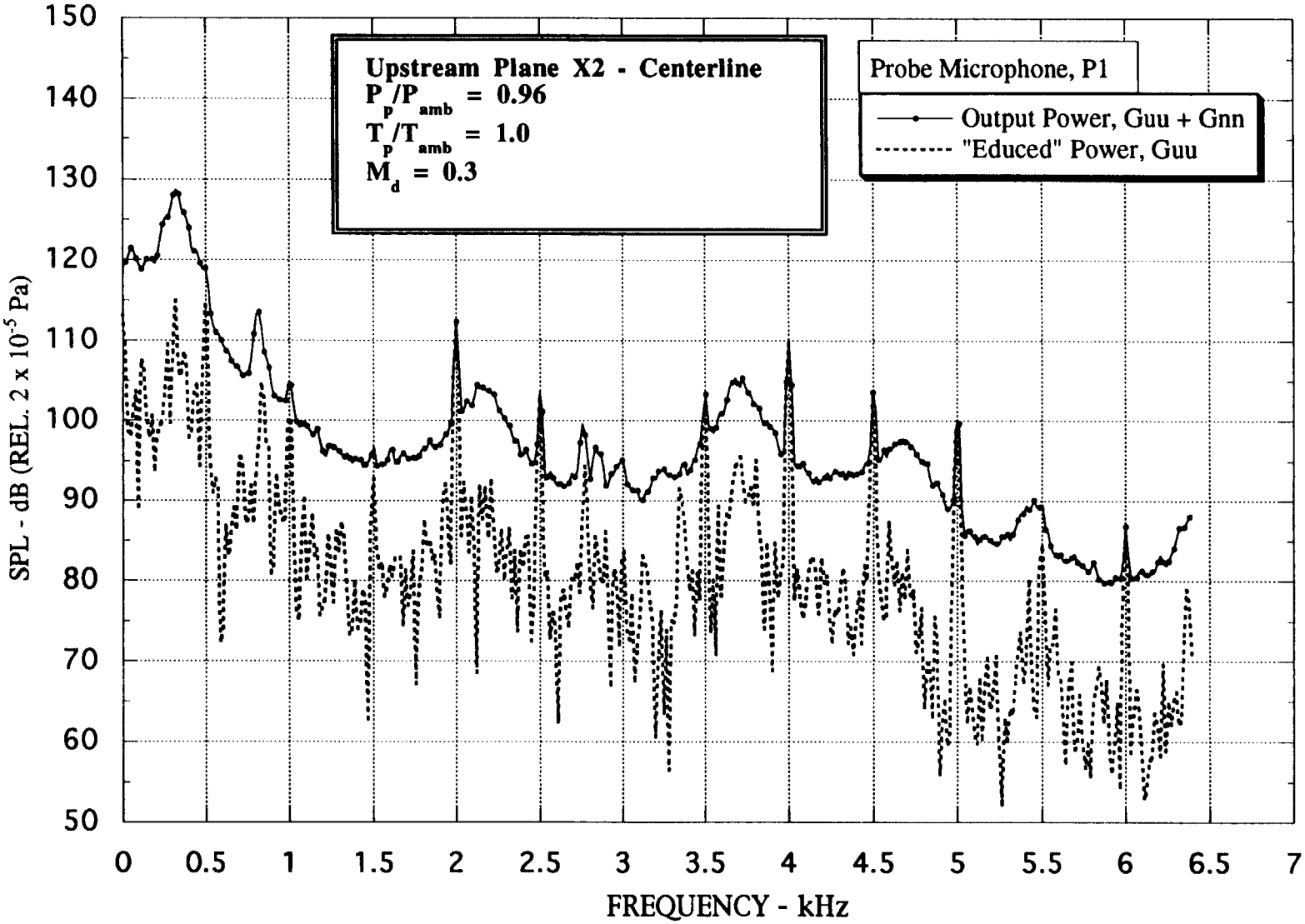

Figure 3.15 Comparison of output power and educed power spectra for a probe microphone placed in a mean flow ($M_d = 0.3$; $\Delta f = 16$ Hz; 64 avgs.).

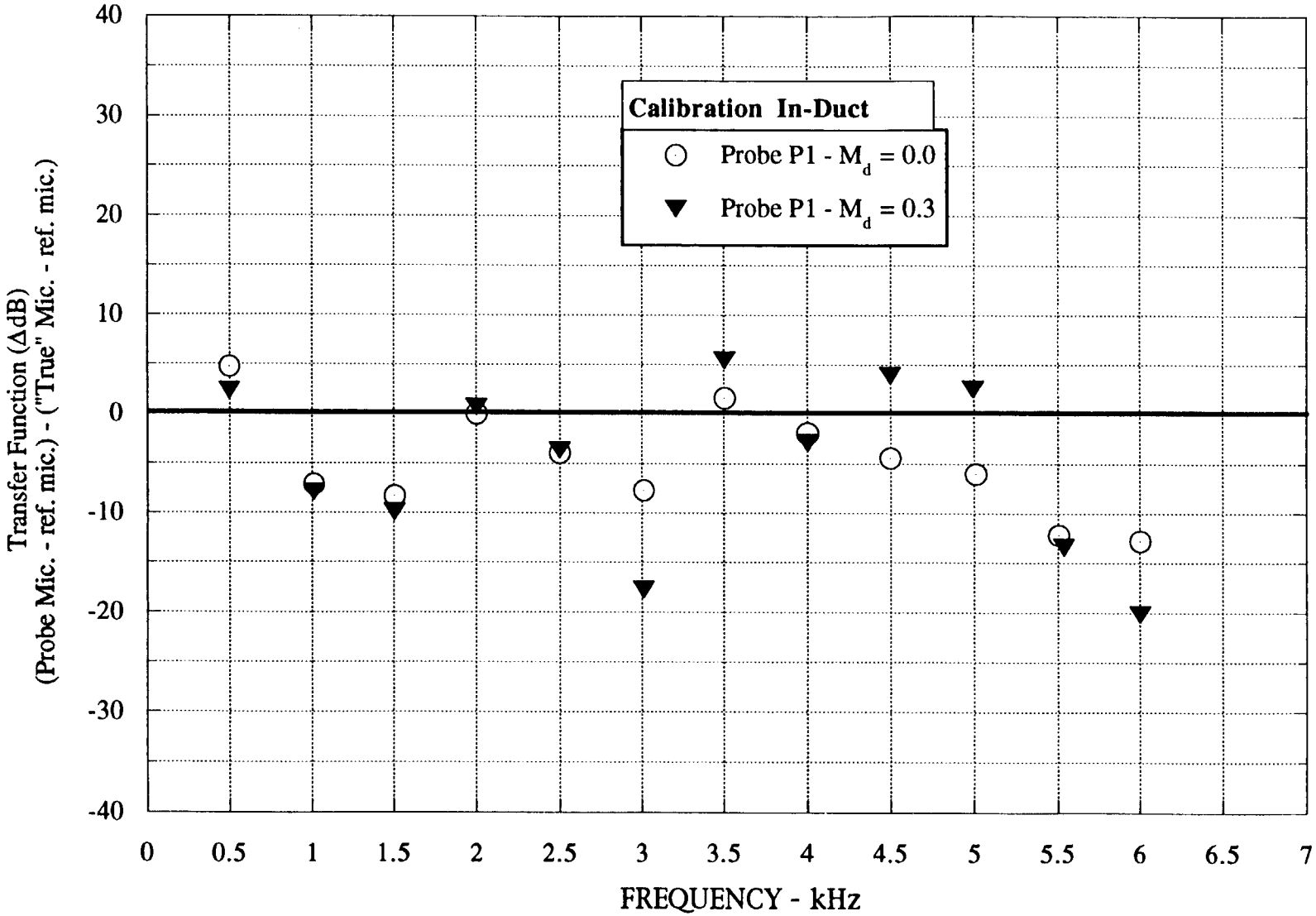

Figure 3.16 Calibration transfer function for a probe microphone placed in a mean flow using a multitone input signal (M_d = 0.3; Δf = 16 Hz; 64 avgs.).

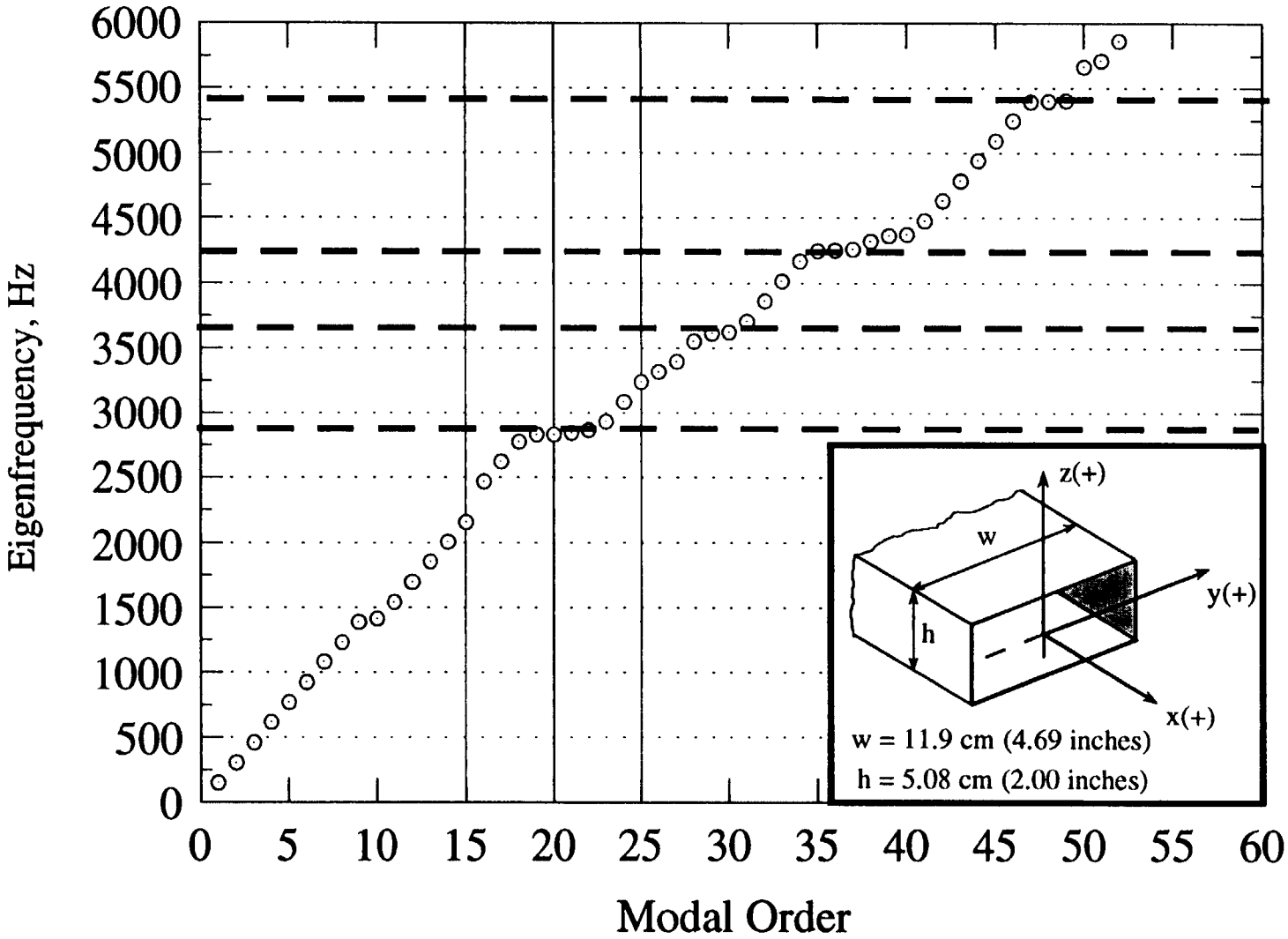

Figure 3.17 Resonant frequencies corresponding to the flow-duct dimensions tested in this study.

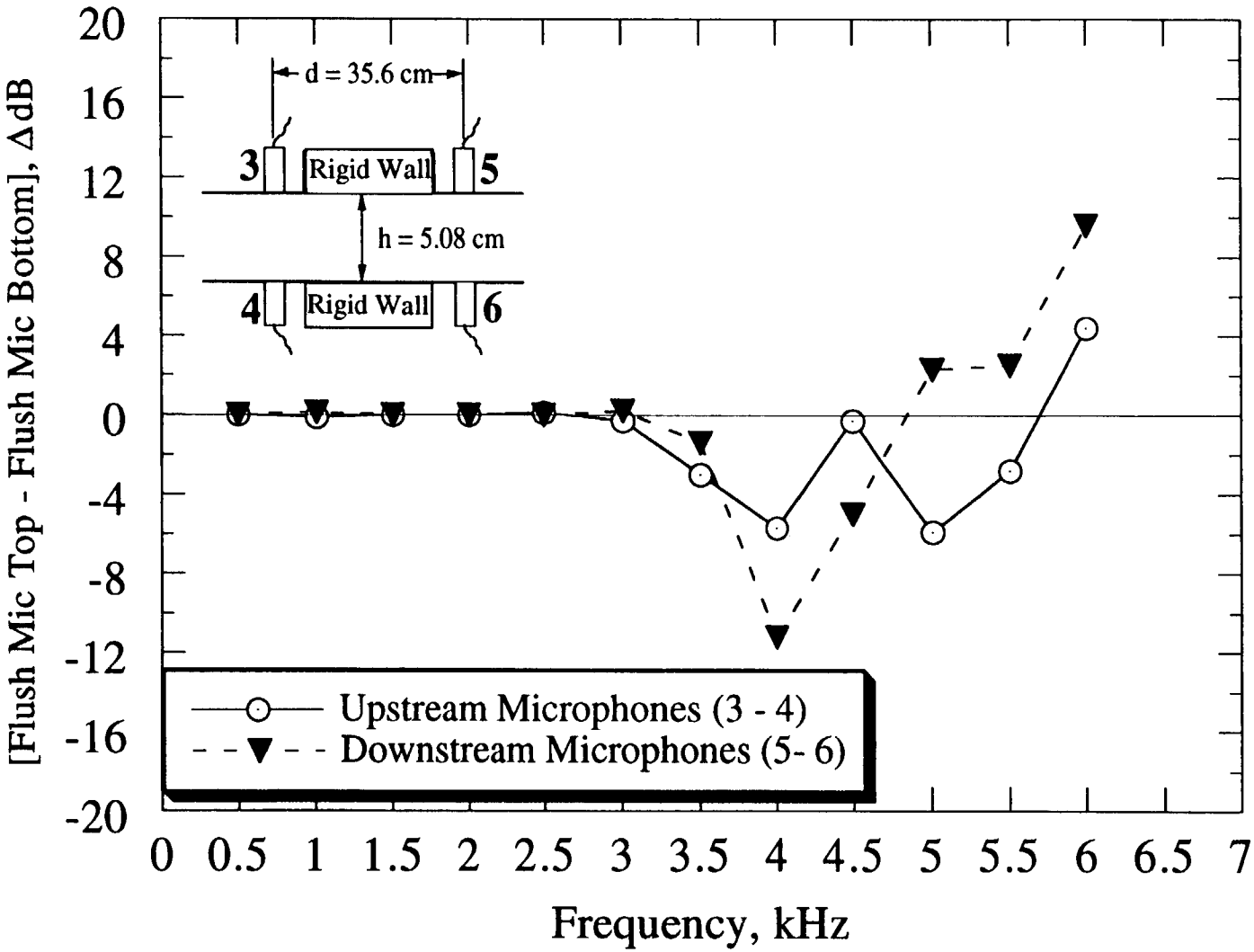

Figure 3.18 Sound pressure level differences between top and bottom of duct walls for an unlined duct ($M_d = 0.0$; $\Delta f = 16$ Hz; 64 avgs.).

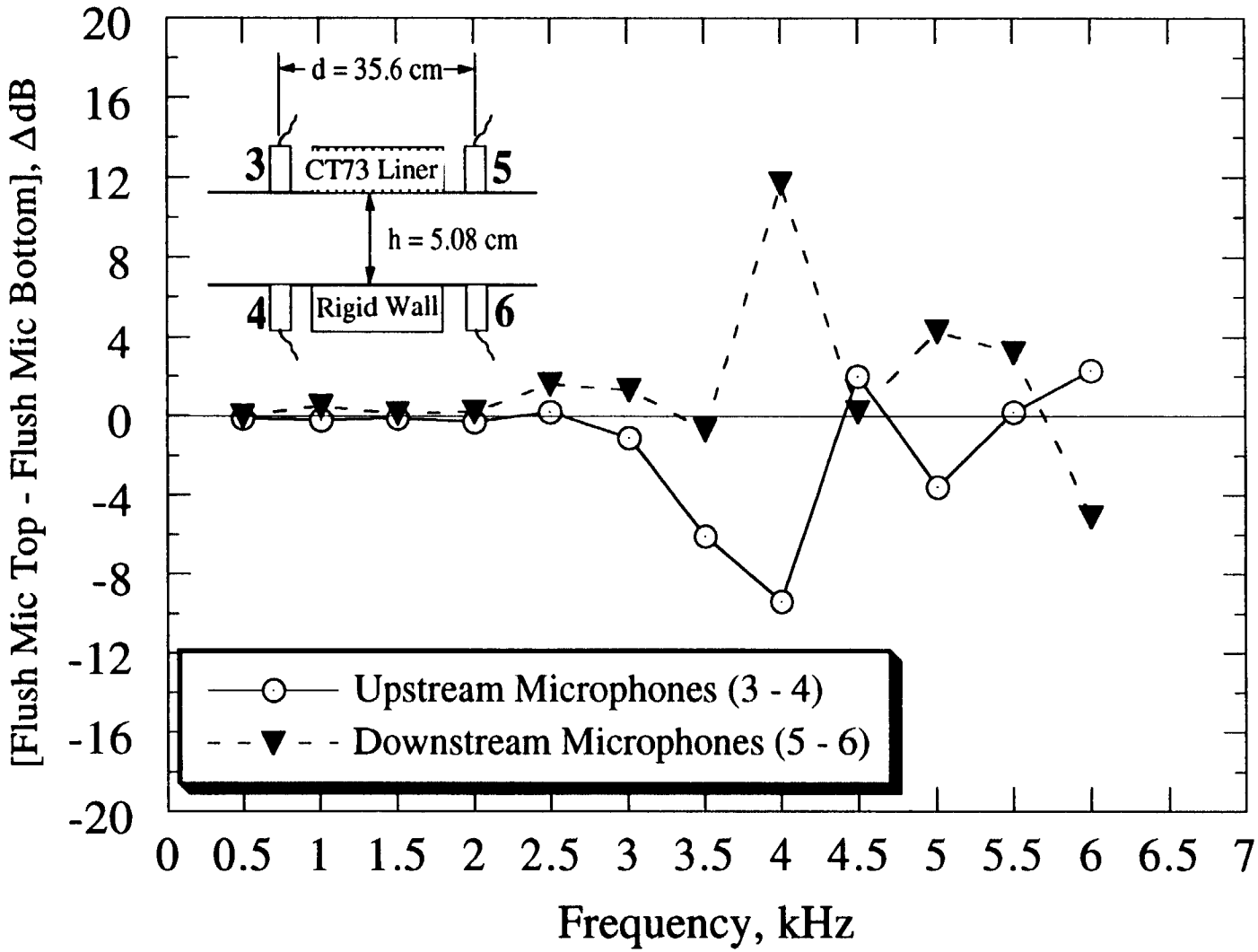

Figure 3.19 Sound pressure level differences between top and bottom of duct walls for a lined duct (M_d = 0.0; Δf = 16 Hz; 64 avgs.).

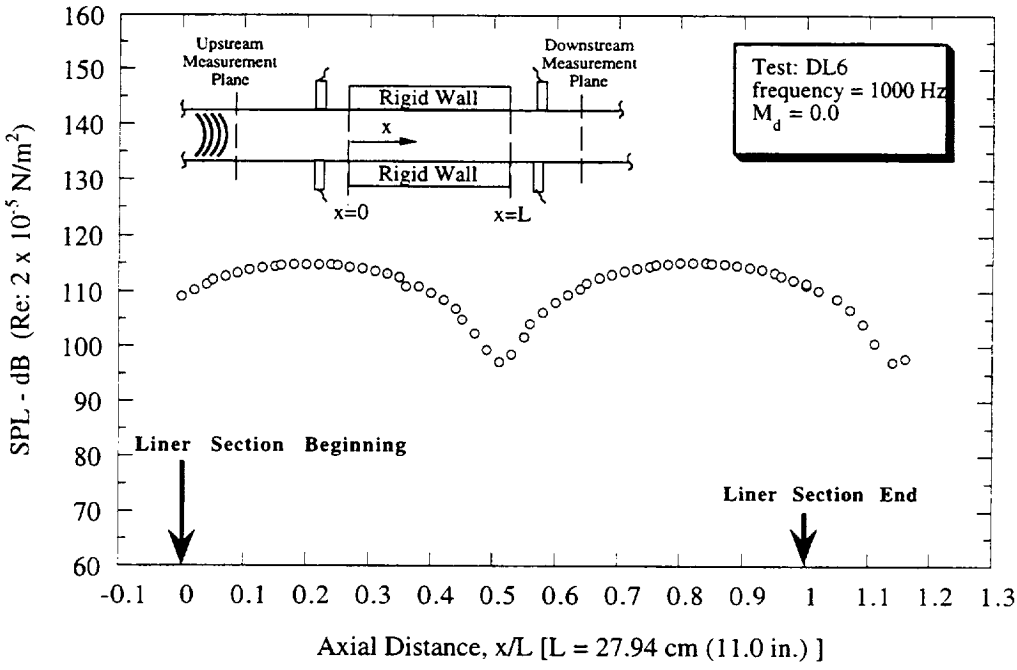

(a) An unlined duct

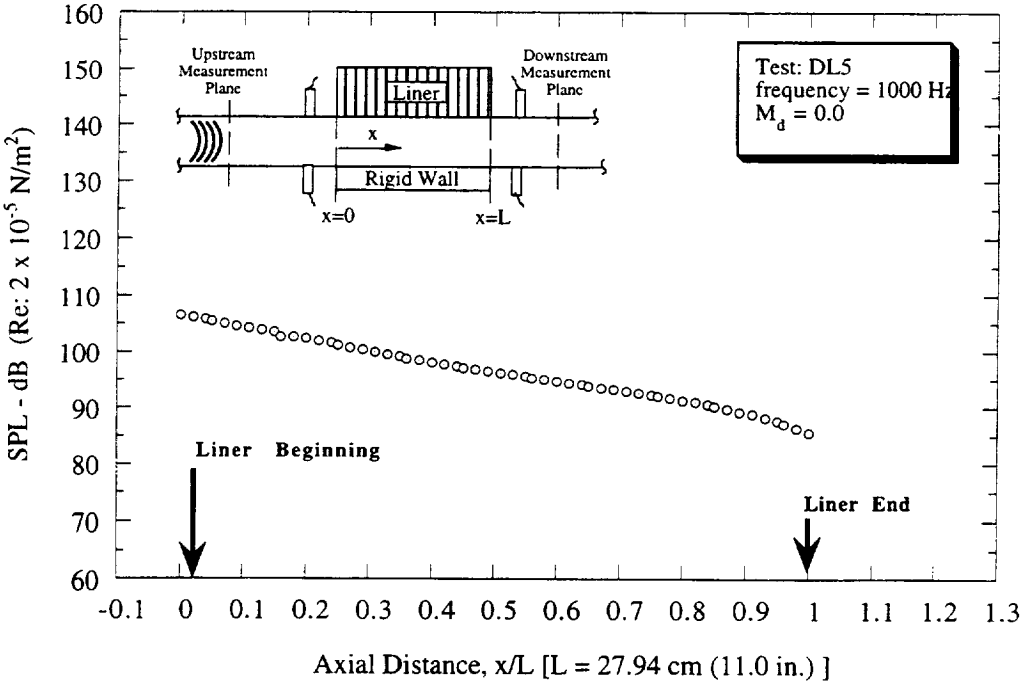

(b) A lined duct

Figure 3.20 Typical axial centerline acoustic sound pressure levels at a frequency of 1000 Hz (M_d = 0.0; Δf = 16 Hz; 64 avgs).

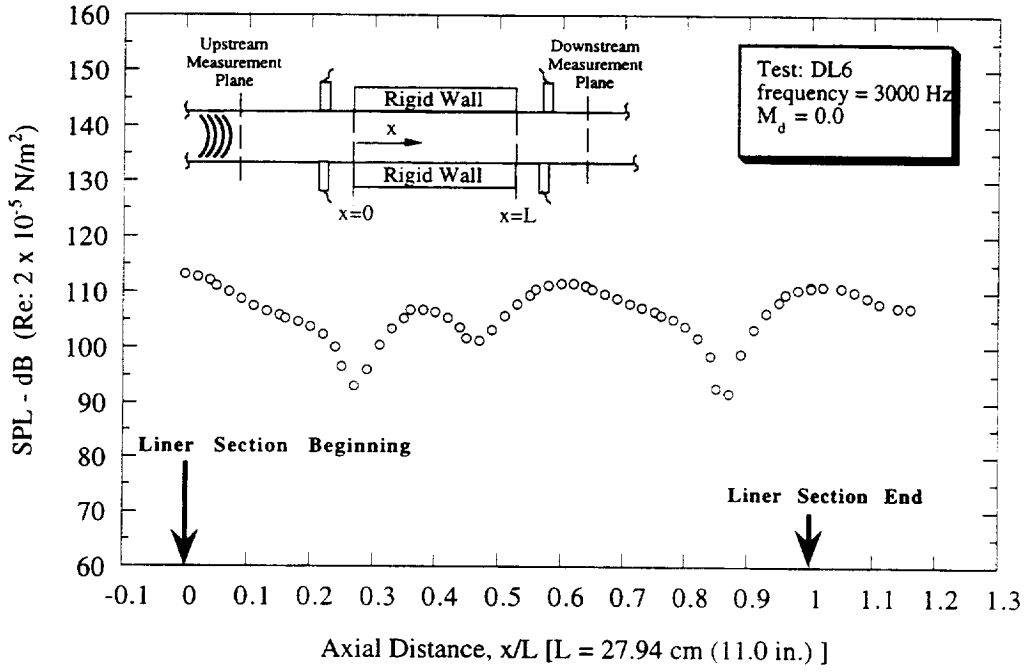

(a) An unlined duct

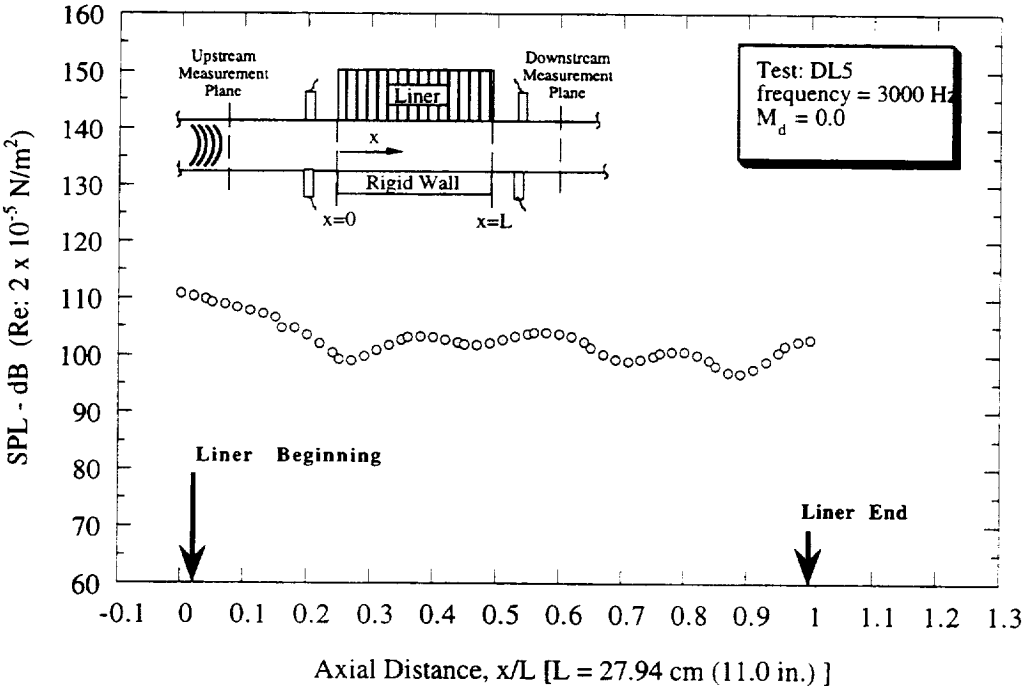

(b) A lined duct

Figure 3.21 Typical axial centerline acoustic sound pressure levels at a frequency of 3000 Hz (M_d = 0.0; Δf = 16 Hz; 64 avgs).

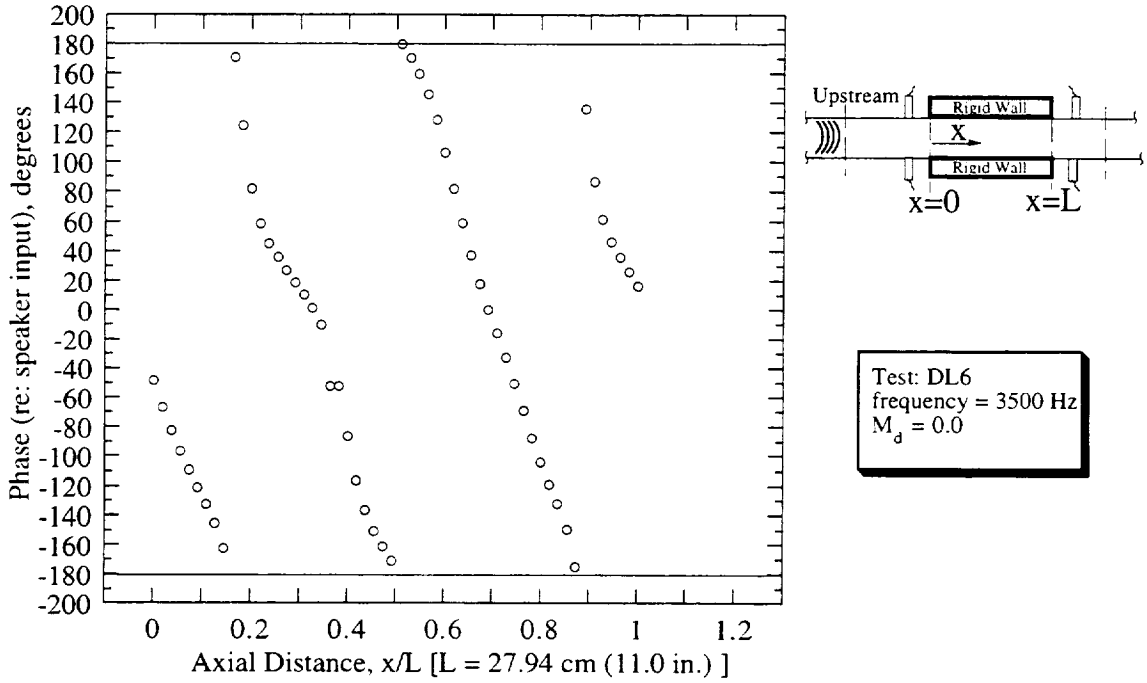

(a) An unlined duct

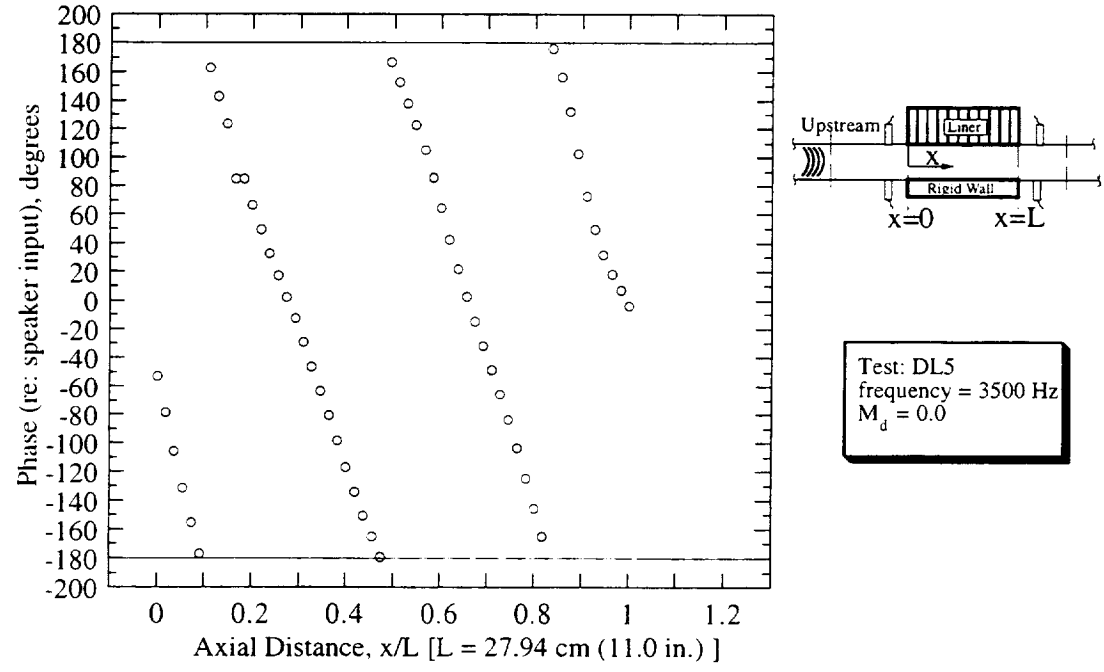

(b) A lined duct

Figure 3.22 Typical axial centerline phase data at a frequency of 3500 Hz (Md = 0.0; Df = 16 Hz; 64 avgs.).

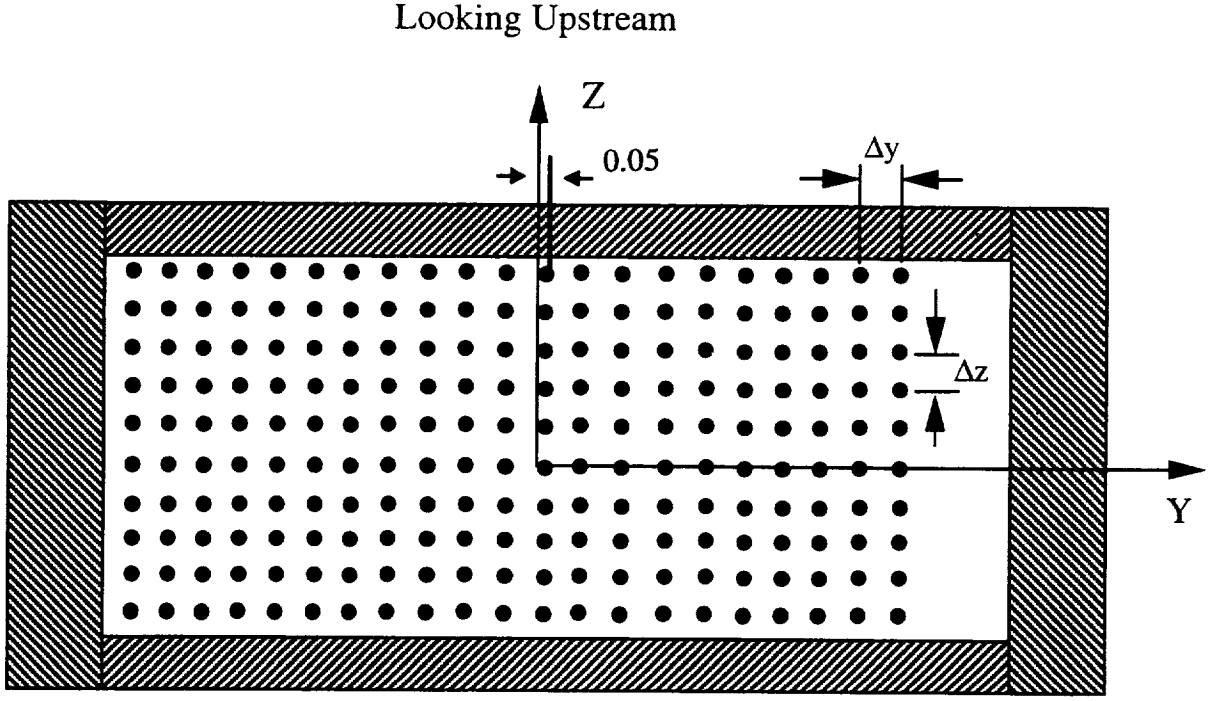

$\Delta z = 0.20$ in.
$\Delta y = 0.20$ in.

Figure 3.23 Typical grid of acoustic measurement locations in flow-duct facility.

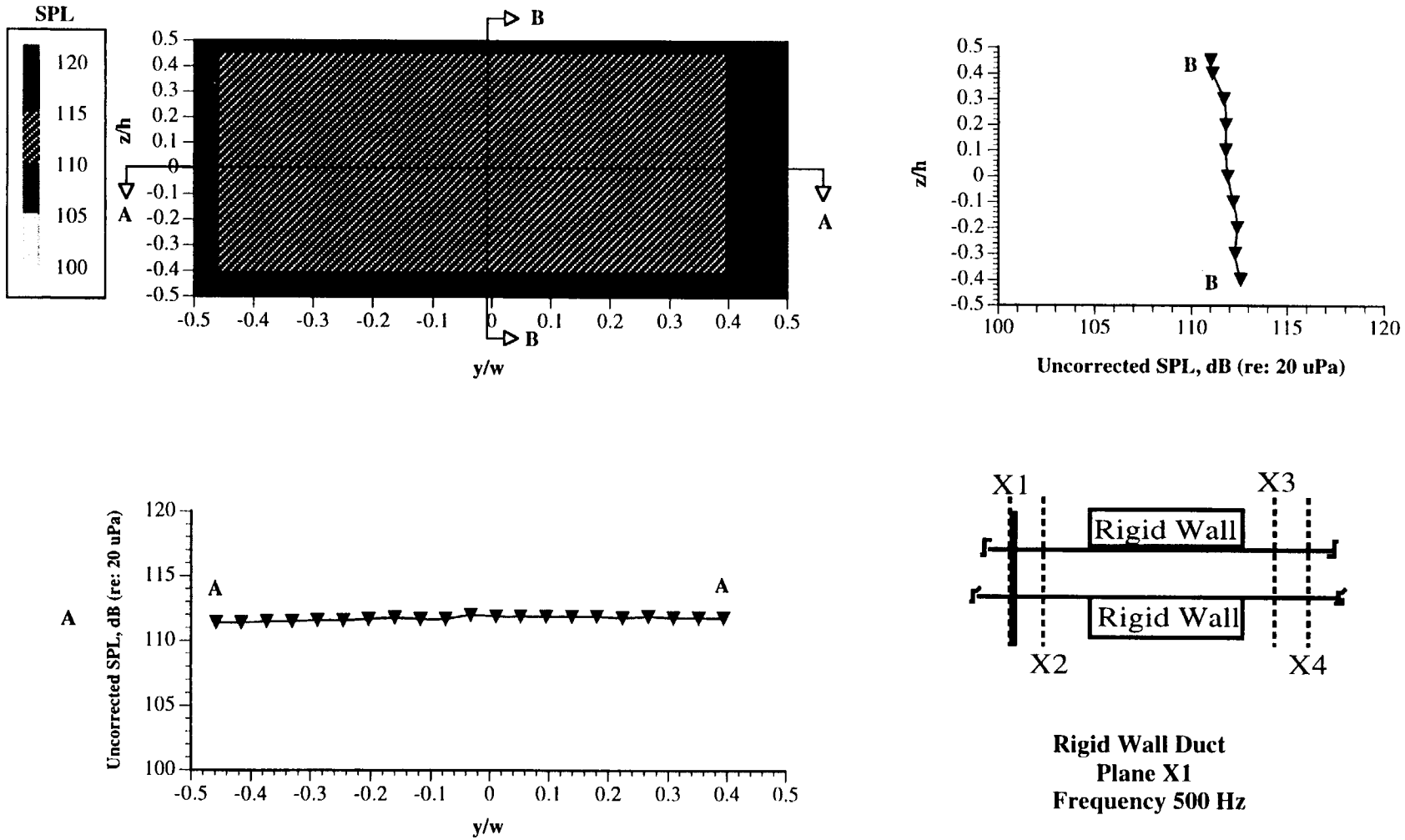

Figure 3.24 Typical planar acoustic sound pressure levels at 500 Hz at plane X1 for an unlined duct (M_d = 0.0; Δf = 16 Hz; 64 avgs.).

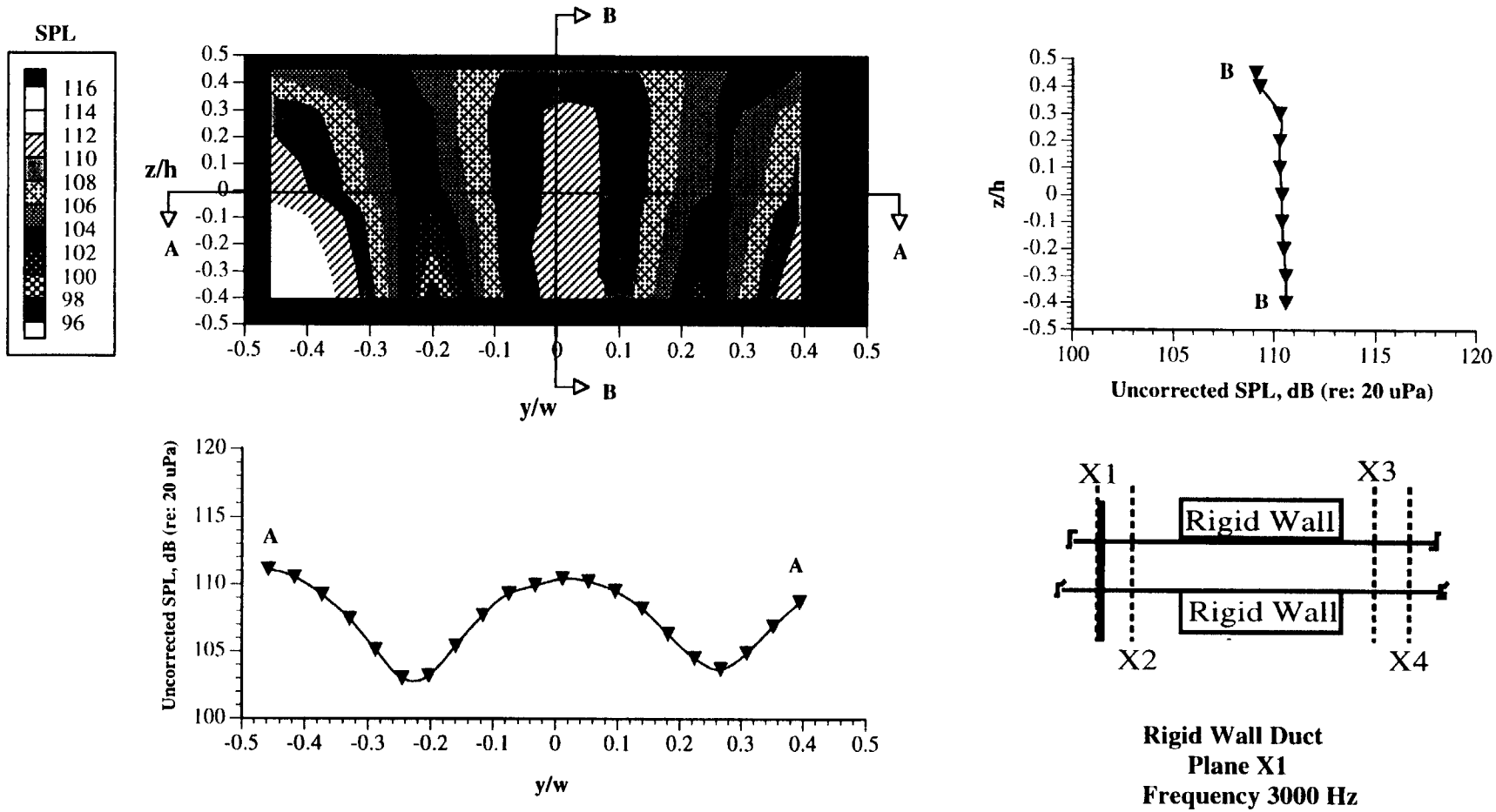

Figure 3.25 Typical planar acoustic sound pressure levels at 3000 Hz at plane X1 for an unlined duct ($M_d = 0.0$; $\Delta f = 16$ Hz; 64 avgs.).

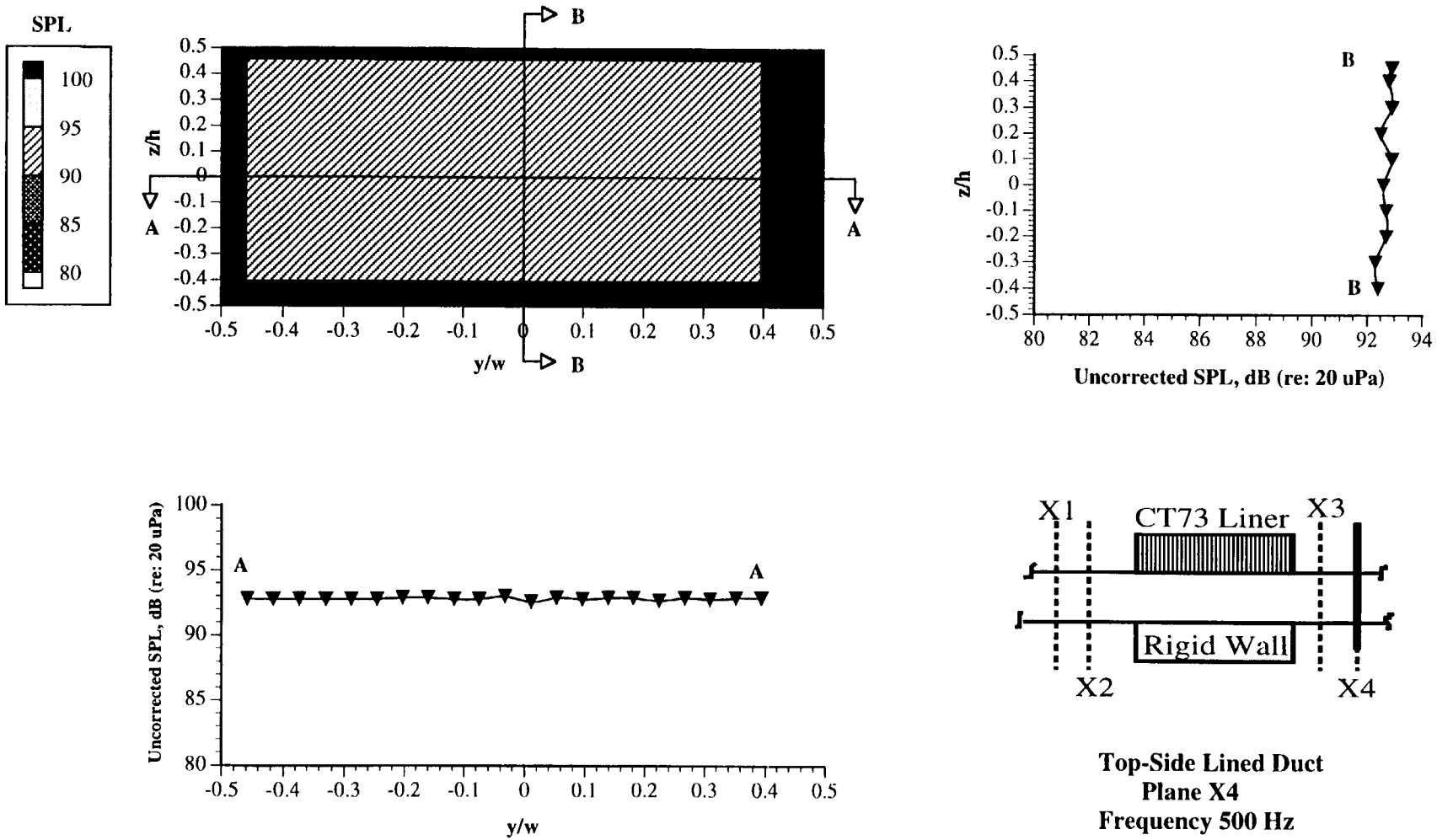

Figure 3.26 Typical planar acoustic sound pressure levels at 500 Hz at plane X4 for a lined duct ($M_d = 0.0$; $\Delta f = 16$ Hz; 64 avgs.).

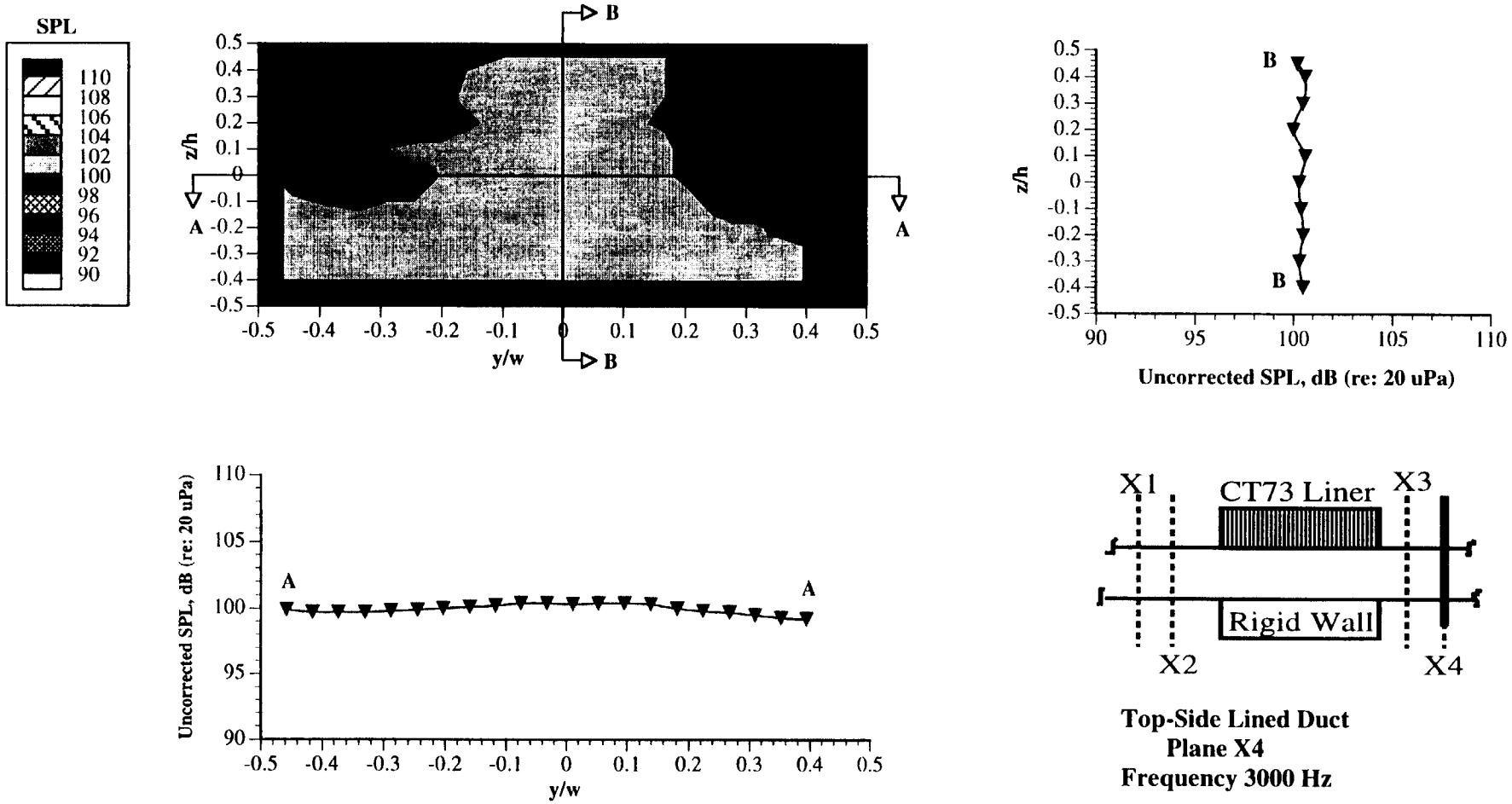

Figure 3.27 Typical planar acoustic sound pressure levels at 3000 Hz at plane X4 for a lined duct (M_d = 0.0; Δf = 16 Hz; 64 avgs.).

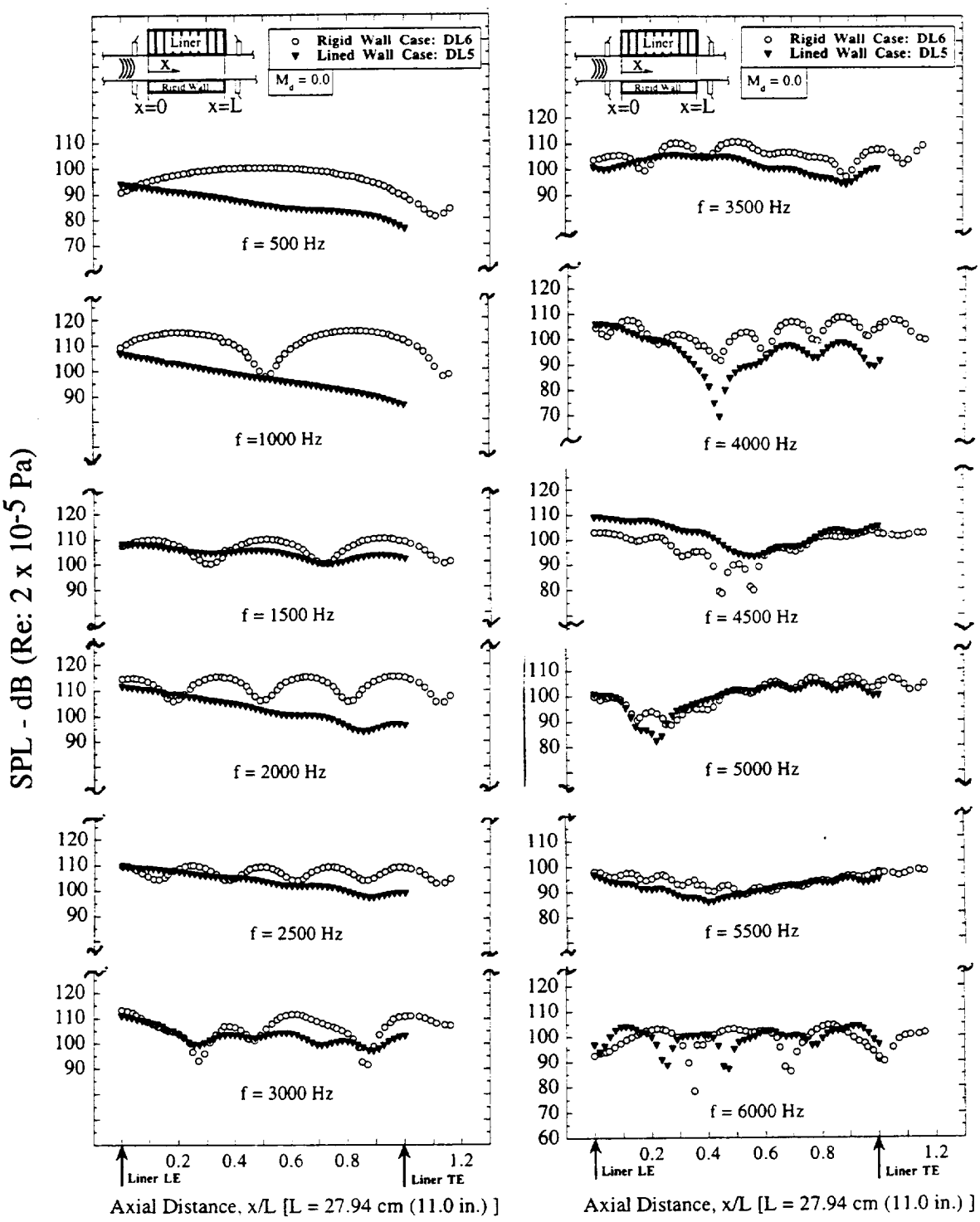

Figure 4.1 Sound pressure levels along axial centerline for rigid-wall duct and lined duct at selected frequencies (M_d = 0.0; Δf = 16 Hz; 64 avgs.).

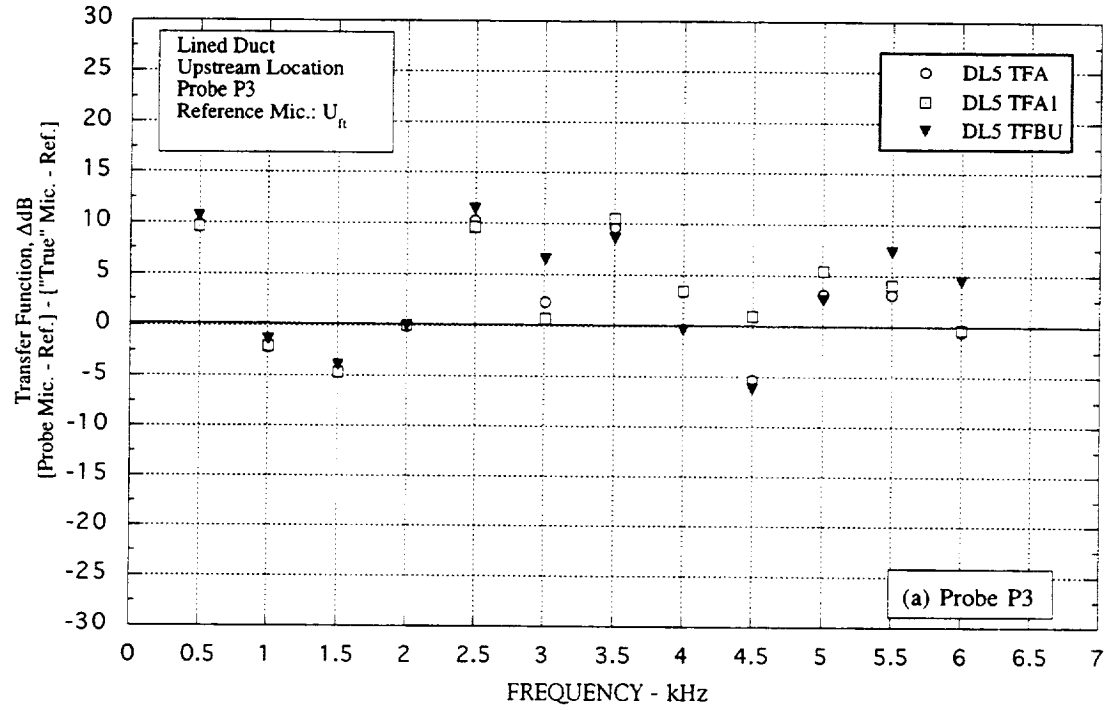

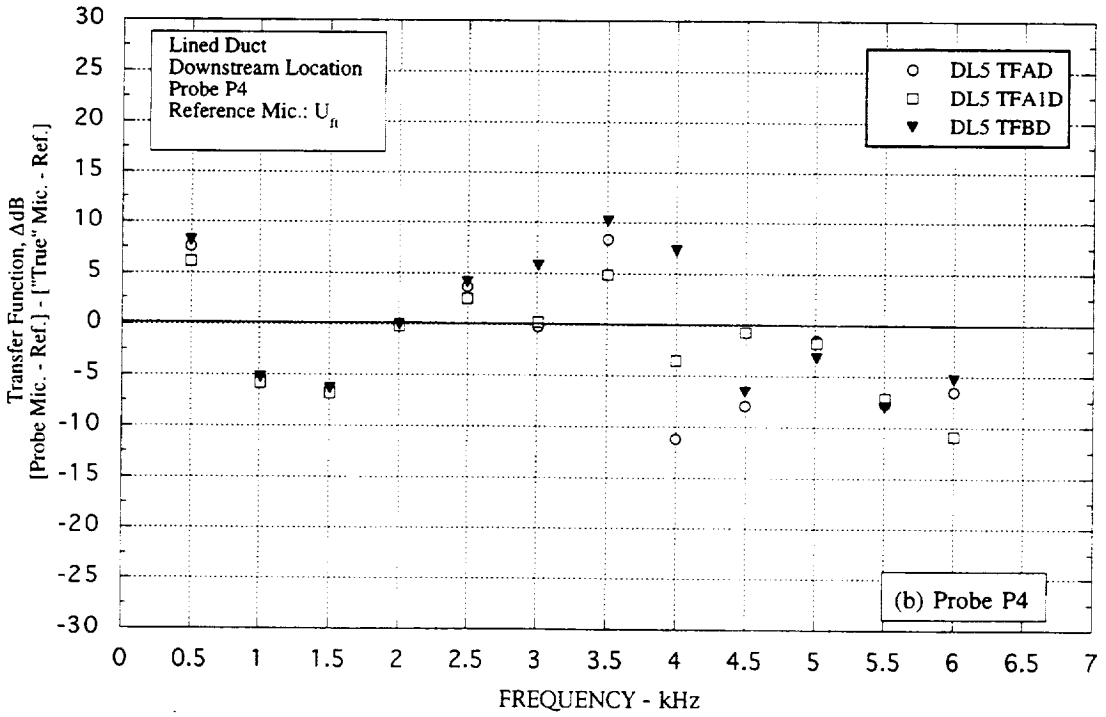

Figure 4.2 Lined wall in-duct calibrations for upstream and downstream probe microphones ($M_d = 0.0$; $\Delta f = 16$ Hz; 64 avgs.).

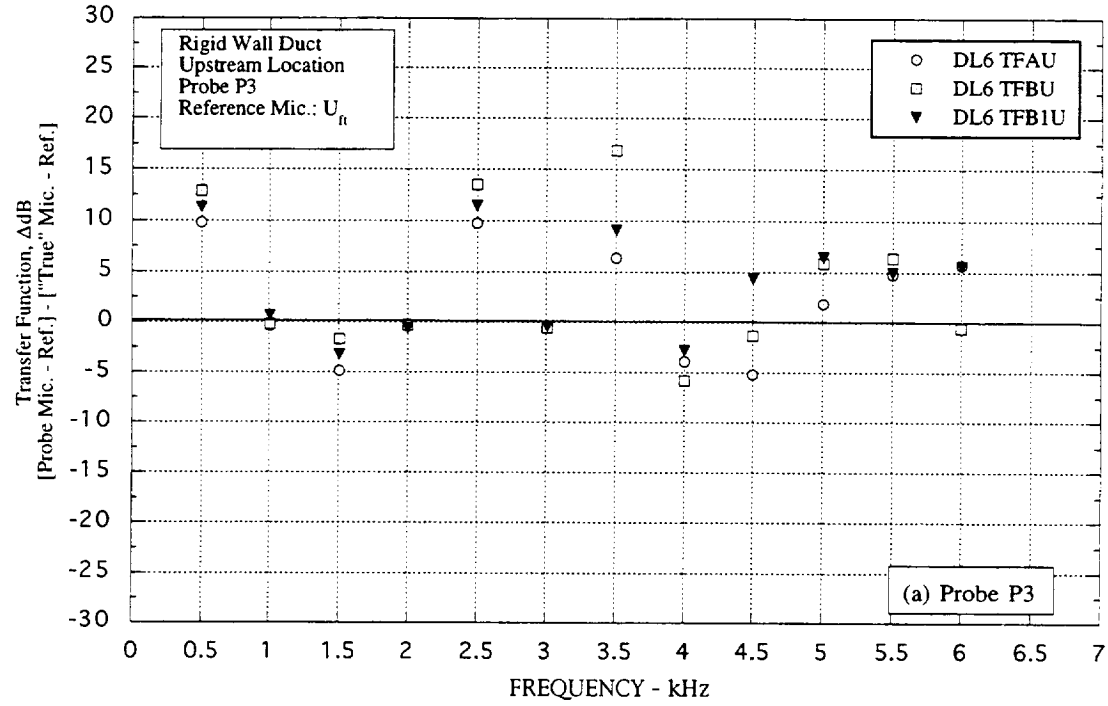

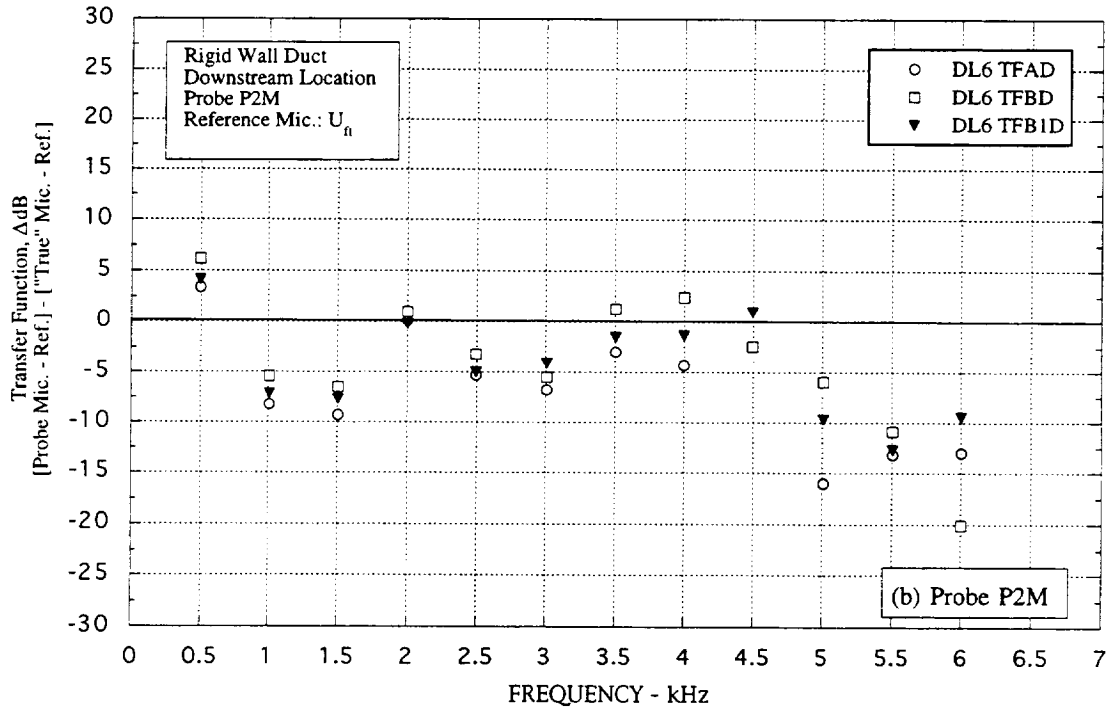

Figure 4.3 Rigid wall in-duct calibrations for upstream and downstream probe microphones ($M_d = 0.0$; $\Delta f = 16$ Hz; 64 avgs.).

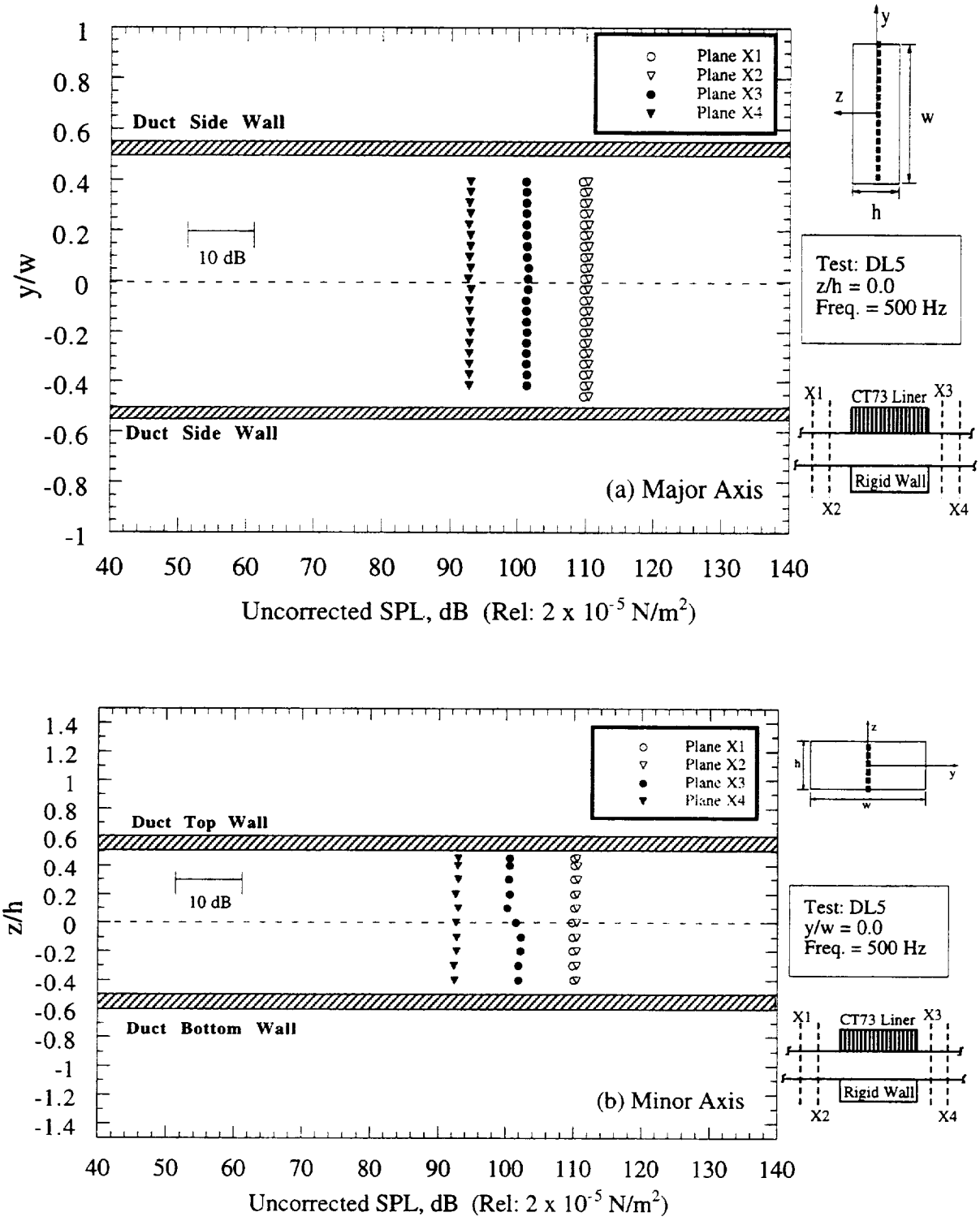

Figure 4.4 Uncorrected sound pressure levels for the lined duct at f = 500 Hz in upstream and downstream planes (M_d = 0.0; Δf = 16 Hz; 64 avgs.).

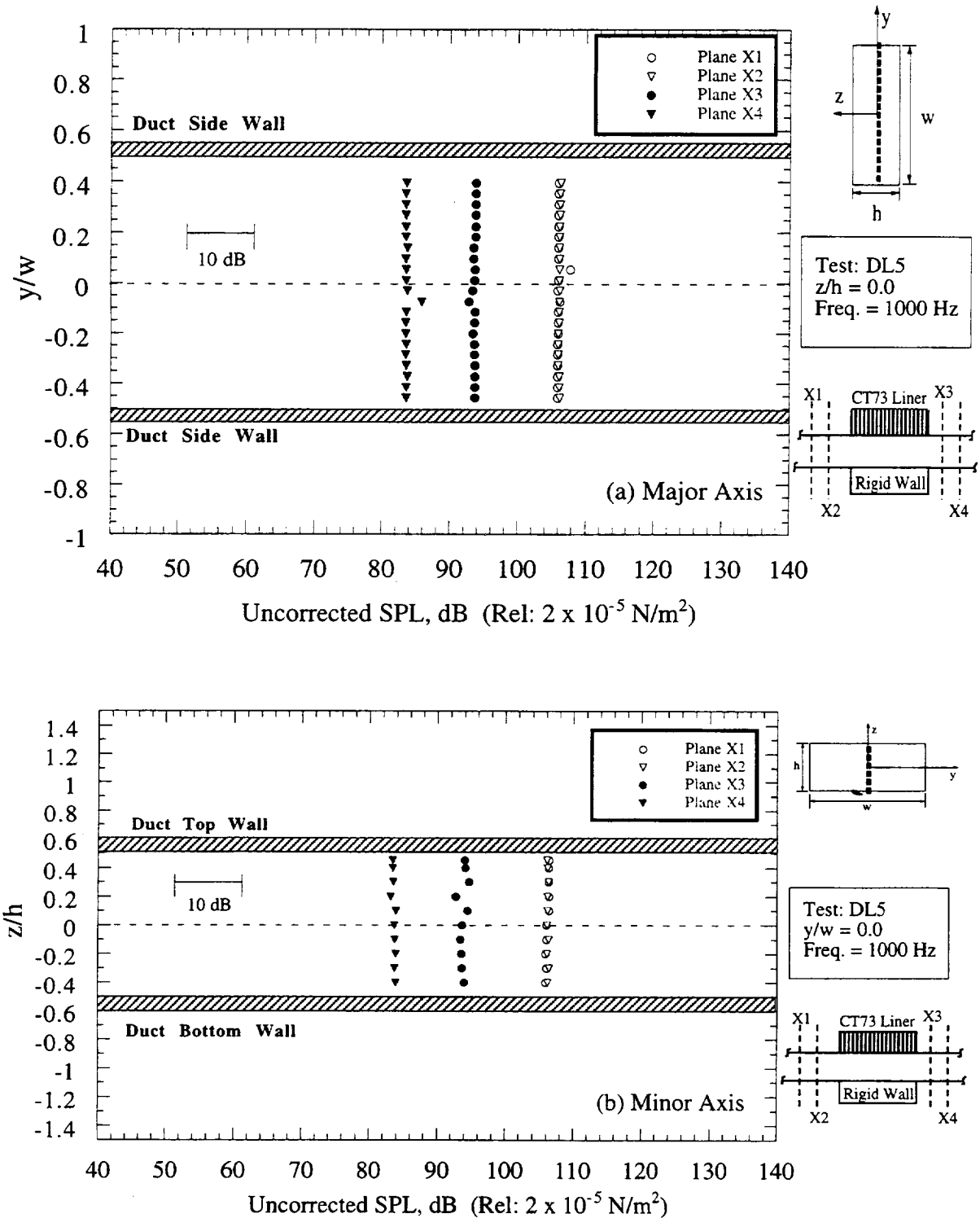

Figure 4.5 Uncorrected sound pressure levels for the lined duct at f = 1000 Hz in upstream and downstream planes (M_d = 0.0; Δf = 16 Hz; 64 avgs.).

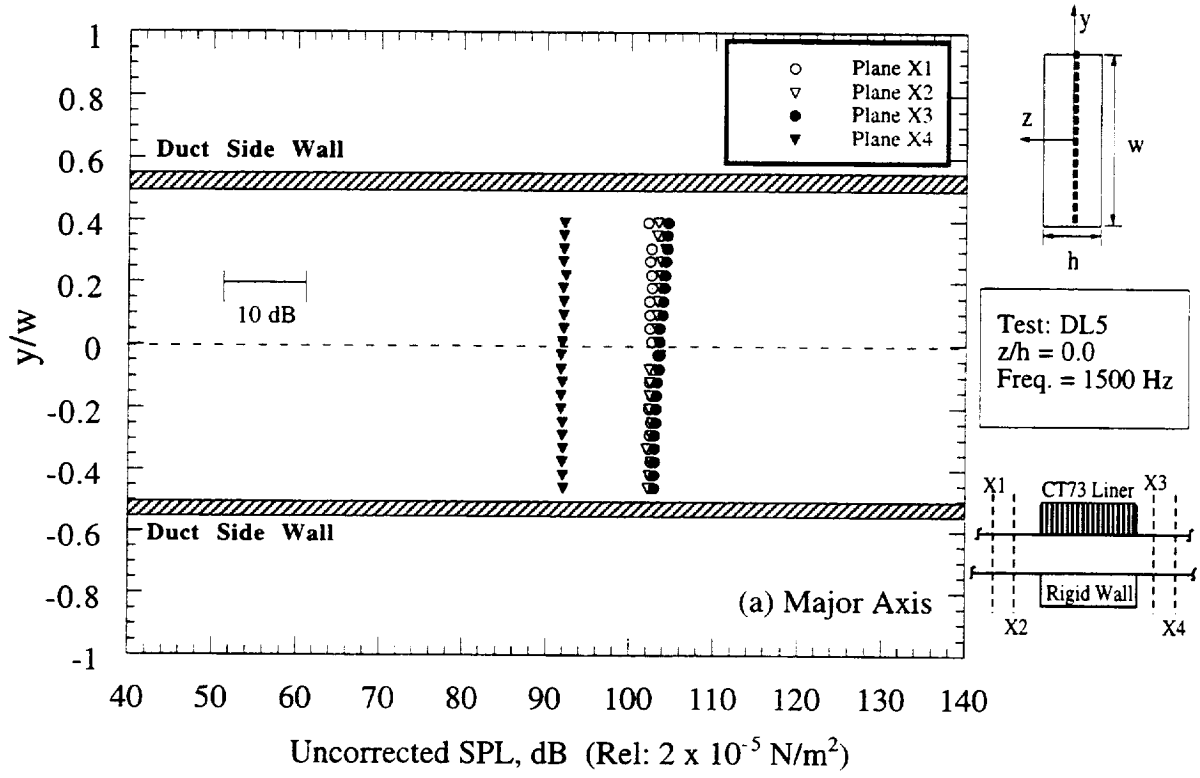

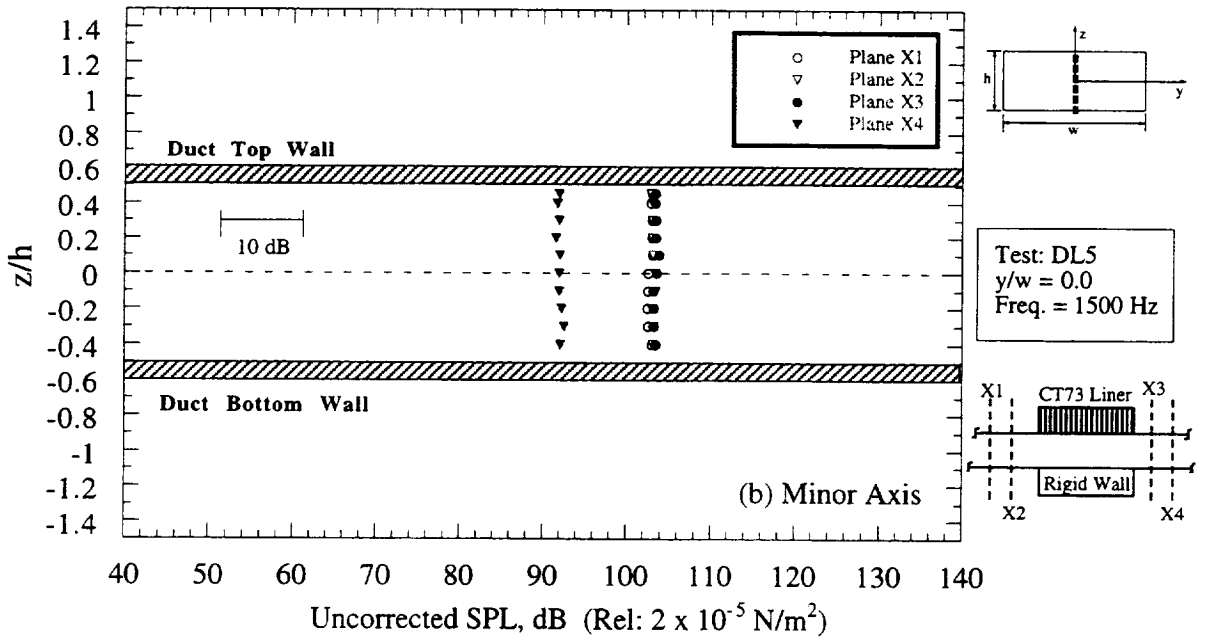

Figure 4.6 Uncorrected sound pressure levels for the lined duct at f = 1500 Hz in upstream and downstream planes (M_d = 0.0; Δf = 16 Hz; 64 avgs.).

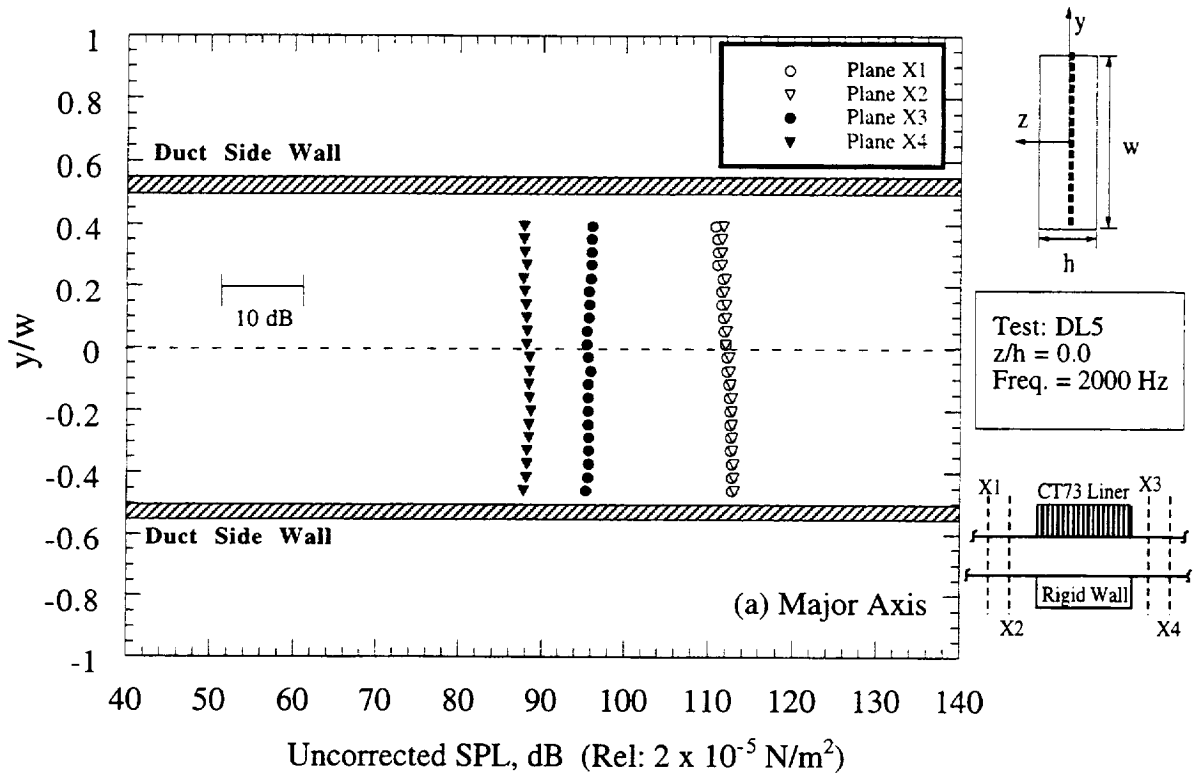

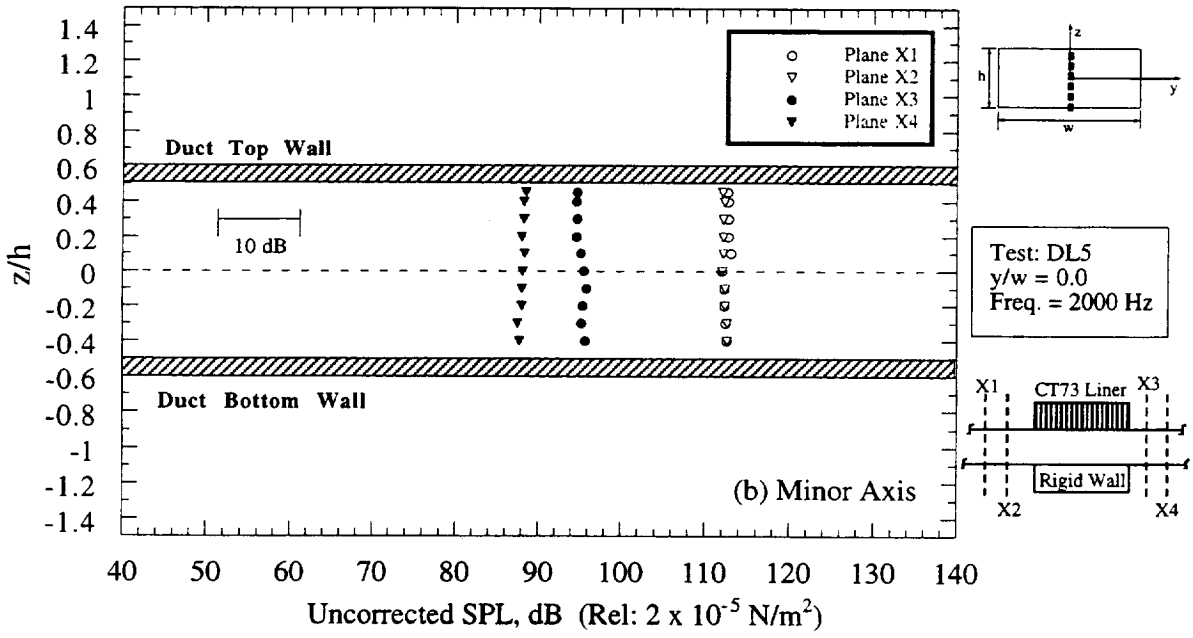

Figure 4.7 Uncorrected sound pressure levels for the lined duct at f = 2000 Hz in upstream and downstream planes (M_d = 0.0; Δf = 16 Hz; 64 avgs.).

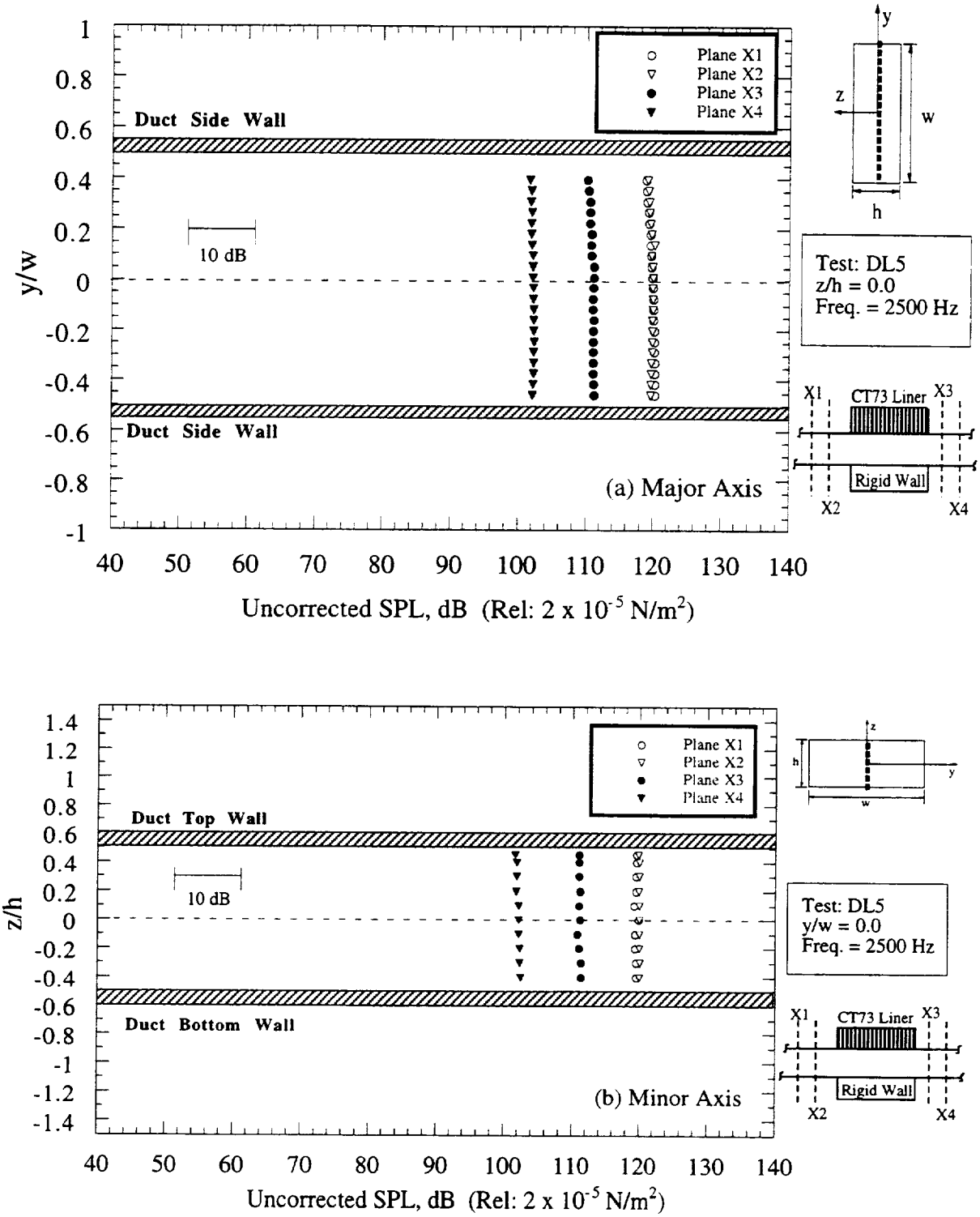

Figure 4.8 Uncorrected sound pressure levels for the lined duct at f = 2500 Hz in upstream and downstream planes (M_d = 0.0; Δf = 16 Hz; 64 avgs.).

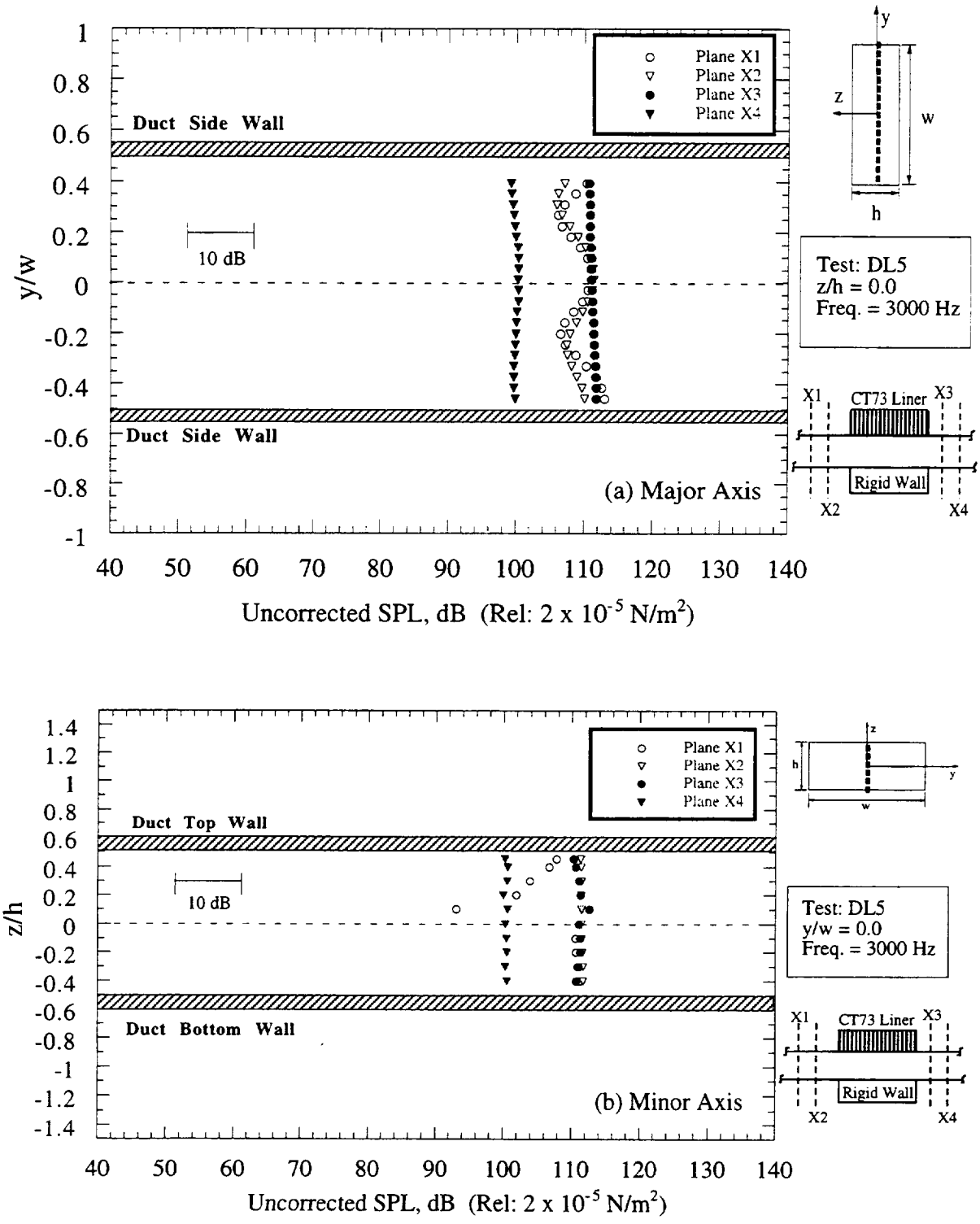

Figure 4.9 Uncorrected sound pressure levels for the lined duct at f = 3000 Hz in upstream and downstream planes (M_d = 0.0; Δf = 16 Hz; 64 avgs.).

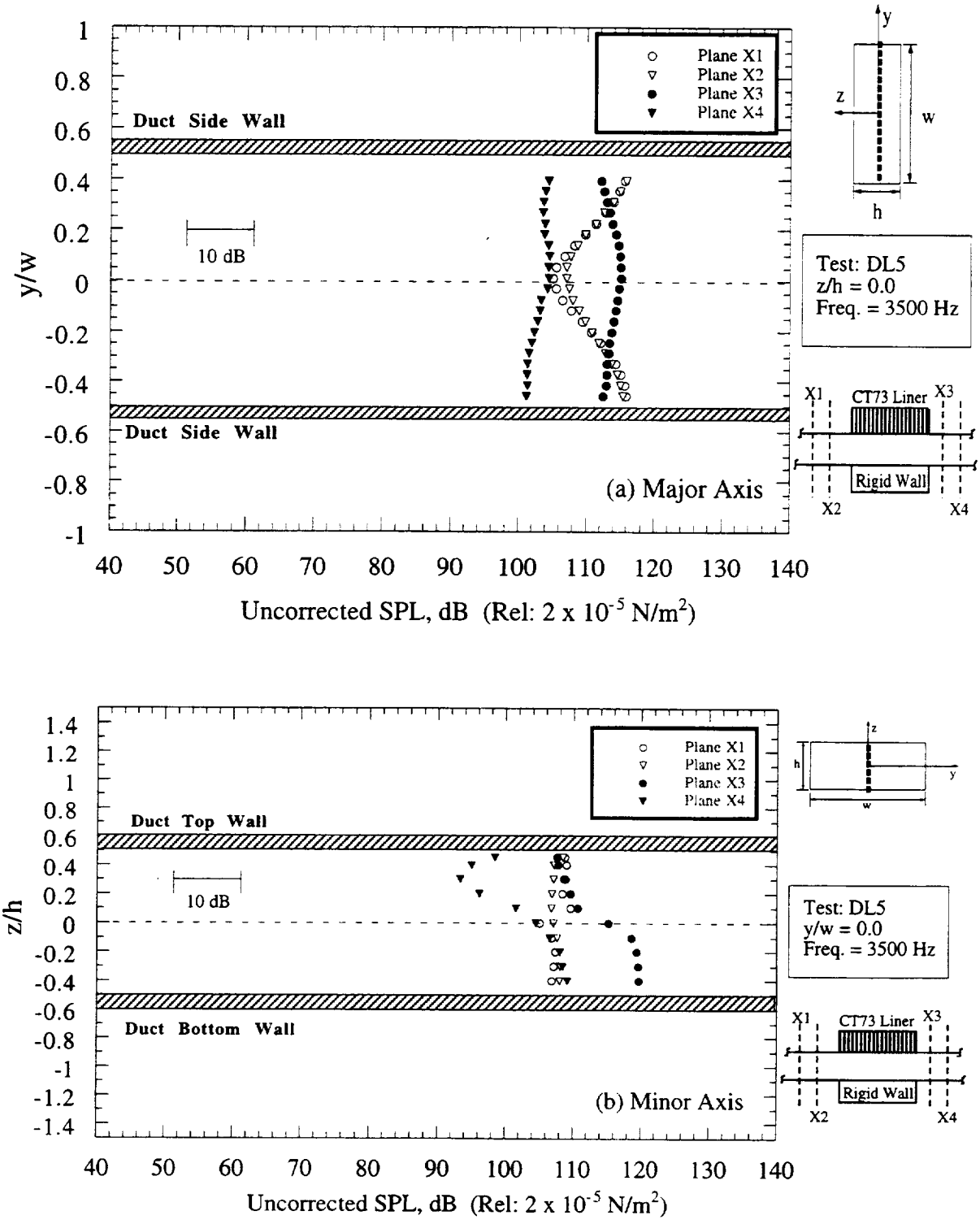

Figure 4.10 Uncorrected sound pressure levels for the lined duct at f = 3500 Hz in upstream and downstream planes (M_d = 0.0; Δf = 16 Hz; 64 avgs.).

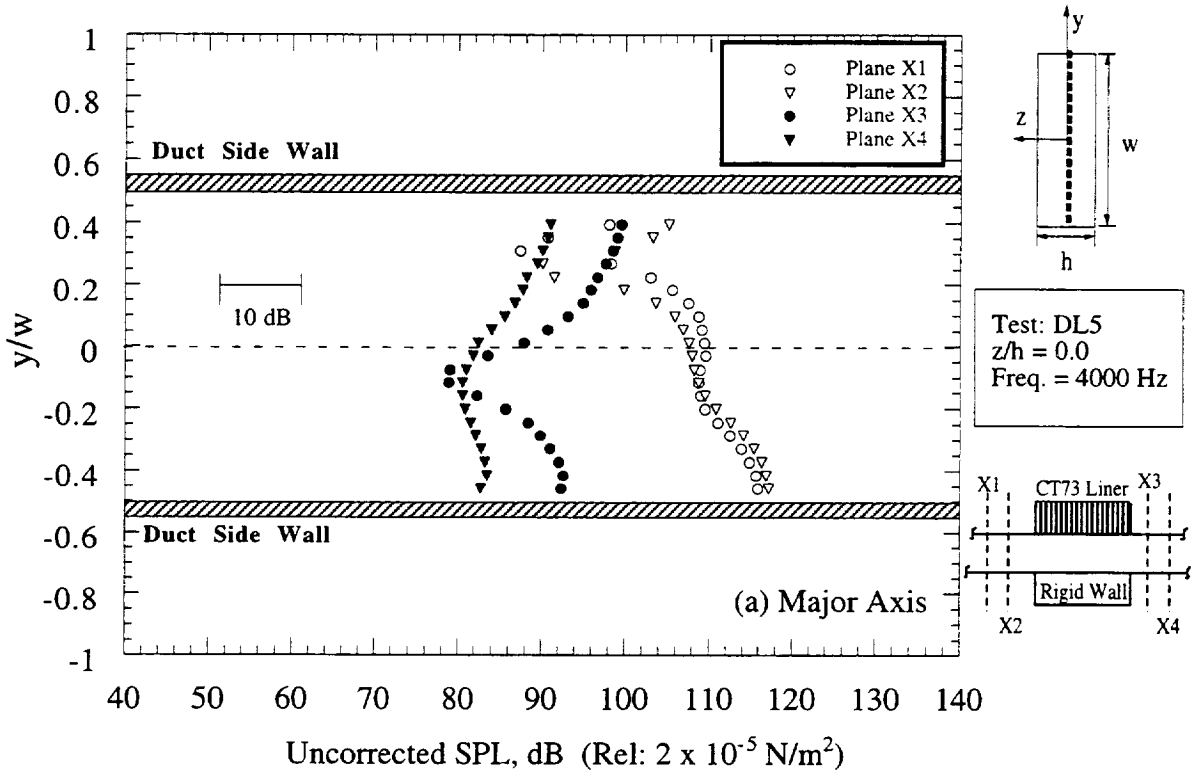

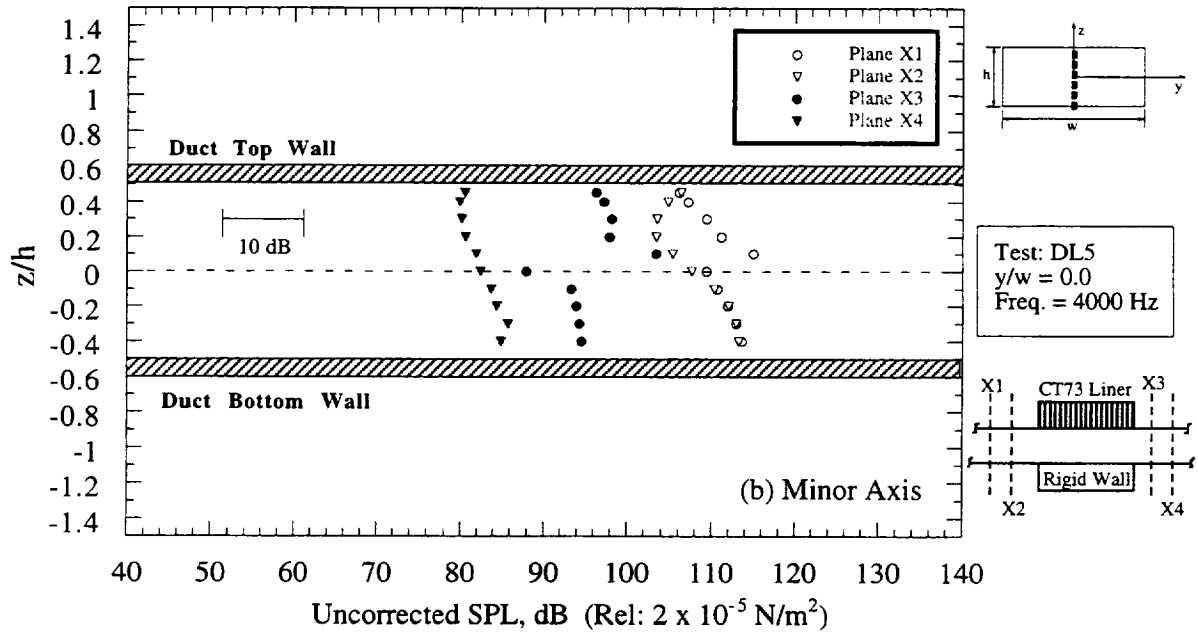

Figure 4.11 Uncorrected sound pressure levels for the lined duct at f = 4000 Hz in upstream and downstream planes (M_d = 0.0; Δf = 16 Hz; 64 avgs.).

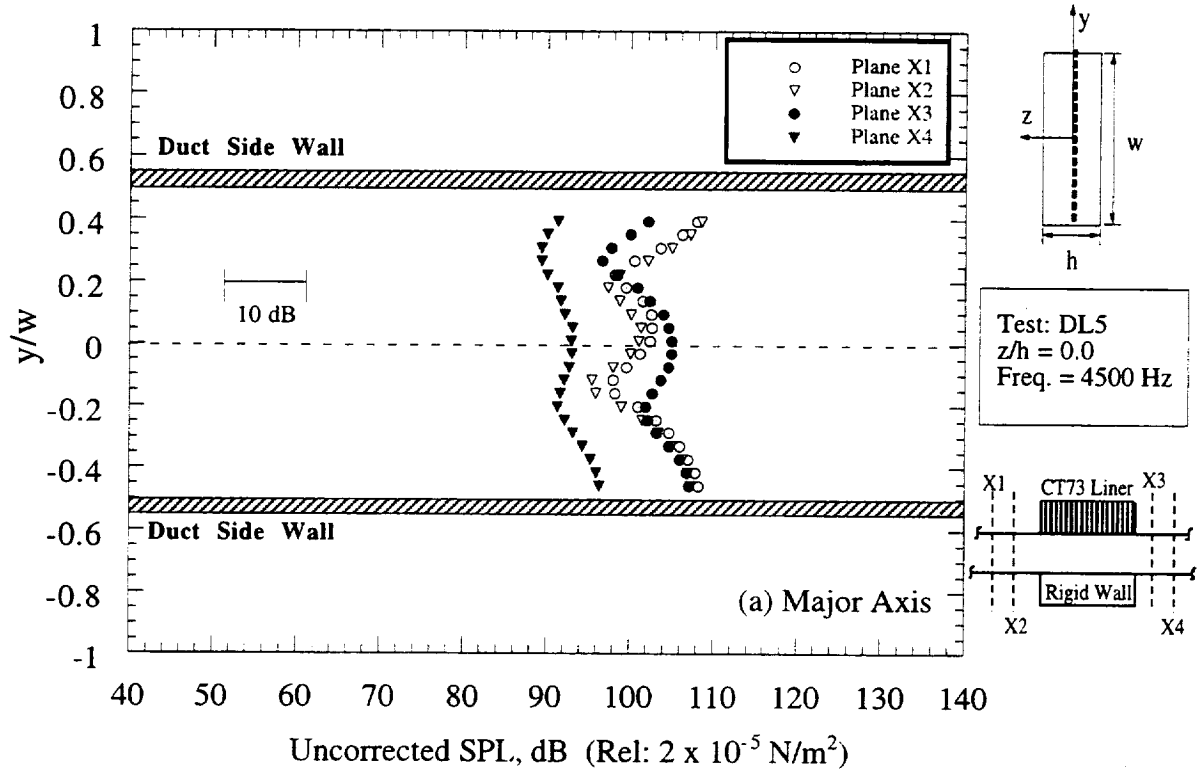

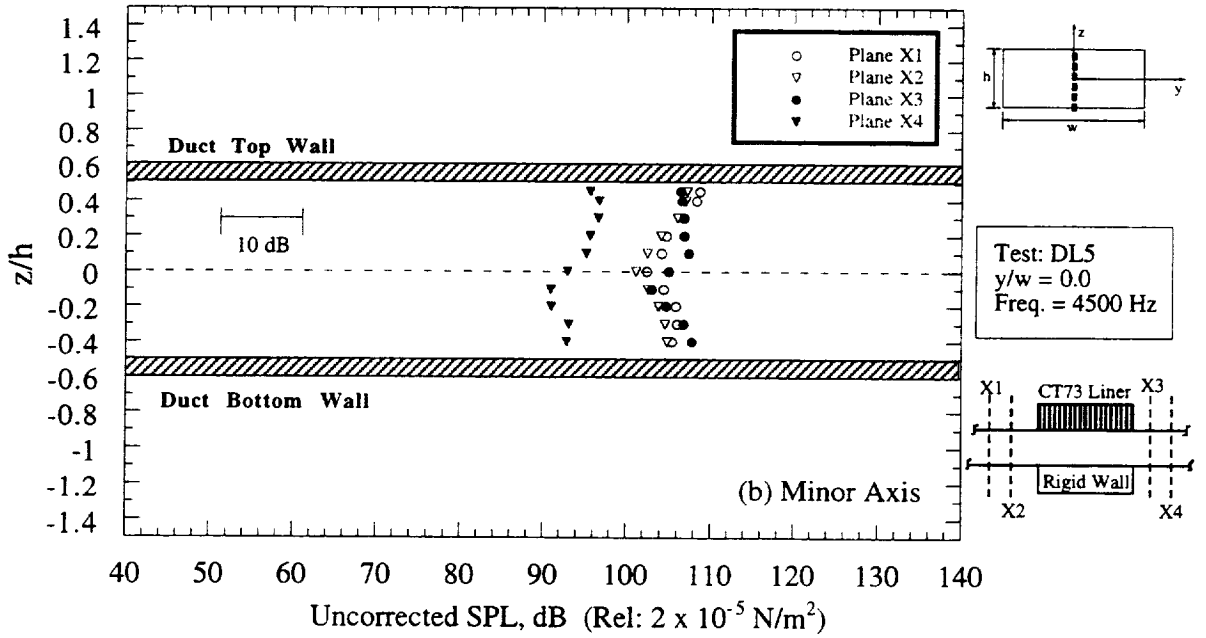

Figure 4.12 Uncorrected sound pressure levels for the lined duct at f = 4500 Hz in upstream and downstream planes (M_d = 0.0; Δf = 16 Hz; 64 avgs.).

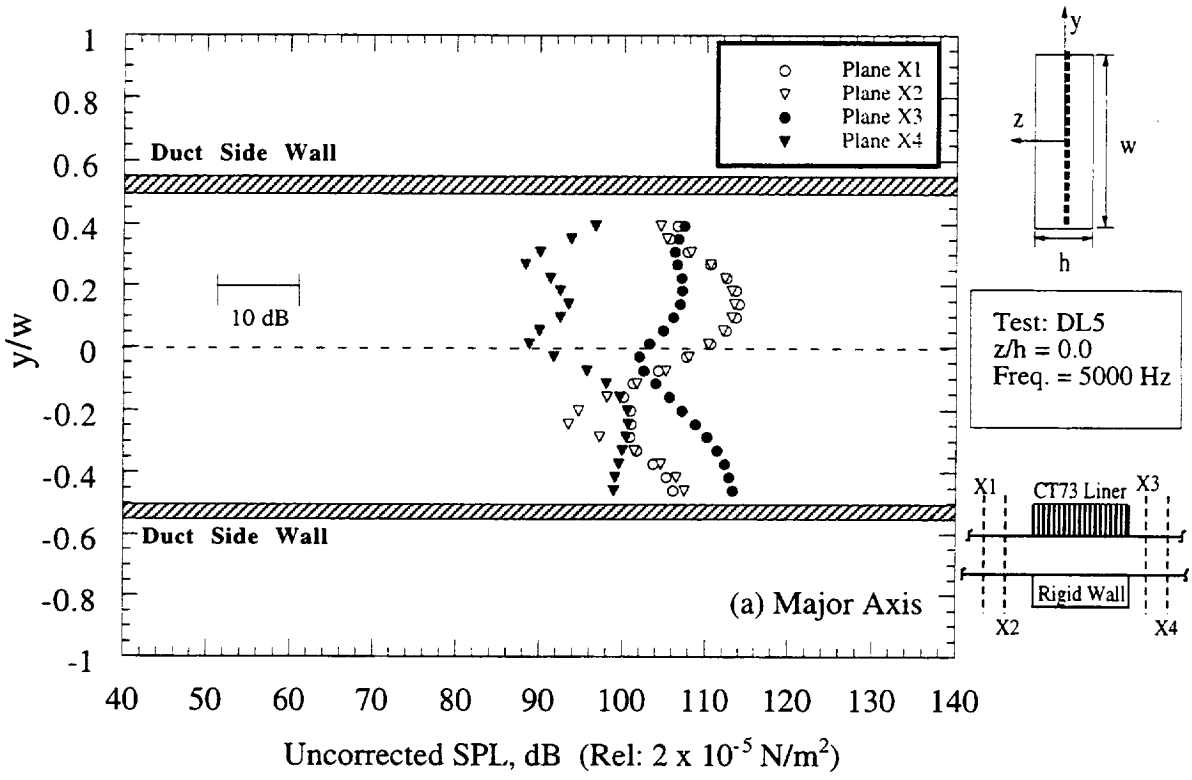

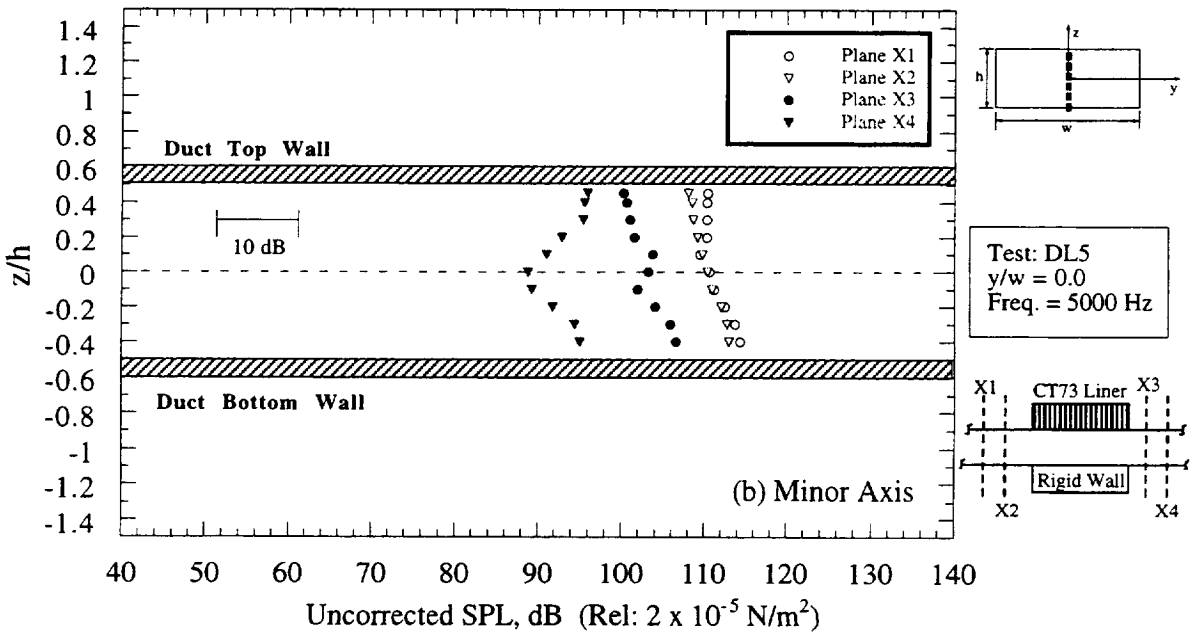

Figure 4.13 Uncorrected sound pressure levels for the lined duct at f = 5000 Hz in upstream and downstream planes (M_d = 0.0; Δf = 16 Hz; 64 avgs.).

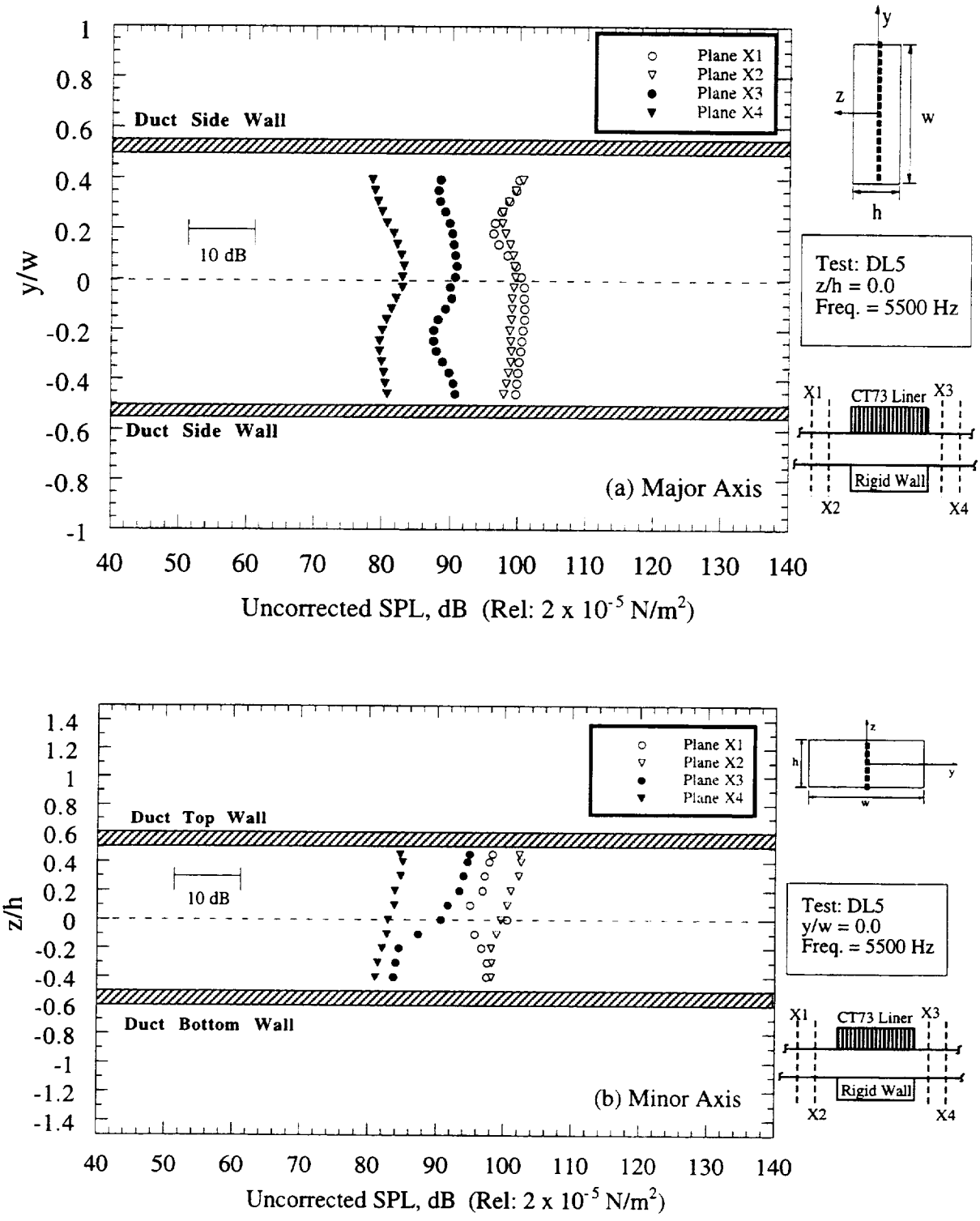

Figure 4.14 Uncorrected sound pressure levels for the lined duct at f = 5500 Hz in upstream and downstream planes (M_d = 0.0; Δf = 16 Hz; 64 avgs.).

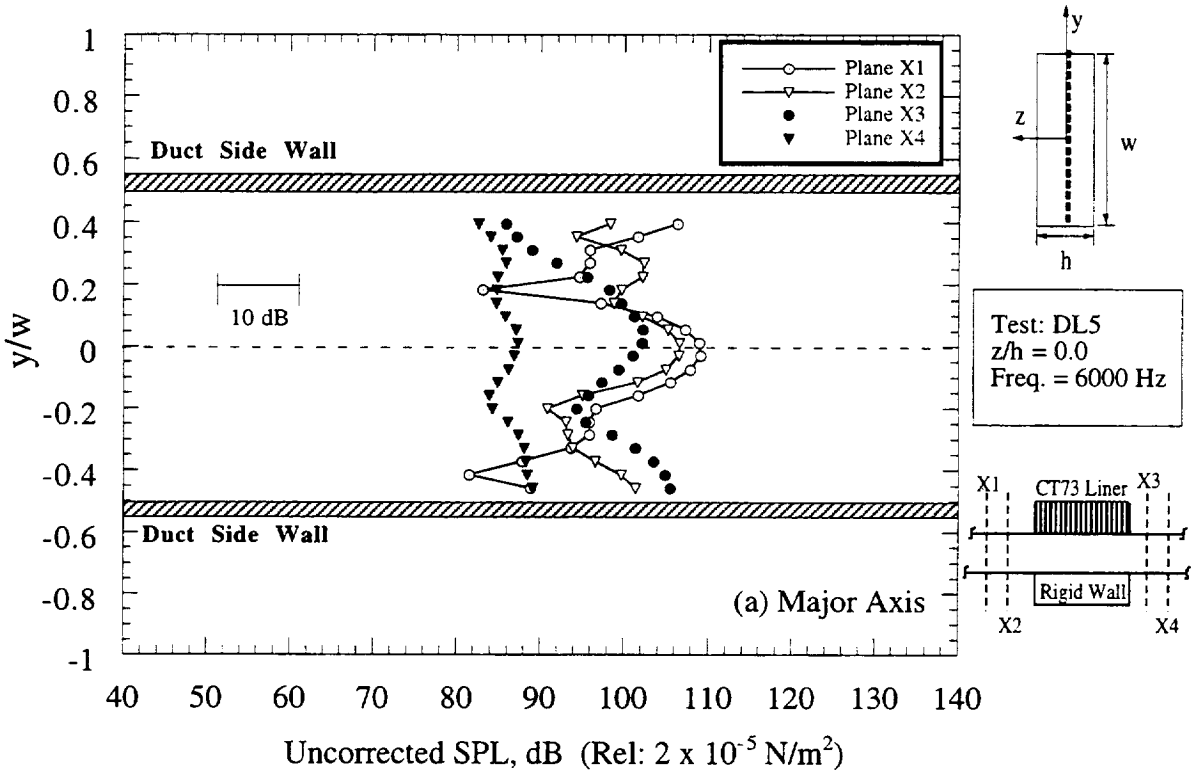

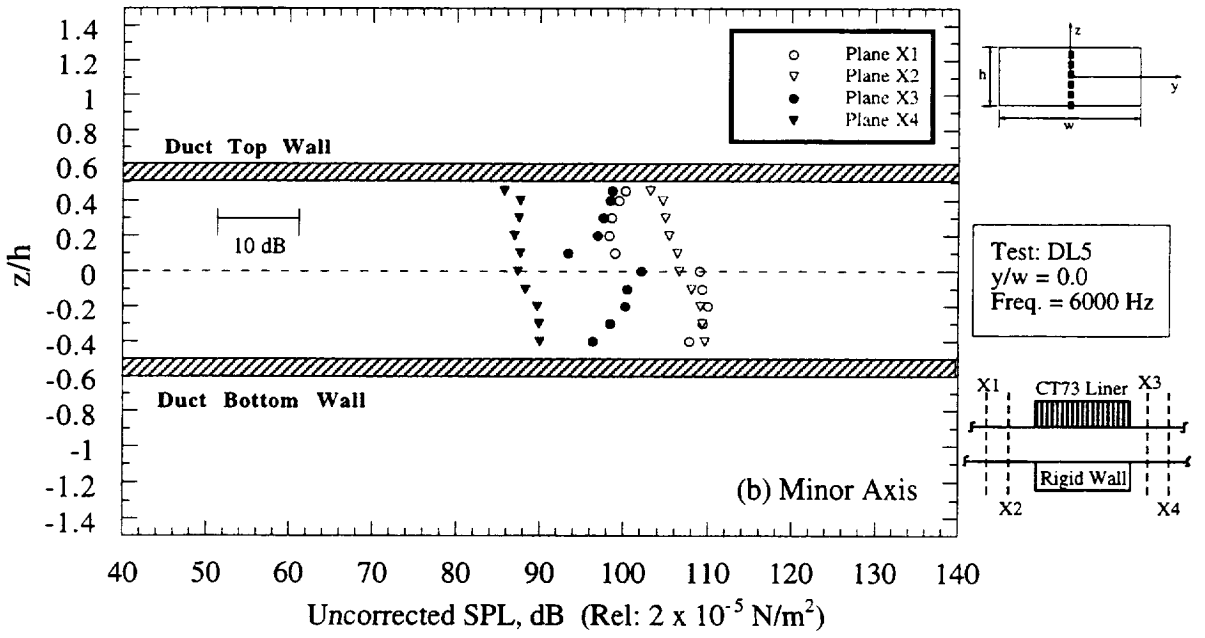

Figure 4.15 Uncorrected sound pressure levels for the lined duct at f = 6000 Hz in upstream and downstream planes (M_d = 0.0; Δf = 16 Hz; 64 avgs.).

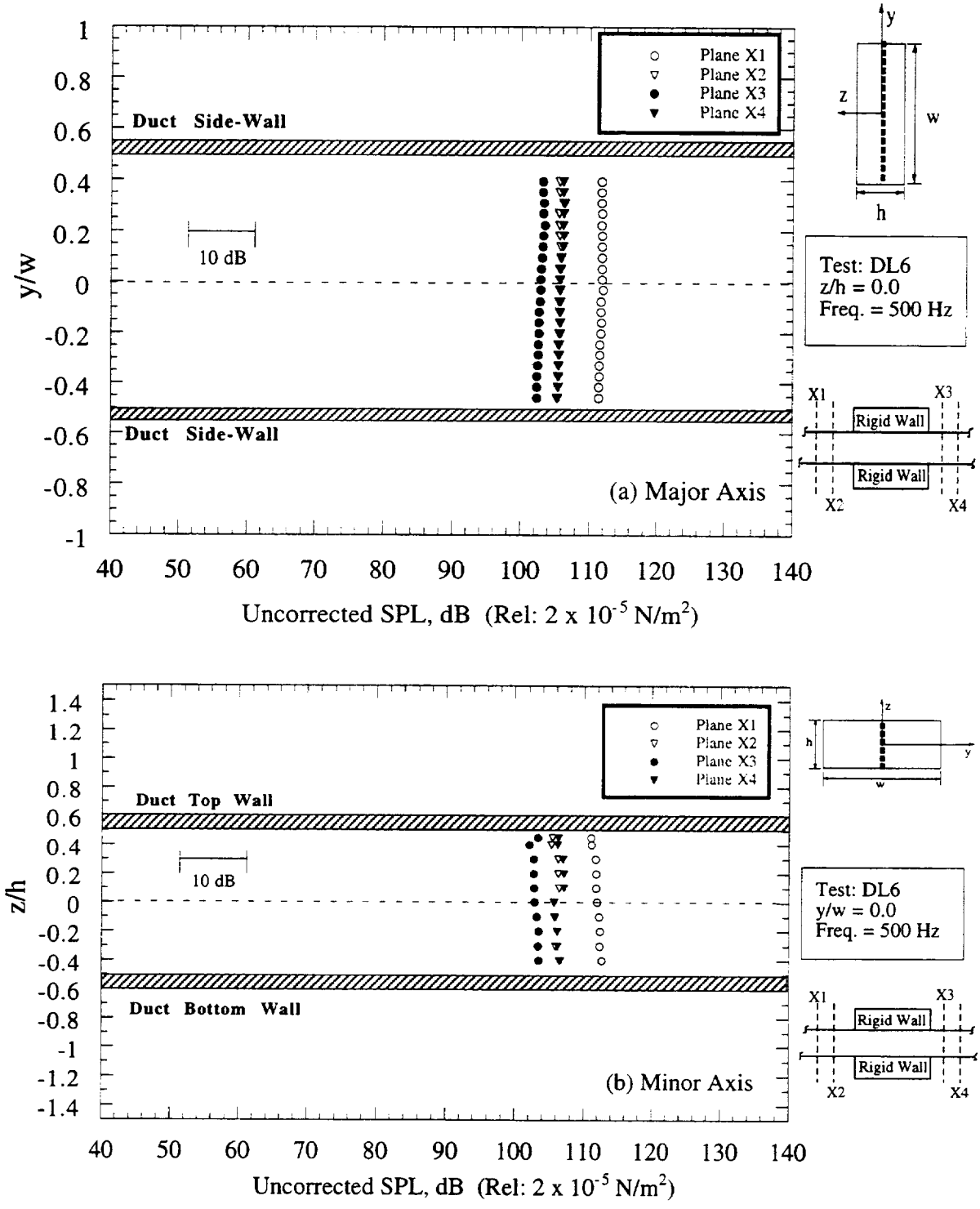

Figure 4.16 Uncorrected sound pressure levels for rigid-walled duct at f = 500 Hz in upstream and downstream planes (M_d = 0.0; Δf = 16 Hz; 64 avgs.).

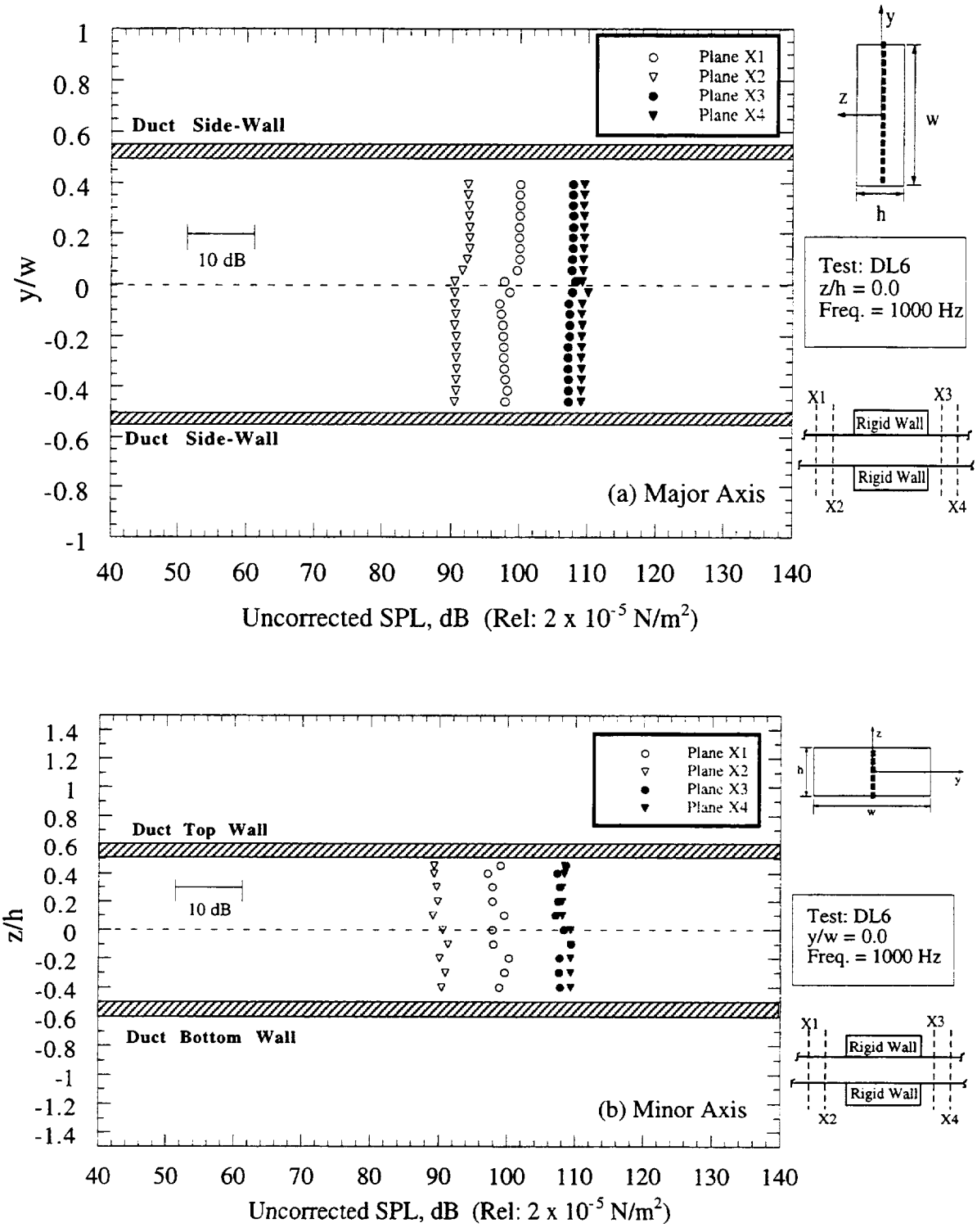

Figure 4.17 Uncorrected sound pressure levels for rigid-walled duct at f = 1000 Hz in upstream and downstream planes (M_d = 0.0; Δf = 16 Hz; 64 avgs.).

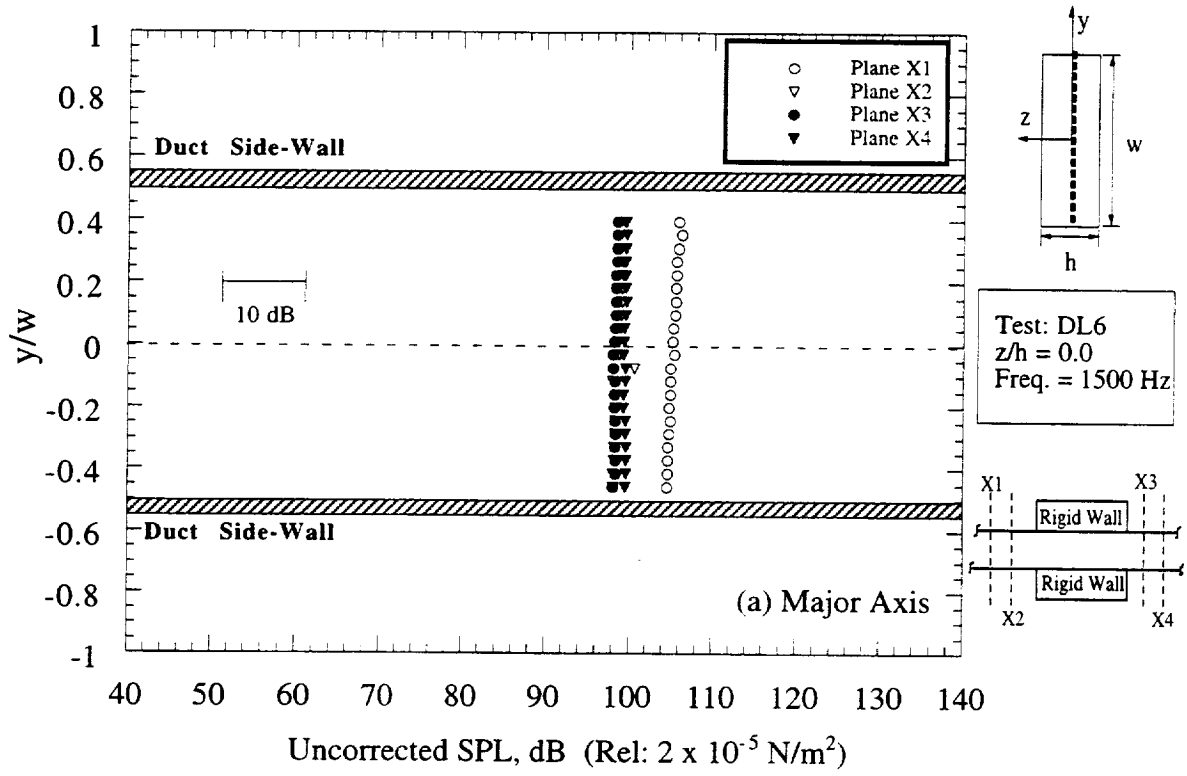

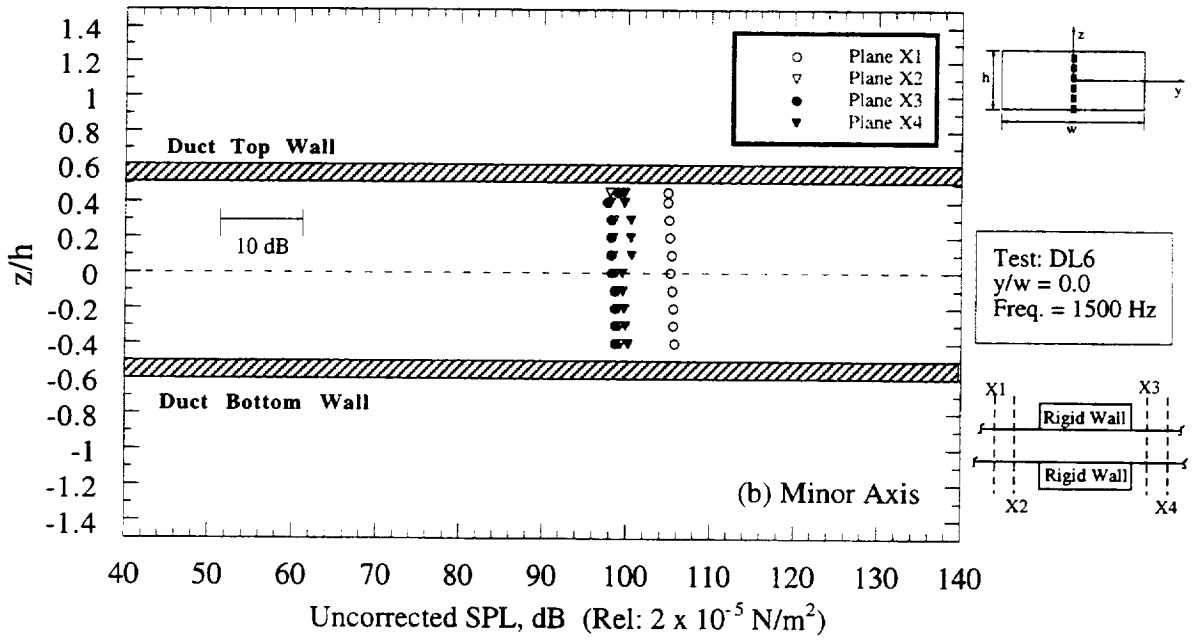

Figure 4.18 Uncorrected sound pressure levels for rigid-walled duct at f = 1500 Hz in upstream and downstream planes (M_d = 0.0; Δf = 16 Hz; 64 avgs.).

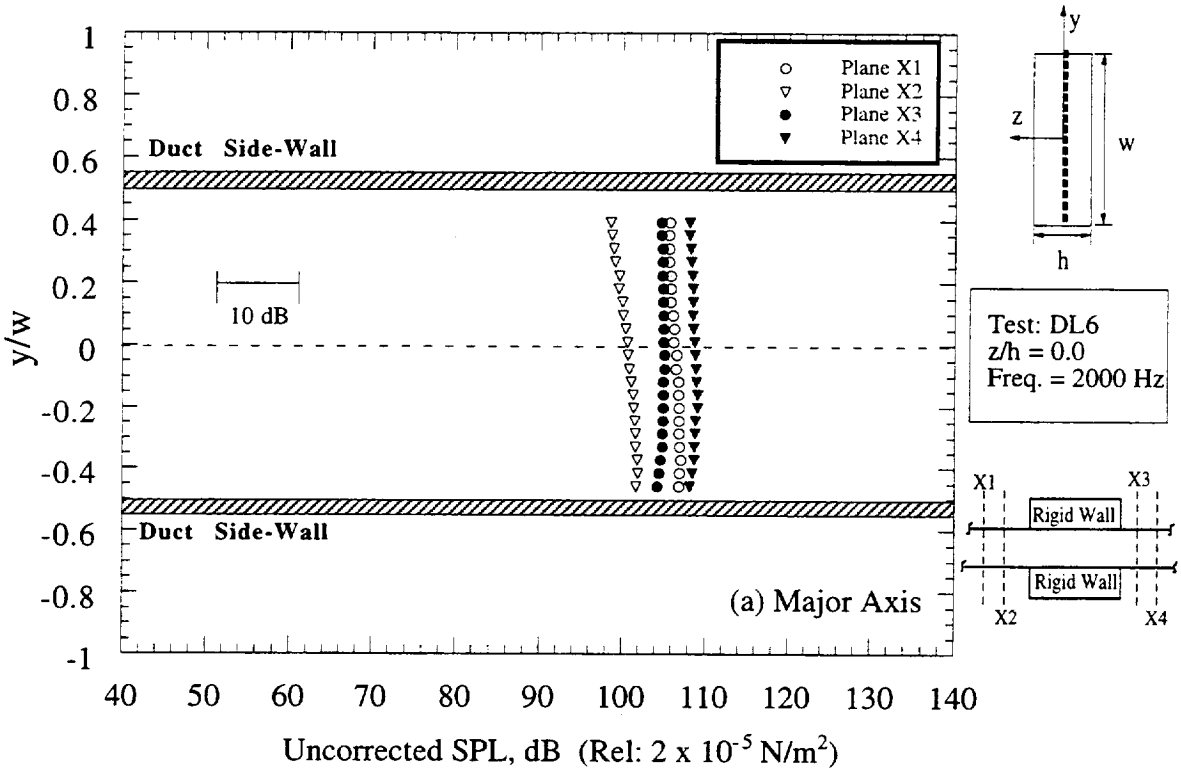

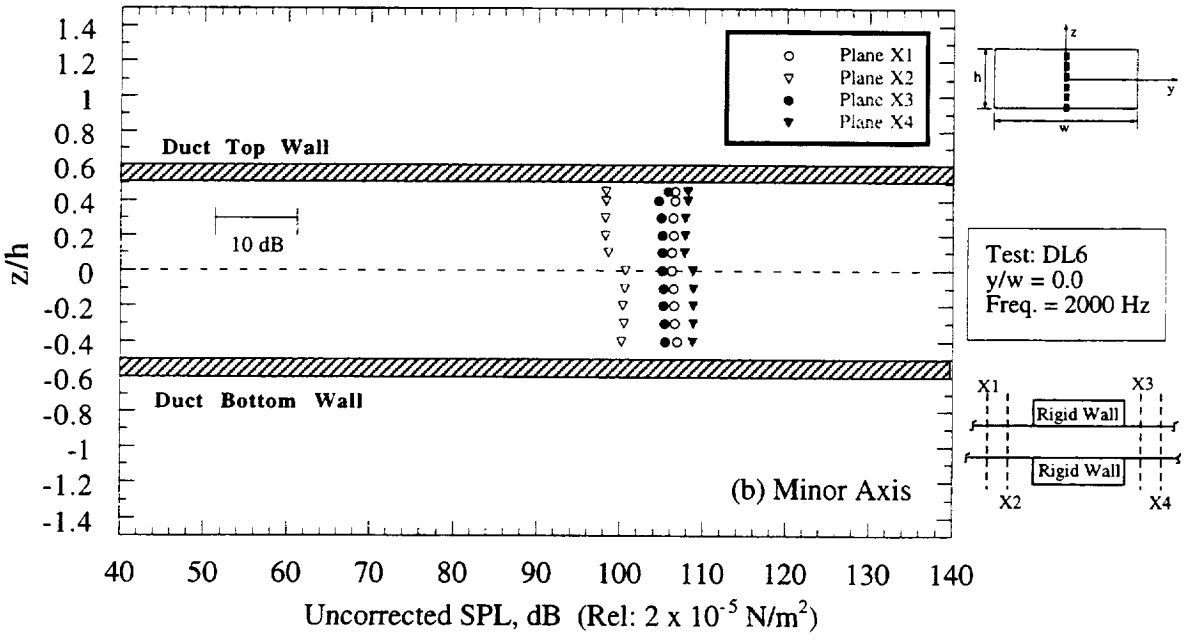

Figure 4.19 Uncorrected sound pressure levels for rigid-walled duct at f = 2000 Hz in upstream and downstream planes (M_d = 0.0; Δf = 16 Hz; 64 avgs.).

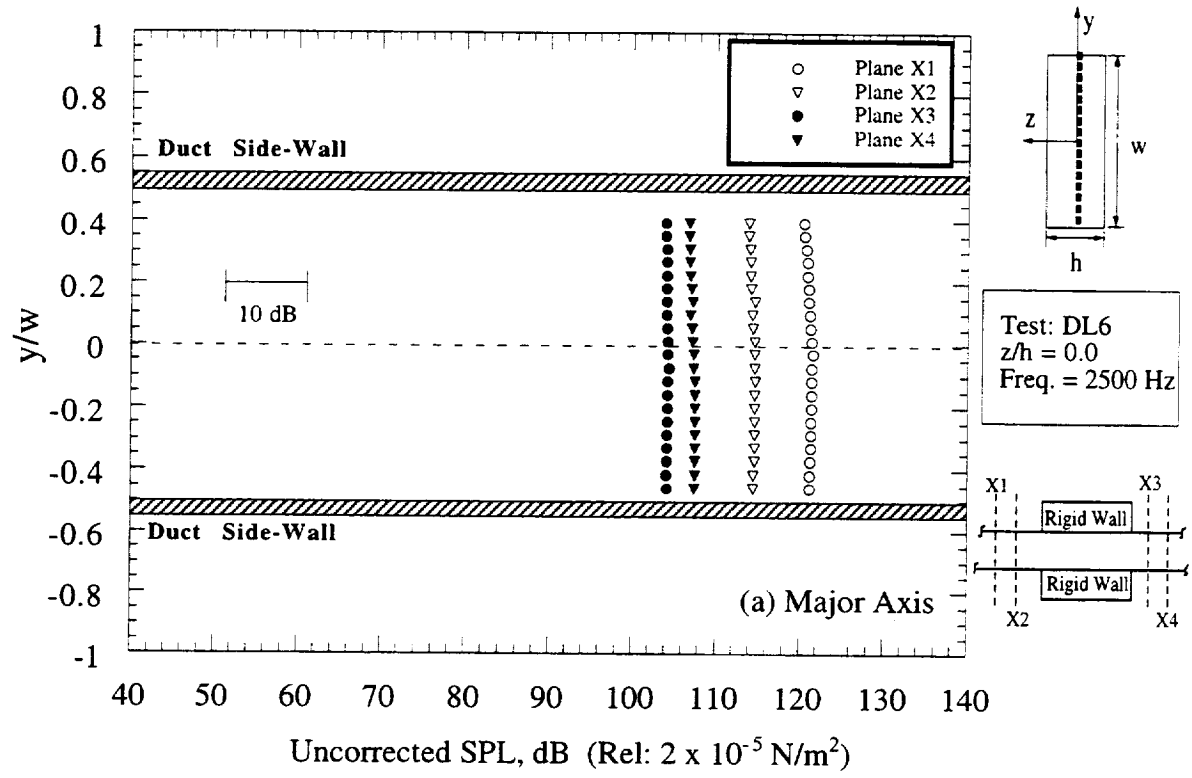

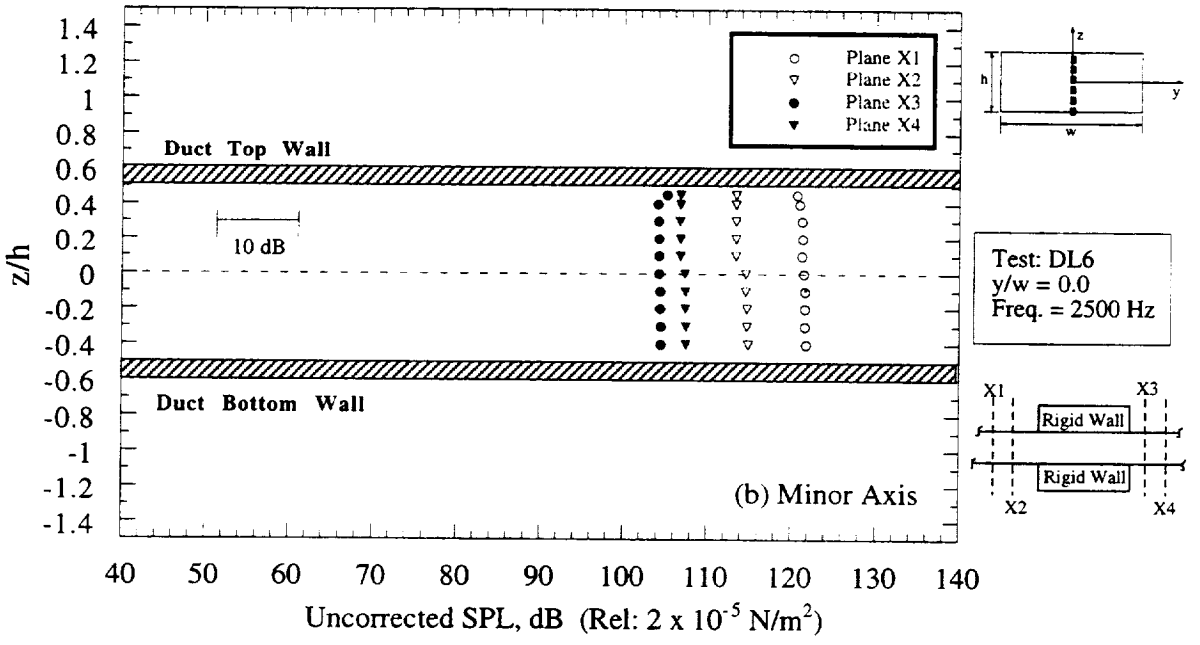

Figure 4.20 Uncorrected sound pressure levels for rigid-walled duct at f = 2500 Hz in upstream and downstream planes (M_d = 0.0; Δf = 16 Hz; 64 avgs.).

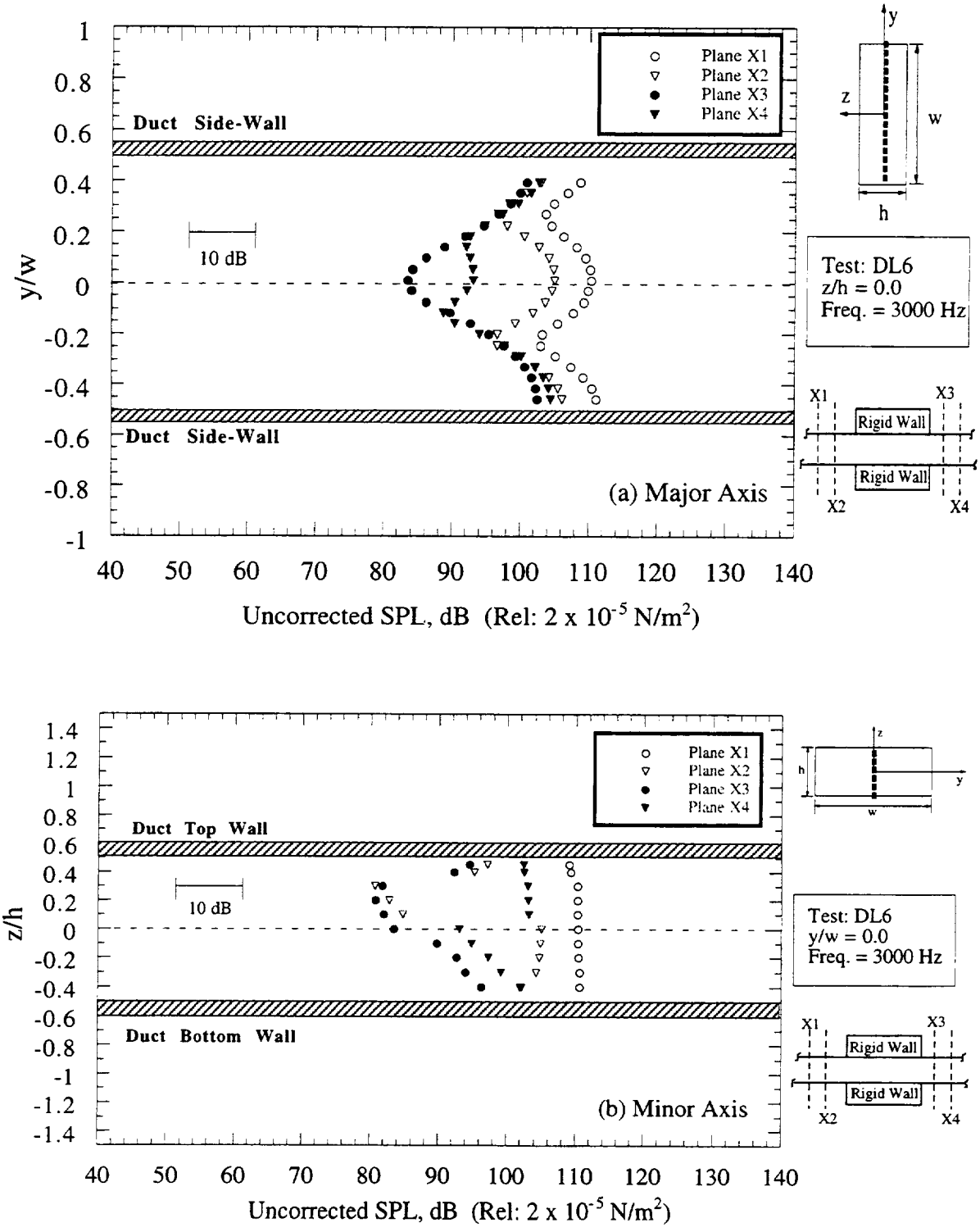

Figure 4.21 Uncorrected sound pressure levels for rigid-walled duct at f = 3000 Hz in upstream and downstream planes (M_d = 0.0; Δf = 16 Hz; 64 avgs.).

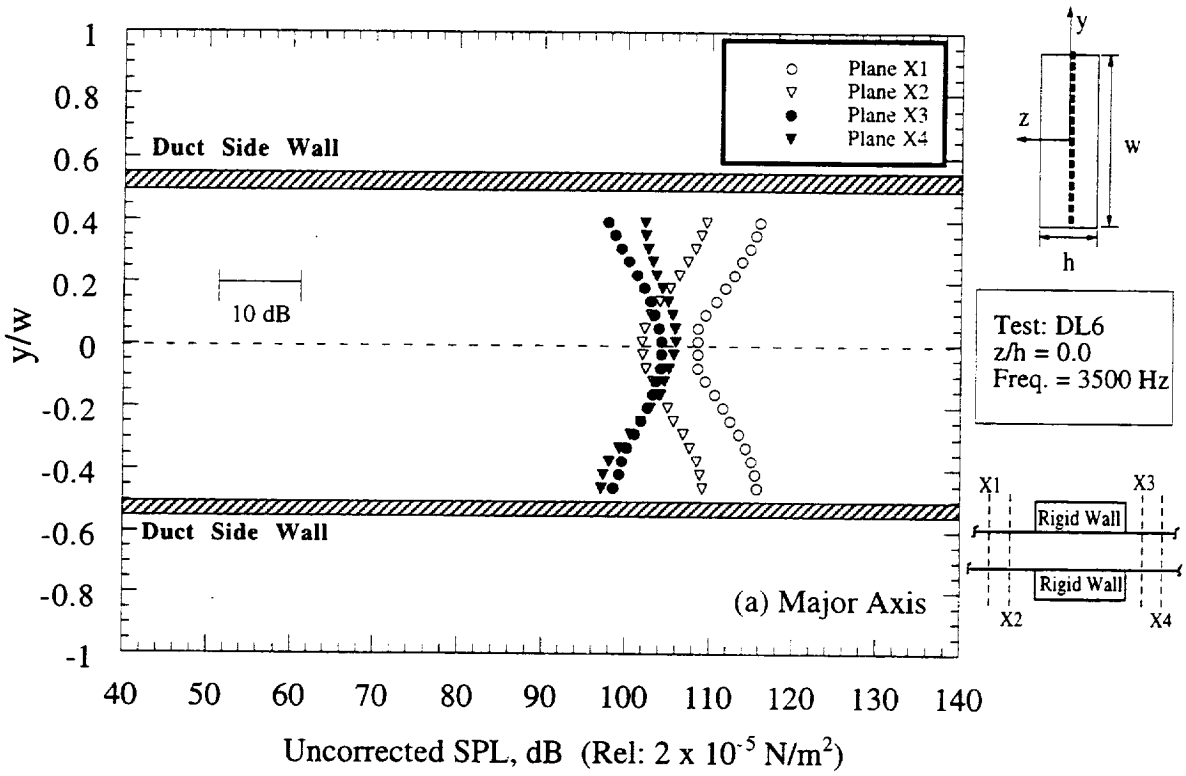

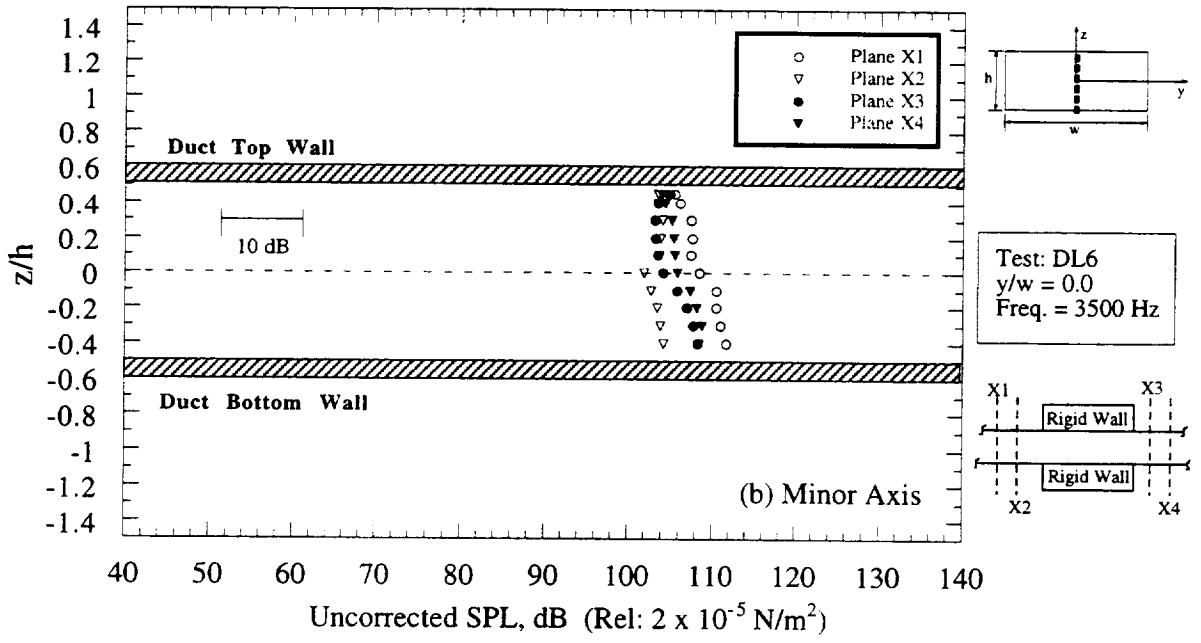

Figure 4.22 Uncorrected sound pressure levels for rigid-walled duct at f = 3500 Hz in upstream and downstream planes (M_d = 0.0; Δf = 16 Hz; 64 avgs.).

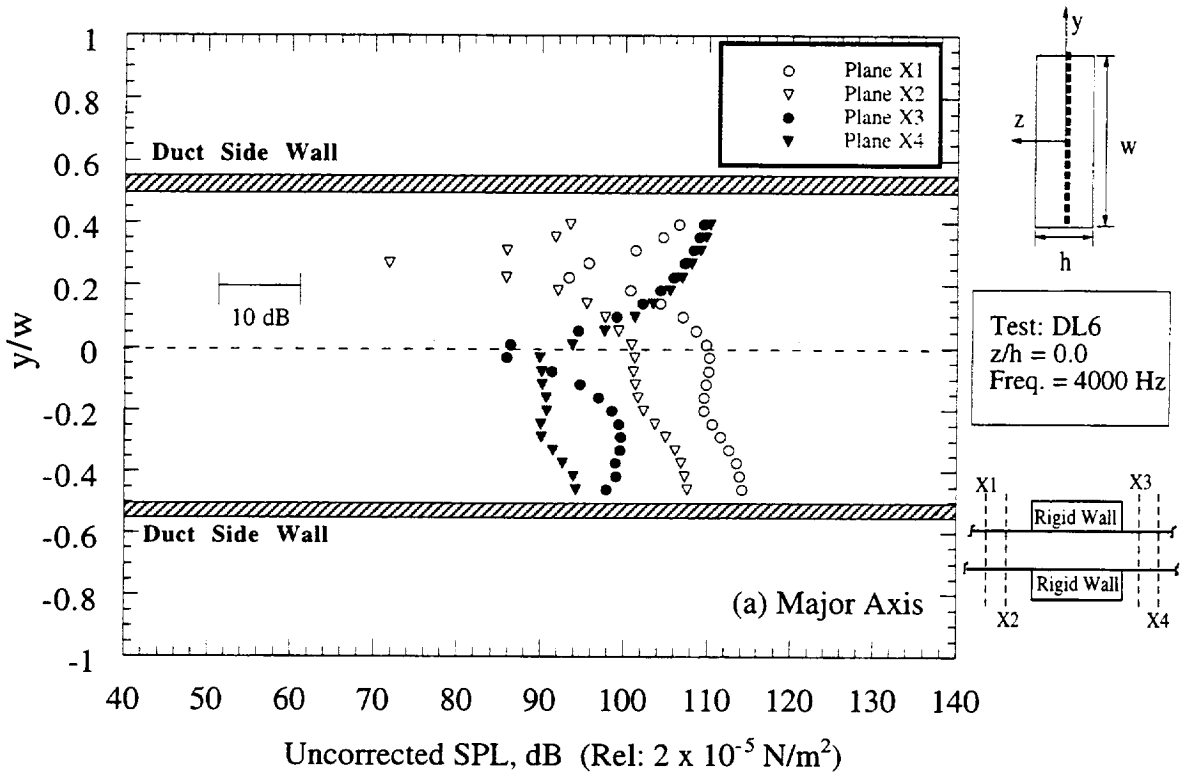

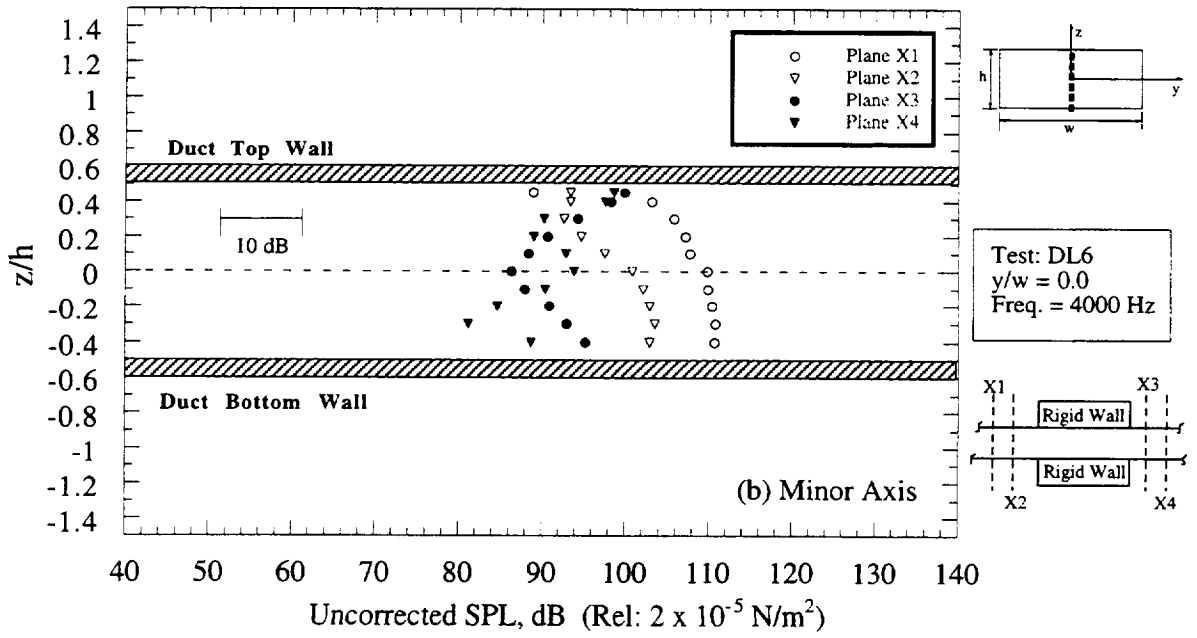

Figure 4.23 Uncorrected sound pressure levels for rigid-walled duct at f = 4000 Hz in upstream and downstream planes (M_d = 0.0; Δf = 16 Hz; 64 avgs.).

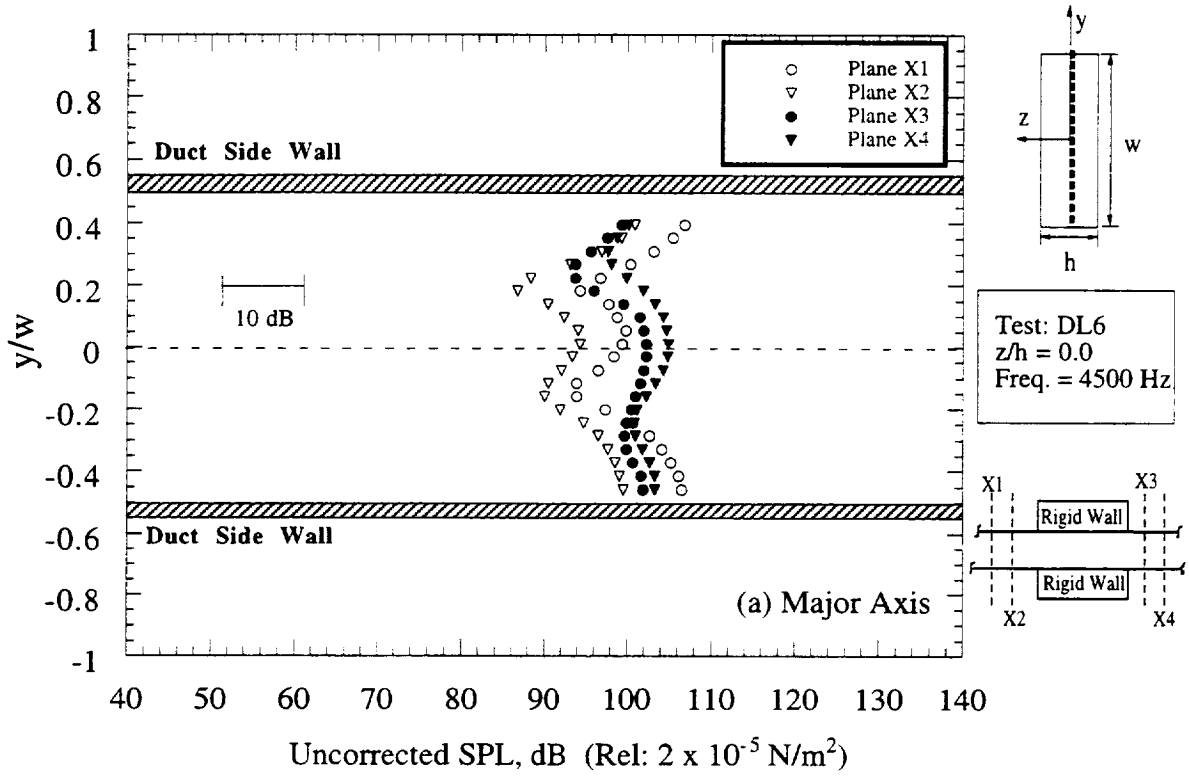

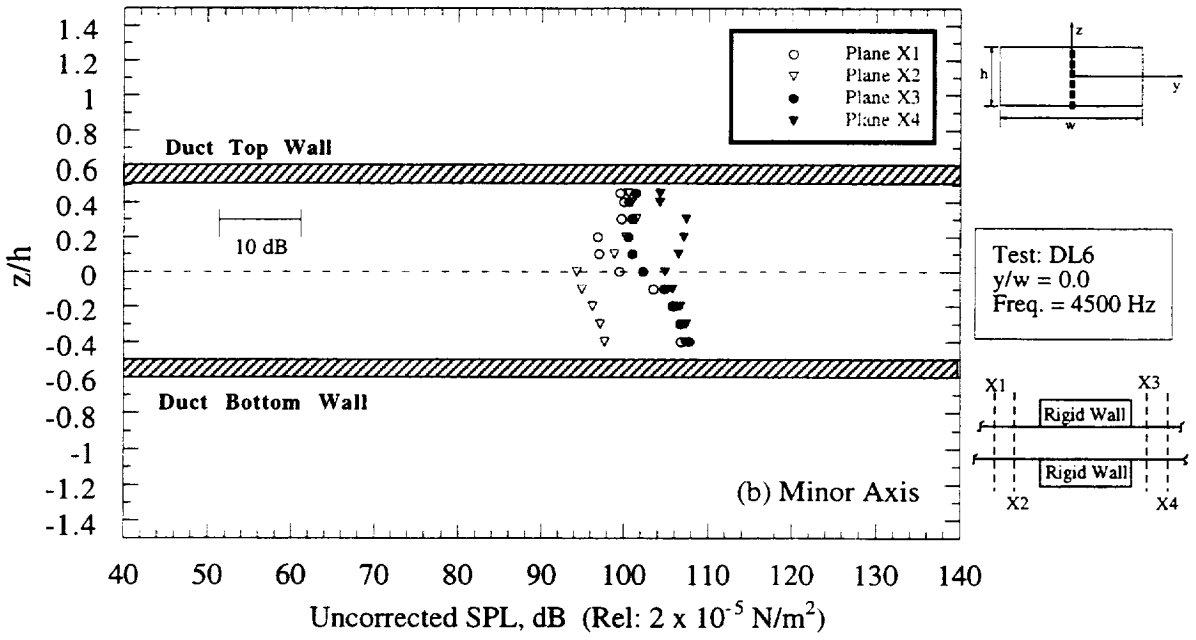

Figure 4.24 Uncorrected sound pressure levels for rigid-walled duct at f = 4500 Hz in upstream and downstream planes (M_d = 0.0; Δf = 16 Hz; 64 avgs.).

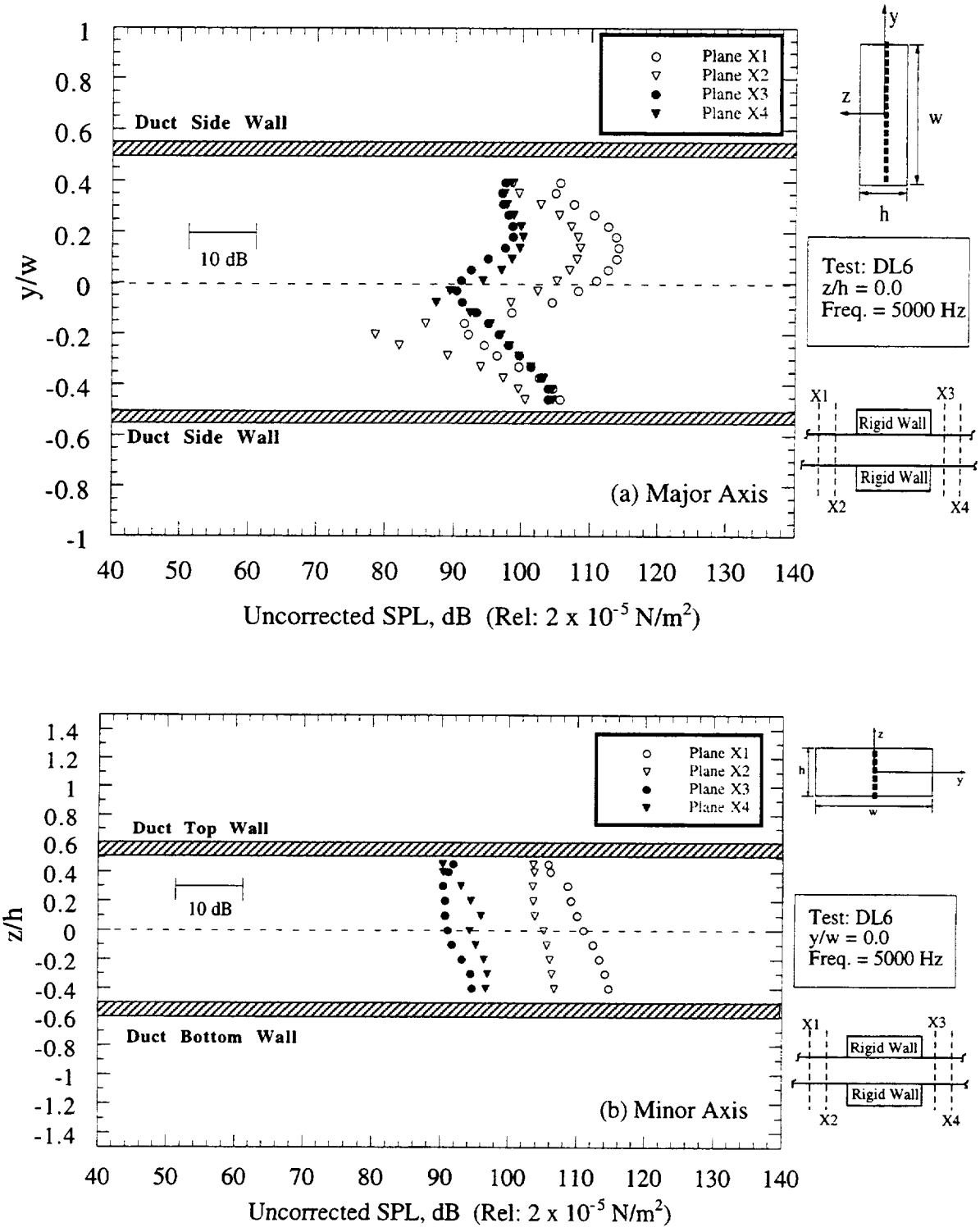

Figure 4.25 Uncorrected sound pressure levels for rigid-walled duct at f = 5000 Hz in upstream and downstream planes (M_d = 0.0; Δf = 16 Hz; 64 avgs.).

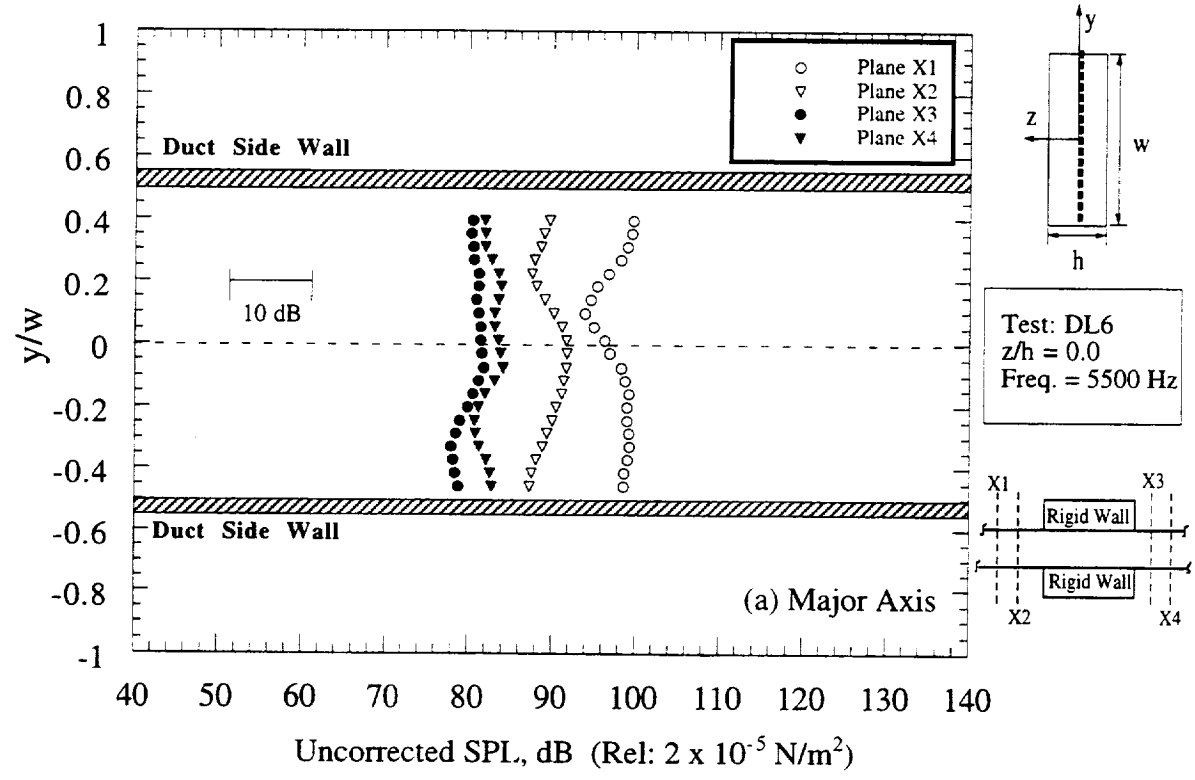

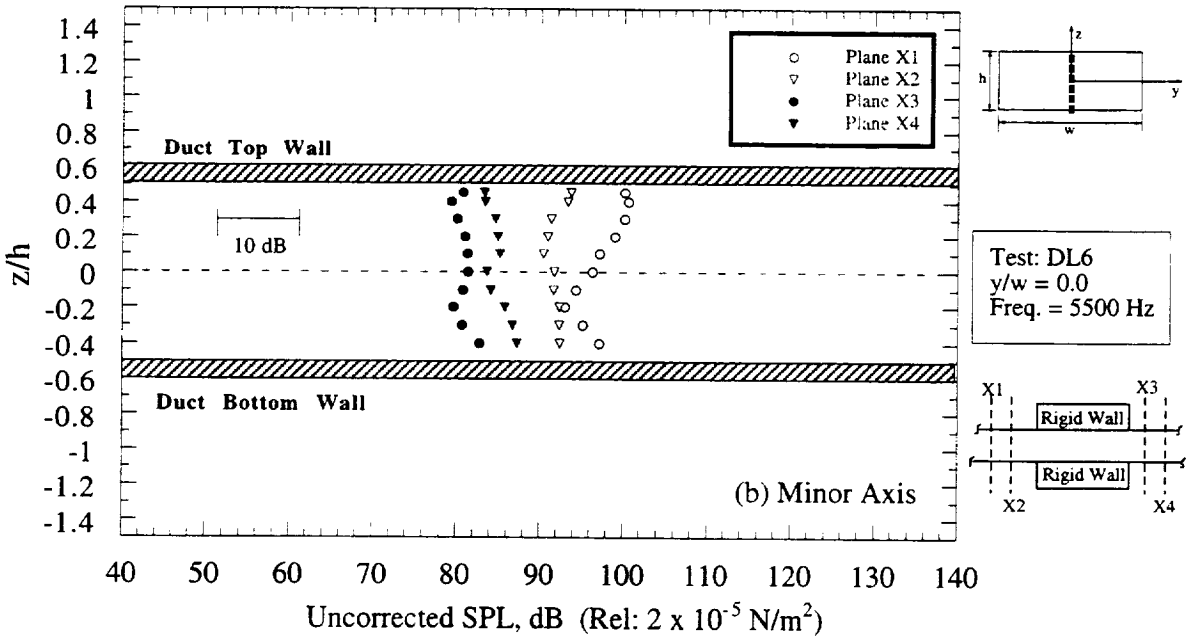

Figure 4.26 Uncorrected sound pressure levels for rigid-walled duct at f = 5500 Hz in upstream and downstream planes (M_d = 0.0; Δf = 16 Hz; 64 avgs.).

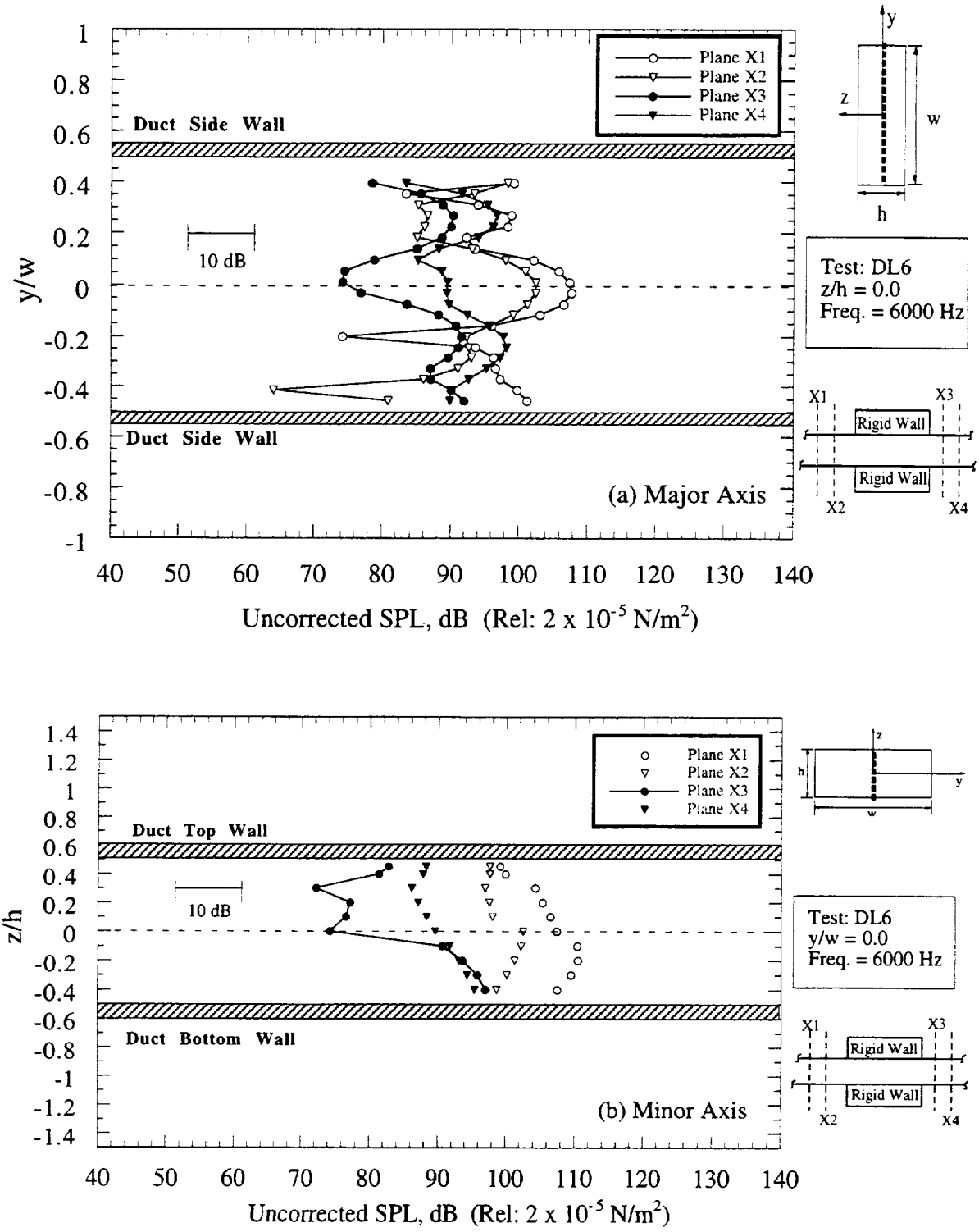

Figure 4.27 Uncorrected sound pressure levels for rigid-walled duct at f = 6000 Hz in upstream and downstream planes (M_d = 0.0; Δf = 16 Hz; 64 avgs.).

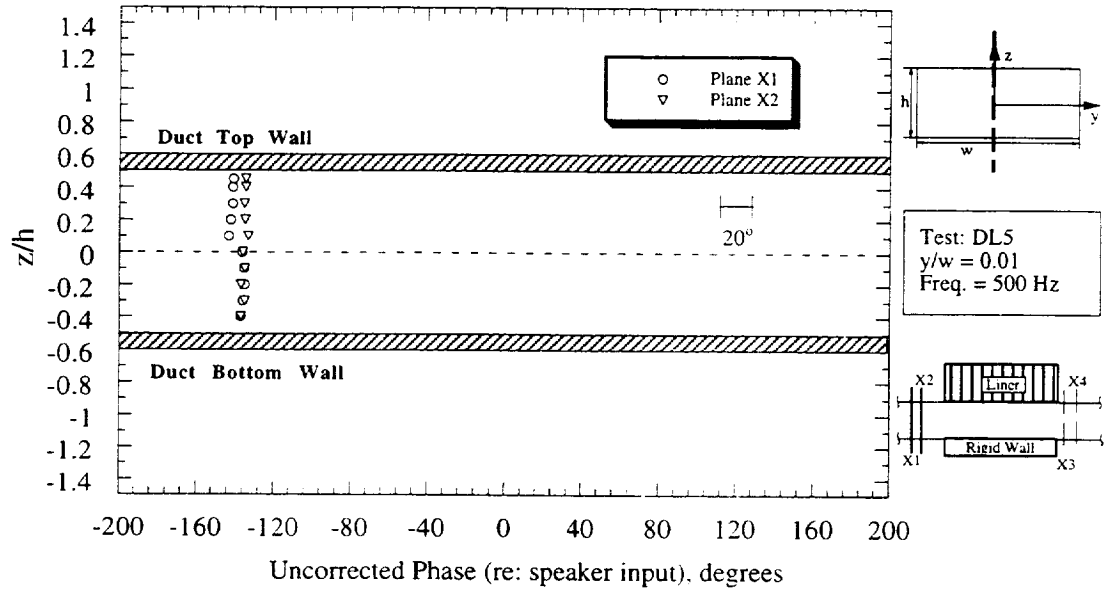

(a) Minor axis

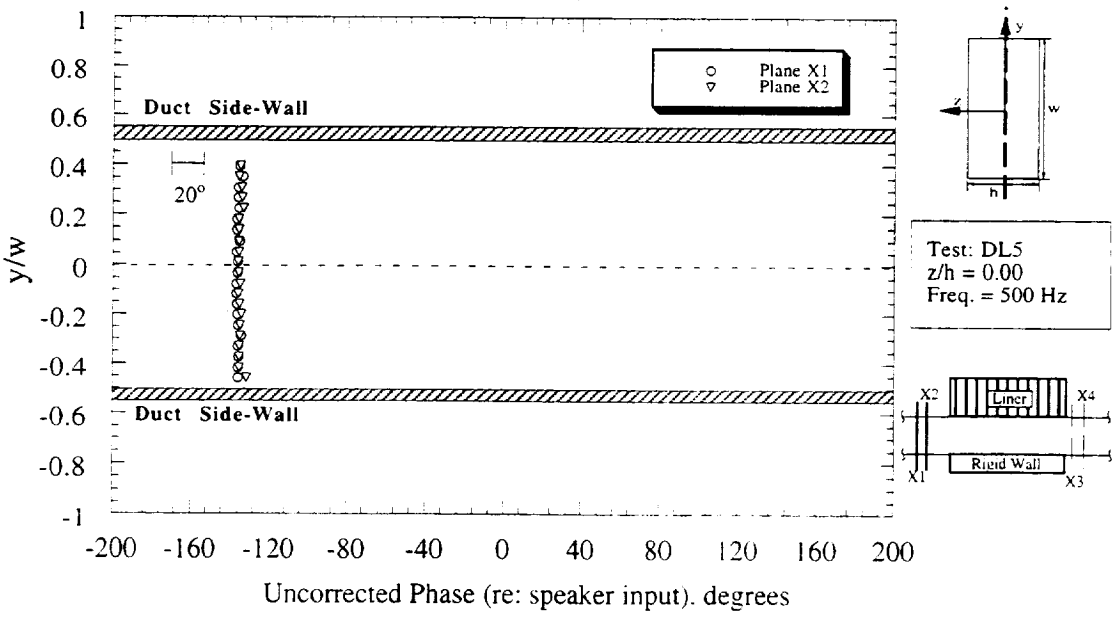

(b) Major axis

Figure 4.28 Uncorrected phase (re: speaker input) at 500 Hz at upstream location for (a) minor axis and (b) major axis ($M_d = 0.0$; $\Delta f = 10$ Hz; 64 avgs.).

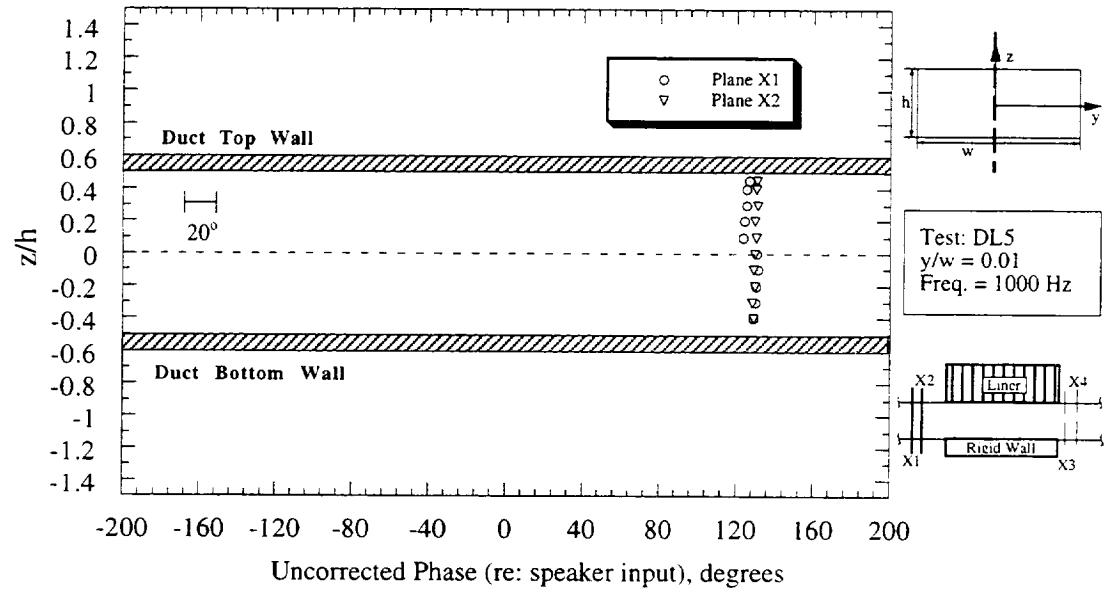

(a) Minor axis

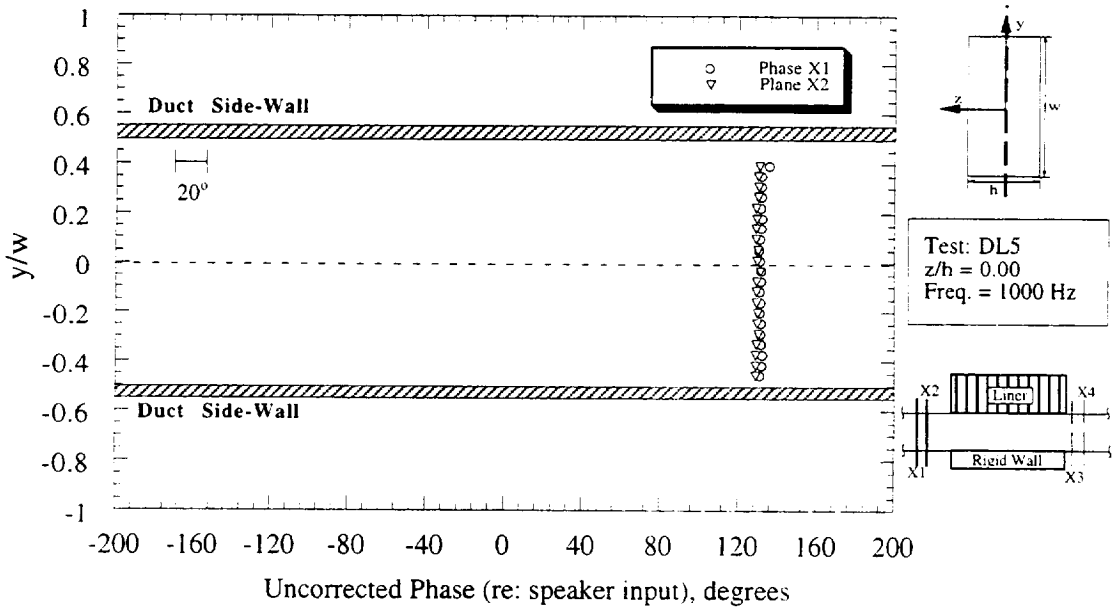

(b) Major axis

Figure 4.29 Uncorrected phase (re: speaker input) at 1000 Hz at upstream location for (a) minor axis and (b) major axis ($M_d = 0.0$; $\Delta f = 10$ Hz; 64 avgs.).

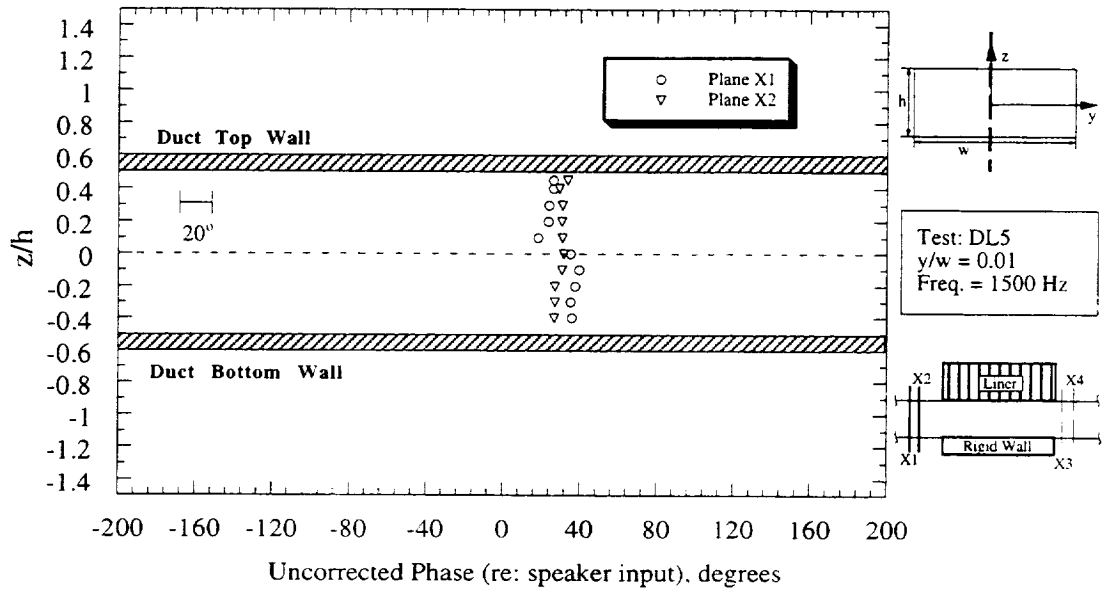

(a) Minor axis

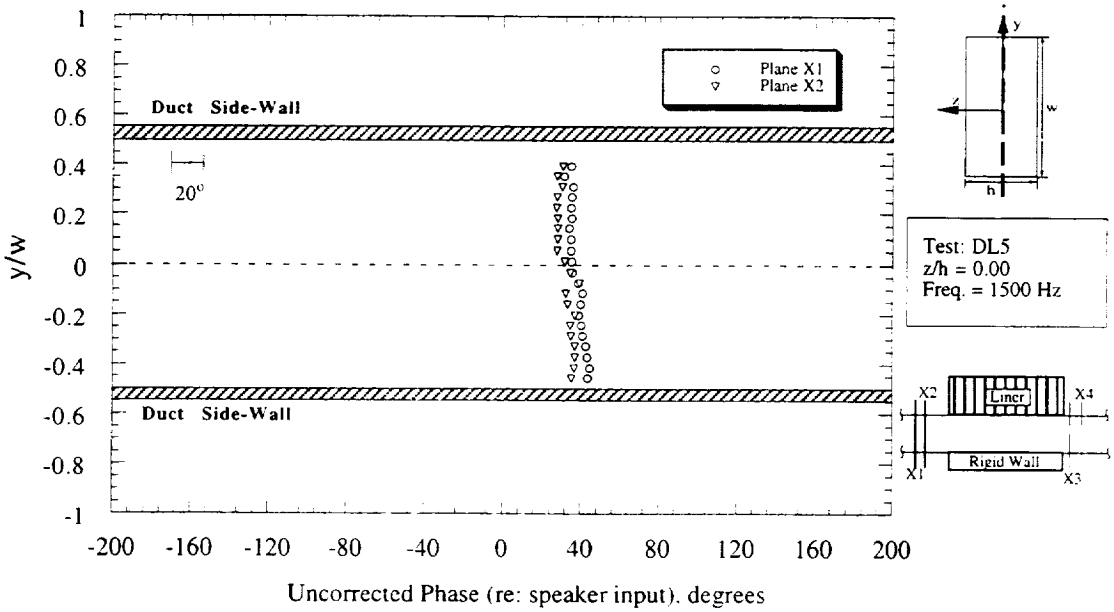

(b) Major axis

Figure 4.30 Uncorrected phase (re: speaker input) at 1500 Hz at upstream location for (a) minor axis and (b) major axis ($M_d = 0.0$; $\Delta f = 10$ Hz; 64 avgs.).

REPORT DOCUMENTATION PAGE

Form Approved
OMB No. 0704-0188

1. AGENCY USE ONLY (Leave blank)	2. REPORT DATE	3. REPORT TYPE AND DATES COVERED
	March 1997	Contractor Report

4. TITLE AND SUBTITLE
A Unique Test Facility to Measure Liner Performance with a Summary of Initial Test Results

5. FUNDING NUMBERS
NAS1-19061
Task 14
538-03-12-02

6. AUTHOR(S)
K. K. Ahuja and R. J. Gaeta, Jr.

7. PERFORMING ORGANIZATION NAME(S) AND ADDRESS(ES)
Georgia Institute of Technology
GTRI/AERO
Atlanta, GA 30332-0800

8. PERFORMING ORGANIZATION REPORT NUMBER
A8612-014
Final Report

9. SPONSORING/MONITORING AGENCY NAME(S) AND ADDRESS(ES)
National Aeronautics and Space Administration
Langley Research Center
Hampont, VA 23681-0001

10. SPONSORING/MONITORING AGENCY REPORT NUMBER
NASA CR-201667

11. SUPPLEMENTARY NOTES
Langley Technical Monitors: Tony Parrott and Sharon Tanner

12a. DISTRIBUTION/AVAILABILITY STATEMENT
Unclassified - Unlimited
Subject Category 71

12b. DISTRIBUTION CODE

13. ABSTRACT *(Maximum 200 words)*

A very ambitious study was initiated to obtain detailed acoustic and flow data with and without a liner in a duct containing a mean flow so that available theoretical models of duct liners can be validated. A unique flow-duct facility equipped with a sound source, liner box, flush-walled microphones, traversable microphones and traversable pressure and temperature probes was built. A unique set of instrumentation boxes equipped with computer controlled traverses were designed and built that allowed measurements of Mach number, temperature, SPLs and phases in two planes upstream of a liner section and two planes downstream at a large number of measurement points. Each pair of planes provided acoustic pressure gradients for use in estimating the particle velocities. Specially-built microphone probes were employed to make measurements in the presence of the flow. A microphone traverse was also designed to measure the distribution of SPLs and phases from the beginning of the liner to its end along the duct axis. All measurements were made with the help of cross-correlation techniques to reject flow noise and/or other obtrusive noise, if any. The facility was designed for future use at temperatures as high as 1500° F. In order to validate 2-D models in the presence of mean flow, the flow duct was equipped with a device to modify boundary layer flow on the smaller sides of a rectangular duct to simulate 2-D flow.

A massive amount of data was acquired for use in validating duct liner models and will be provided to NASA in an electronic form. It was found that the sound in the plane-wave regime is well behaved within the duct and the results are repeatable from one run to another. At the higher frequencies corresponding to the higher-order modes, the SPLs within a duct are not repeatable from run to run. In fact, when two or more modes have the same frequency (i.e., for the degenerate modes), the SPLs in the duct varied between 2 dB to 12 dB from run to run. This made the calibration of the microphone probes extremely difficult at the higher frequencies.

14. SUBJECT TERMS	15. NUMBER OF PAGES
High temperature liners, sound absorption, probe microphones, impedance measurement, flow-duct facility	132
	16. PRICE CODE: A07

17. SECURITY CLASSIFICATION OF REPORT	18. SECURITY CLASSIFICATION OF THIS PAGE	19. SECURITY CLASSIFICATION OF ABSTRACT	20. LIMITATION OF ABSTRACT
Unclassified	Unclassified		